MATERIALS CHEMISTRY FRONTIERS

REVIEW

View Article Online
View Journal | View Issue

Cite this: *Mater. Chem. Front.*, 2021, **5**, 7134

Current trends in MXene research: properties and applications

Shrabani De,[a] Sourav Acharya,[a] Sumanta Sahoo *[b] and Ganesh Chandra Nayak *[a]

Received 12th April 2021,
Accepted 22nd August 2021

DOI: 10.1039/d1qm00556a

rsc.li/frontiers-materials

A new class of two-dimensional (2D) materials known as MXene became one of the most promising candidates under investigation after the discovery of the first member of this group, $Ti_3C_2T_x$, in 2011. These layered transition metal nitrides, carbonitrides, and carbides have offered an attractive new area in inorganic 2D materials with their fascinating structural and chemical characteristics due to the versatility in elemental compositions and surface terminations. Significantly, the surface hydrophilicity of MXenes facilitates the easy composite formation with carbonaceous materials, polymers, and metal oxides that further opens up an efficient pathway for tuning the characteristics of MXenes for different applications. Despite exponentially increasing interest, MXenes lack proper systematic information. This article is focused on reviewing the most applicable aspects of MXenes including structural features with their relevant characteristics and applicability by describing both experimental and theoretical perspectives. A critical survey on current trends, status, and possibilities of MXenes and MXene-based materials have been represented for energy-related applications as well as electromagnetic interference (EMI) shielding, blends and composites, sensors, organic light-emitting diodes (OLED), and actuators and robotics associated with the limitations and future potentialities.

1. Introduction

Two-dimensional (2D) materials are being immensely investigated for the past 16 years since the discovery of single-layered graphene with unique chemical and physical properties.[1] One striking thing about graphene is that its properties are entirely different from the zero-dimensional (0D), one-dimensional (1D), and three-dimensional (3D) allotropes of carbon. The 2D characteristics are quite unique. However, it is required to explore the atypical chemical, physical and electronic properties because of electron caging in two dimensions. Graphene is the most efficient candidate among the carbon-based 2D materials, which have spectacular optical, electronic, thermal, and mechanical properties, quantum hall effect, high specific surface area, elevated carrier mobility, exceptional morphology, and tunable band gap.

[a] *Department of Chemistry, Indian Institute of Technology (ISM), Dhanbad-826004, Jharkhand, India. E-mail: gcnayak@iitism.ac.in*
[b] *Department of Chemistry, Madanapalle Institute of Technology and Science, Madanapalle, Andhra Pradesh, 517325, India. E-mail: sumanta95@gmail.com*

Shrabani De

Ms Shrabani De received her BSc degree from Burdwan University, India in 2014. She completed her MSc from IIT(ISM), Dhanbad, India in the year of 2017. She is currently pursuing her PhD at the department of Chemistry, IIT(ISM), Dhanbad, India. Ms De is currently working on the development of MXene based materials for different energy storage applications.

Sourav Acharya

Mr Sourav Acharya received his BSc degree from Burdwan University (India) in 2015. He completed his MSc from Indian Institute of Technology(ISM), Dhanbad (India) in 2017. He is currently pursuing his PhD at the department of Chemistry, IIT(ISM), Dhanbad (India). Mr Acharya is currently working on the development of different nanocomposites for energy storage and water cleaning application.

Graphene with these unique properties becomes suitable for diversified applications such as energy storage and conversion, sensing, electronics, optical devices, DNA sequencing, and hybrid materials.[2–12] Inspired by the mammoth success of graphene research, scientists were further interested in exploring 2D materials beyond graphene. In this aspect, it is significant to notice that the layered metal oxides, transition metal dichalcogenides, layered double hydroxide, graphitic carbon nitride, hexagonal boron nitride, silicene, borophene, and phosphorene are graphene-like materials with multifunctional properties. The common characteristics of these layered 2D materials are the van der Waals interaction, which is involved between two adjacent sheets, as well as a strong covalent bond is also present in each sheet. This category of materials has tunable electronic structure starting from insulator to the semiconductor; even up to the range of metal, which enabled those to be used in versatile applications such as chemical sensor, catalyst, solar cell, supercapacitor, and optoelectronics.[13]

However, a few of these materials as mentioned above exist due to academic interest and a few of them suddenly gained interest due to their magnificent characteristics resulting in practical applications. Among the second type of materials, early group transition metal carbides, nitrides, or carbonitrides, typically called MXenes (uttered as 'maxenes') are a fast-developing class of 2D materials.[14] These types of materials are generally synthesized by the delamination of their corresponding 3D MAX phases. Since its discovery, MXene has exhibited unique but diverse properties. For example, it shows analogous conductivity with that of few-layered graphene.[15] In this aspect, it is essential to note that Khazaei *et al.* reported that, at lower temperatures, semiconducting MXenes can reach very high Seebeck coefficients.[16] According to the density functional theory (DFT) calculation, the in-plane elastic constant of MXene is above 500 GPa, which means MXene sheets are comparatively stiff.[17] Due to its magnificent properties, MXene has attained enormous attention for its application in various fields such as an efficient electrode material for energy storage[18] and supporting material for metal nanoparticles used as a catalyst in fuel cell.[19] As another example, Wang *et al.* observed that MXene has good enzyme immobilization capability. It is also biocompatible with redox protein, which makes it a potential candidate as an electrochemical biosensor.[20] In a word, currently, MXenes are considered one of the hot topics for material scientists worldwide.

This review article focuses on recent developments on MXene and related compounds with different synthesis techniques, properties, and characterization techniques covering both theoretical aspects and experimental studies. We also briefly discuss the applications of MXene and MXene-based composites in various fields, including supercapacitor, secondary batteries, hydrogen storage, fuel cell, solar cell, electromagnetic interference (EMI) shielding, energy harvesting, blends and composites, electro-catalysis, sensors, organic light-emitting diodes (OLED), actuators, and robotics (briefly illustrated in Fig. 1). Besides, the obstacles and future research prospects are also provided for further exploration of this fascinating material.

2. Introduction of MXene

MXene, a novel category of 2D materials with metallic property is prepared by selective elimination of the 'A' layer from the MAX phase using selective etching reagent. MAX phase is stoichiometrically denoted by the formula $M_{n+1}AX_n$, (n = 1–3) where 'M' is the prior transition metals including Ti, Sc, V, Zr, Hf, Nb, Mo, Cr, *etc.*, 'A' is the sp elements of 12 to 16 group

Sumanta Sahoo

Dr Sumanta Sahoo is working as an Asst. Professor in Madanapalle Institute of Technology & Science, Andhra Pradesh, India. He received his PhD degree IIT Kharagpur, West Bengal, India in 2013. He also worked at the Korea Advanced Institute of Science and Technology (KAIST) (2013–2014) (Postdoctoral Researcher), South Korea, Yeungnam University (2015–2017) (Research Professor), South Korea, and Indian Institute of Technology (ISM), Dhanbad, India (2018–2019) (National Postdoctoral Fellow). Dr Sahoo is currently working in MXene and graphene-based composite materials for energy-related applications. Dr Sahoo has published more than 50 peer-reviewed research/review articles in refereed international journals, wrote 3 book chapters and edited a book.

Ganesh Chandra Nayak

Dr G. C. Nayak received a PhD in Materials Science from the IIT Kharagpur, INDIA in 2012. After his PhD, he joined the IIT (ISM) Dhanbad, INDIA as an Assistant Professor in the year of 2012. He was promoted to Associate Professor in 2019. Dr Nayak's research interest includes Synthesis and applications of 2D nanomaterials for microwave absorption and energy storage. He has guided 4 PhD students and published more than 65 papers in peer-reviewed journals along with 6 book chapters.

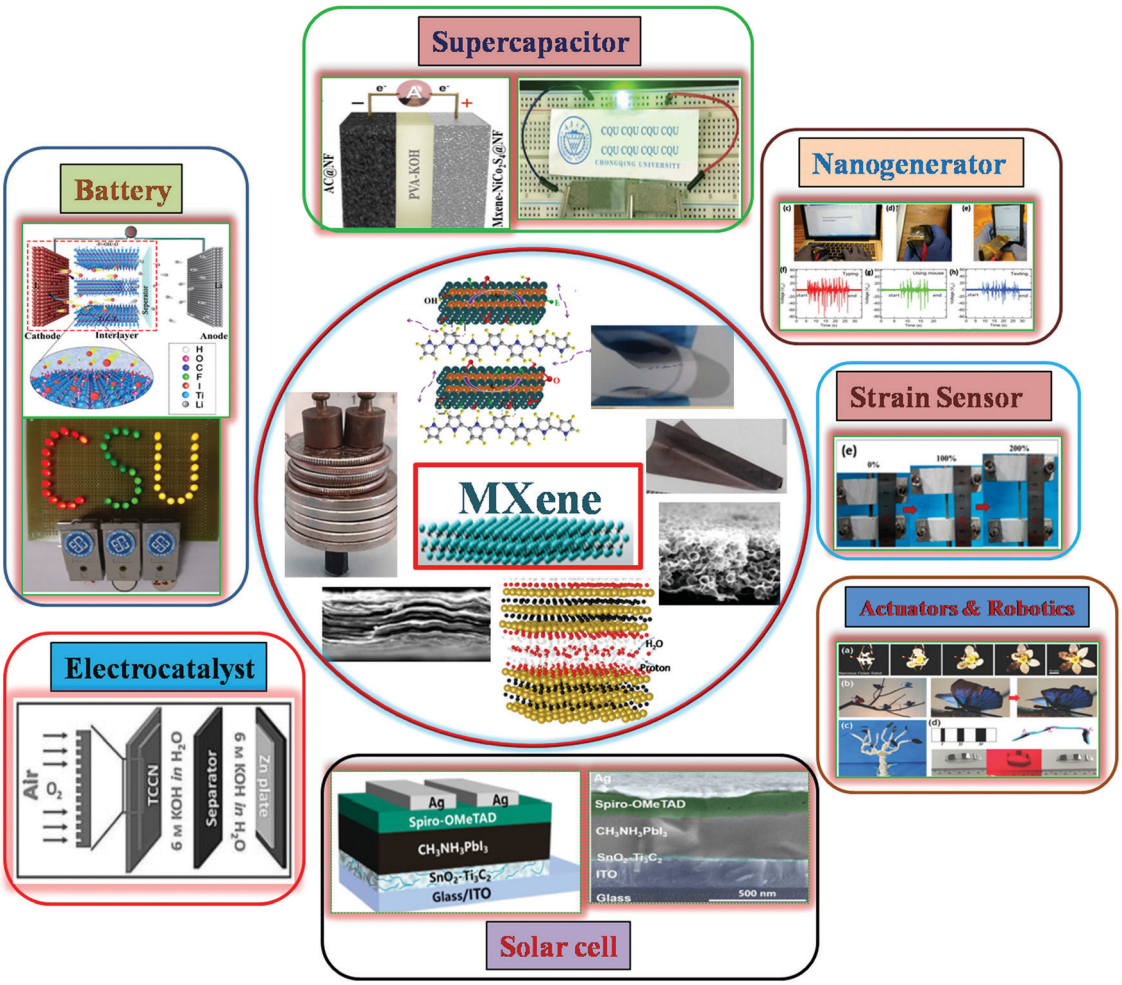

Fig. 1 Schematics representing the progress of the applications of MXene in different fields. Reused with consent from ref. 21–34.

elements such as Al, Ga, Si, P, *etc.*, and 'X' is C, N or both as presented in Fig. 2.[21,35–38]

MAX phases are constructed with a hexagonal lattice structure with a space group of $P6_3/mmc$, where 'A' atoms are sandwiched between two MX layers. Herein, it is vital to know the crystal structure of MAX phases to explore its distinctive properties. Fig. 3 depicts the crystal structure of MAX phases with n values 1 to 3.[22] In general, during the etching method, the 'A' atoms are wiped out from the MAX phase, resulting in a multi-layered MXene, which can be converted to a monolayer by ultrasonication. MXene has a general representation $M_{n+1}X_nT_x$, where T_x is the surface terminal groups including –OH, –F, or –O, from the etching process.[39] It is necessary to remember that the 2D MXene layers also have hexagonal structures inherited from the MAX phase. Due to such similarity with graphene, it has been named as MXene.[40]

2.1 Historical development of MXenes and related compounds

In the past two years, MXene-based research work has been remarkably expanded, and over 750 institutes from 50 countries are studying MXene and articles are frequently published in peer-reviewed journals.[38] In 2011, MXene was first synthesized by Gogotsi *et al.* at Drexel University, USA, without any previous prediction about its stability.[14] Till then, above 30 MXene compositions have been established experimentally, as shown in Fig. 4 (labeled in blue). Moreover, dozens of them have also been explored theoretically (labeled in grey in Fig. 4). An exclusive feature of MXenes was discovered when two transition metals were fused in the MXene structure. Also, during the formation of solid solutions such as $(Ti,Nb)CT_x$ (labelled in green in Fig. 4), transition metals can generate an orderly structure in a 2D, a single flake of MXene either by in-plane (for $n = 1$) arranged structure formation such as $(Mo_{2/3}Y_{1/3})_2CT_x$, or atomic sandwich formation of transition metal planes (for $n \geq 2$) such as $Mo_2TiC_2T_x$. Though ordered MXenes were fabricated in 2014, various new MXene subfamily compositions have been developed (labeled in red in Fig. 4).[41] Due to the rush in preparing new ordered MAX phases, around 30 new, 2D double transition metal, ordered MAX phases were reported since 2017, and their magnetic properties were also explored.[42–44] In Fig. 2(b), the transition metals labeled in blue strips are only reported for the synthesis of MAX phases. Since the last three years, around 100 plausible stoichiometry of MXenes and their precursors have been

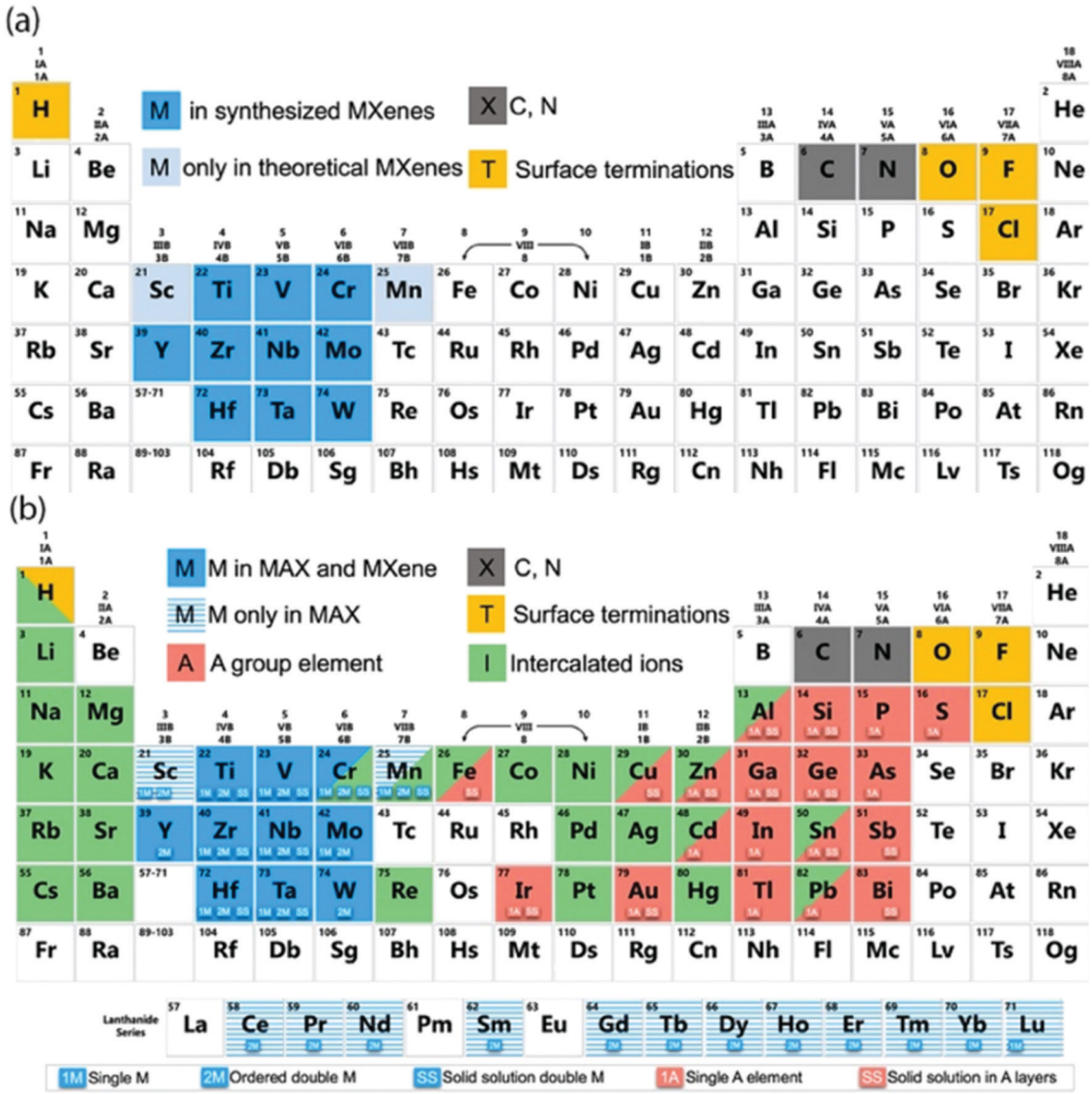

Fig. 2 In periodic table (a) elements utilized for MXene synthesis (experimentally and theoretically), (b) elements employed for MAX phase and MXene synthesis with different variations. Reused with consent from ref. 38. Copyright (2019) American Chemical Society.

established by computational studies.[44–48] The preparation of solid solution on M or/and X, provides further opportunity to fabricate a huge number of non-stoichiometric MXenes and accurately tune the features by mixing appropriate transition metals or even developing carbonitrides.

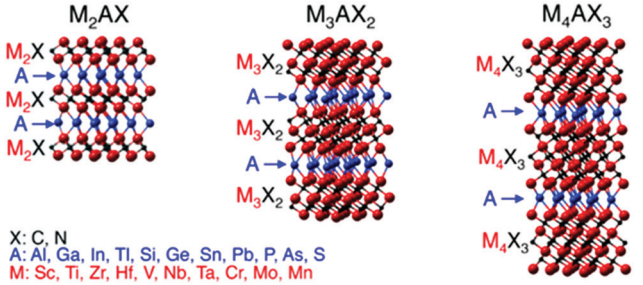

Fig. 3 Crystal structures of M_2AX, M_3AX_2 and M_4AX_3, Reused with consent from ref. 22.

Another critical development observed in the past year is the fluoride-free fabrication of MXene. It is noteworthy that, in most of the initially reported fabrication processes, researchers employed fluoride-containing materials in both aqueous and molten salts for the synthesis of MXenes.[22] An electrochemical route for such fluoride-free synthesis of Ti_2CT_x MXene in dilute hydrochloric acid was reported.[49] On the other hand, Huang *et al.* utilized $ZnCl_2$ salt to manufacture new MAX phase and fluorine-free MXene in the year 2019.[50] This method remarkably widens the synthesis process of MXenes, and now researchers can avoid fluoride-containing hazardous chemicals for the fabrication of MXenes. To date, above 70% of the MXene related researches have been aimed at $Ti_3C_2T_x$, which is the foremost discovered MXene.[38]

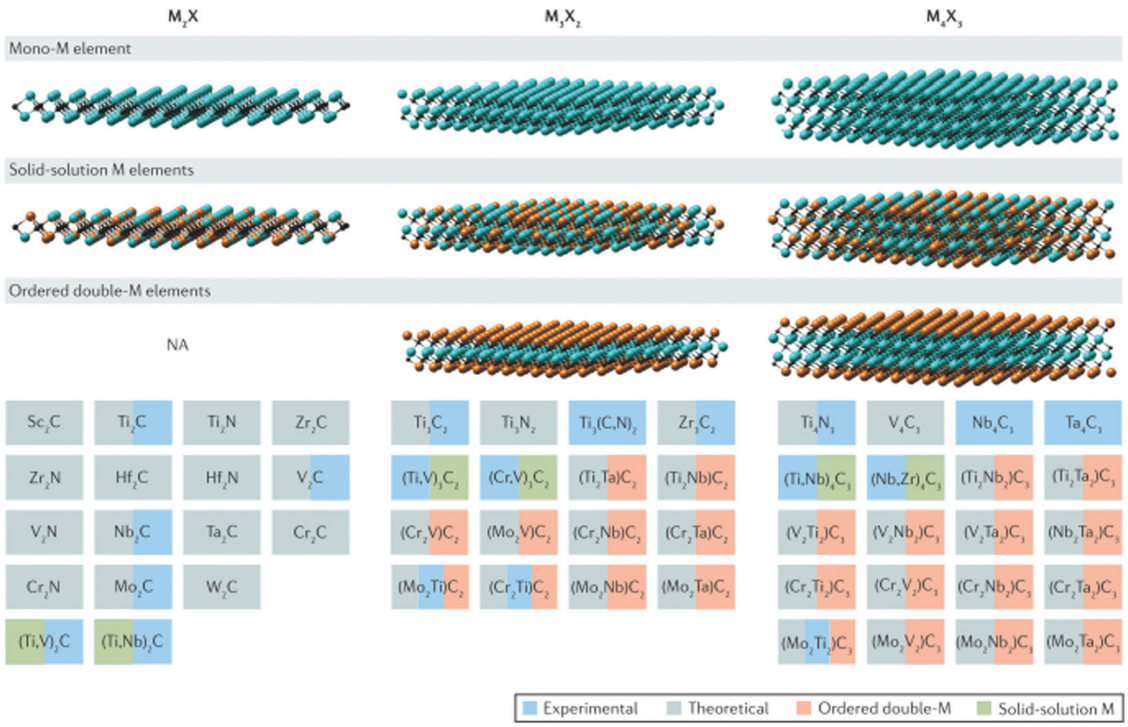

Fig. 4 Crystal structures with examples of three different MXenes: M_2X, M_3X_2 and M_4X_3 in three different conformations: mono M elements, solid solution M elements and ordered double-M elements. (NA – not applicable). Reused with permission from ref. 22.

2.2 Importance of MXenes

MXenes have a unique fusion of properties like high mechanical strength and excellent electrical conductivity of transition metal carbides, nitrides, or carbonitrides. Moreover, the surface functionalization makes MXene sheets hydrophilic and offers easy bond formation with different materials leading to the formation of a stable colloidal solution with water due to high negative zeta potential and capability of outstanding absorption of electromagnetic radiation leading to several applications for MXene. In Fig. 5, different applications of MXenes are represented as a pie chart.[38] The year of the first paper publication of each application is exhibited in the second circle of Fig. 5 to understand the recent trend of MXene research. The first reported use of MXene was in energy applications. Even a vast portion of MXene application is based on the energy storage field. However, for the past two years, the biomedical application of MXenes has become an attractive topic, including biosensors, theranostics, photothermal therapy of cancer, neural electrodes, and dialysis.[38,51] Another hottest topic of MXene research is electromagnetic applications such as printable antennas and electromagnetic interference shielding.[52] Like structural and electronics applications, most of the reported works are based on theoretical studies rather than a few experimental works. There are some predicted properties like topological insulators and ferromagnetism that are yet to be established experimentally.

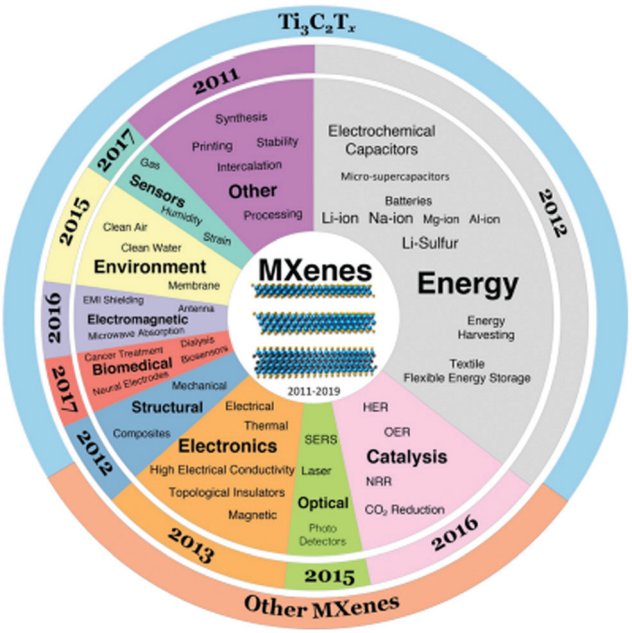

Fig. 5 Pie chart of the previously studied properties and applications of MXene (up to the year of 2017). Reused with permission from ref. 38. Copyright (2019) American Chemical Society.

2.3 Different types of MAX phases and MXenes

Since the discovery of MXene, over 70 MAX phases are established experimentally. Among them, V_2AlC, Ti_2AlC, Nb_2AlC, Ti_2AlN, Ti_3AlC_2, Zr_3AlC_2, Ti_3SiC_2, V_4AlC_3, Ti_4AlC_3, Ta_4AlC_3 and Nb_4AlC_3 have been already etched into V_2C, Ti_2C, Nb_2C, Ti_2N, Ti_3C_2, Zr_3C_2, V_4C_3, Ti_4C_3, Ta_4C_3 and Nb_4C_3 MXenes.[15,53–59] It is experimentally observed that the solution

of two transition metals (M′ and M″) or 'A' components (A′ and A″) or 'X' elements (C and N) leads to the generation of MAX phase alloys and subsequently the formation of different MXene alloys. In this context, it is necessary to mention that the $(Ti_{0.5}Nb_{0.5})_2C$, TiNbC, Ti_3CN, $(V_{0.5}Cr_{0.5})_3C_2$, $(Nb_{0.8}Zr_{0.2})_4C_3$, and $(Nb_{0.8}Ti_{0.2})_4C_3$ alloy MXenes have already been developed experimentally.[15,60] It has recently been observed that, by choosing proper stoichiometry of M, A, and X elements, two kinds of ordered MAX phases consisting of double transition metals can be prepared, known as iMAX and oMAX phases. The iMAX phases $(M'_{2/3}M''_{1/3})_2AX$, consist of in-plane ordered double transition metals. In contrast to the oMAX phases and conventional MAX phases, iMAX phases consist of both M′ and M″ in every layer of transition metals, as shown in Fig. 6(a–c).[40] After exfoliation of iMAX phases, the derived MXenes are also called iMXenes, which also consist of two different transition metals in each layer of transition metals (Fig. 6(f)). Among the experimentally synthesized phases, $(M'_{2/3}M''_{1/3})_2AX$ (where, M′ = Mo, Cr, W; M″ = Y, Sc), and $(M'_{2/3}Zr_{1/3})_2AlC$ (where, M′ = Cr, V) have been already exfoliated.[61,62]

Conversely, oMAX phases ($M'_2M''_2AX_3$ and $M'_2M''AX_2$) are consisting of ordered out-of-plane double transition metals. Fig. 6(b) and (e) show the lattice configuration of $M'_2M''AX_2$ and its corresponding MXene $M'_2M''X_2$ and MXenes consisting of the transition metal M′ in the outer layer and M″ in the inner layer.[40] Among the experimentally prepared oMAX phases, Cr_2TiAlC_2, Mo_2TiAlC_2, Mo_2ScAlC_2 and $Mo_2Ti_2AlC_3$ have already been exfoliated into Cr_2TiC_2, Mo_2TiC_2, Mo_2ScC_2 and $Mo_2Ti_2C_3$ MXenes.[41,63,64]

2.4 Techniques for MXenes synthesis

The bond strength mainly differentiates the M–X and M–A bonds. In fact, the M–X bond is stronger than the M–A bond.[65] Thus, the synthesis process of MXenes is based on the removal of weakly bonded 'A' atom layers. Due to this elimination of 'A' layers from MAX phases, this category of 2D carbides, nitrides, and carbonitrides are called MXenes. The pioneering synthesis process used hydrofluoric acid (HF, aq.) to etch $M_{n+1}AX_n$ (MAX phase) under constant agitation, and the 'A' atoms are replaced by surface terminal groups fluorine (–F), hydroxyl (–OH), oxygen (–O) as depicted in following equations,[15]

$$M_{n+1}AX_n + 3HF = AF_3 + 3/2H_2 + M_{n+1}X_n \quad (1)$$

$$M_{n+1}X_n + 2H_2O = M_{n+1}X_n(OH)_2 + H_2 \quad (2)$$

$$M_{n+1}X_n + 2HF = M_{n+1}X_n(F)_2 + H_2 \quad (3)$$

Herein, eqn (1) shows the removal of 'A' atoms, and eqn (2) and (3) represent the surface terminations with hydroxyl and fluorine, respectively. Later, the presence of oxygen functionalities was also confirmed for MXene.[66] Precisely, the M–A bonds are replaced by M–OH, M–F, and M–O bonds, and the synthesized MXene consist of multilayered sheets, weakly stacked by the van

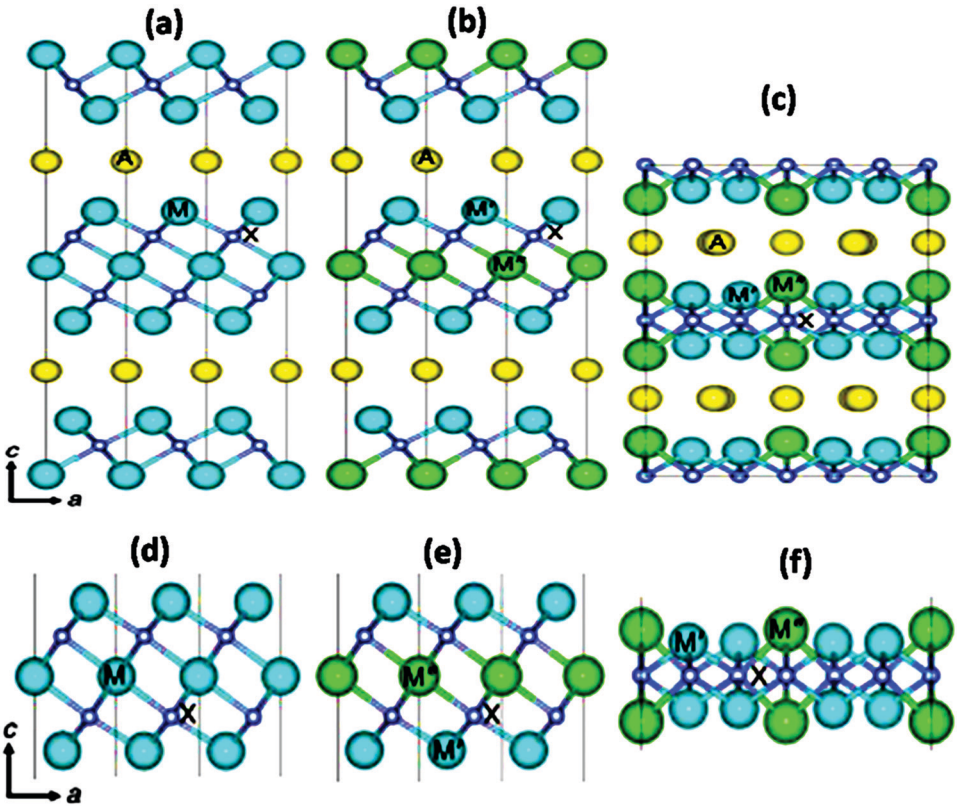

Fig. 6 Crystal structures of (a) M_3AX_2, (b) ordered out of plane double transition metal $M'_2M''AX_2$, (c) double transition metal in the plane $(M'_{2/3}M''_{1/3})_2AX$, (d) M_3X_2, (e) ordered out of plane double transition metal $M'_2M''X_2$ and (f) double transition metal in the plane $(M'_{2/3}M''_{1/3})_2X$. Solid lines designate the boundary of unit cells. Reused with permission from ref. 40.

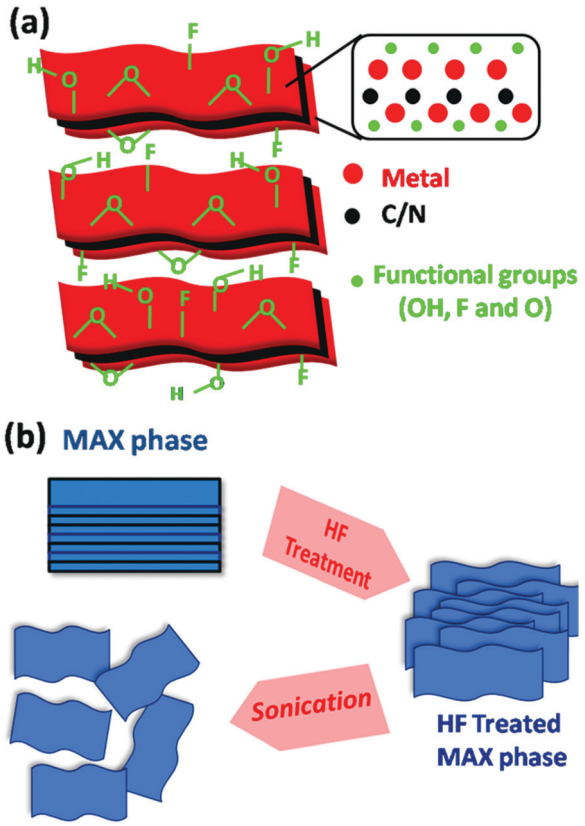

Fig. 7 (a) Surface functionalized MXene and (b) synthesis of MXene from MAX phase.

der Waals force of attraction and can be delaminated into single sheets through ultrasonication,[67,68] as shown in Fig. 7(b). According to the experimental observations, with the rising atomic number of M, stronger etching conditions and longer time are required due to the strength of the M–Al bond.[39] The XRD patterns before and after the etching of Ti_3AlC_2 with HF are exhibited in Fig. 8(a).

After exfoliation and etching, the terminated MXene has higher thermodynamic stability than its pristine counterpart, and these functional groups mostly affect the physicochemical characteristics of MXene.[69,70] In recent years, another alternative route for MXene synthesis has also been reported, in which HF is formed *in situ* by using LiF, NaF, or KF along with HCl.[36] In this method, the MAX phase is mixed in the solution of fluoride salt and HCl, which leads to the formation of a clay-like product after repeated washing. Finally, this clay-like product can be converted into desired morphologies using different post-processing methods. This method also indicates that fluoride formation is vital for the synthesis of MXene. During fluoride salts' reaction with HCl, the metal ions (Li^+, Na^+ or K^+) get inserted between the MXene layers and therefore enhance the interlayer distance. This type of metal ion intercalation is not possible when HF is directly used to prepare MXene. Hope *et al.* observed that the LiF–HCl route reduces the defect content of MXene.[66] Changing the molar ratio from 1.0 Ti_3AlC_2: 5.0 LiF: 11.7 HCl to 1.0 Ti_3AlC_2: 7.5 LiF: 23.4 HCl leads to a lesser toxic pathway (known as minimally intensive layer delamination (MILD) process) that was effectively employed for the synthesis of $Ti_3C_2T_x$ and Ti_3CNT_x.[71,72] Additionally, ammonium fluoride (NH_4F) and ammonium hydrogen bifluoride (NH_4HF_2) have also been efficiently utilized for the fabrication of $Ti_3C_2T_x$ from T_3AlC_2.[73]

MXene can also be synthesized from non-MAX phase materials. The first reported MXene, which is prepared from

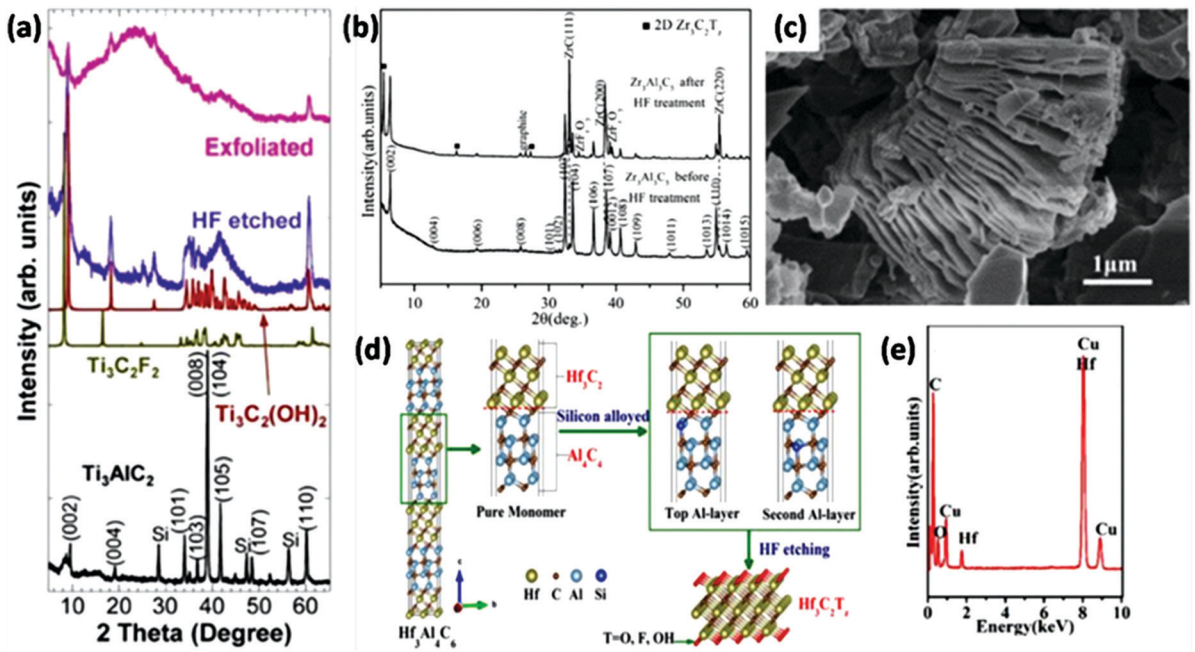

Fig. 8 XRD patterns before and after HF etching of (a) Ti_3AlC_2 and (b) $Zr_3Al_3C_5$, (c) An SEM image of $Zr_3Al_3C_5$ after HF etching, (d) diagrammatic representation of $Hf_3C_2T_x$ preparation method, (e) EDS analysis of HF treated $Hf_3[Al(Si)]_4C_6$. (a) Reused with permission from ref.,14 (b and c) reused with permission from ref. 55 and (d and e) adapted with permission from ref. 75. Copyright (2017) American Chemical Society.

non-MAX phase precursor Mo_2Ga_2C by removing the Ga layer, is Mo_2CT_x.[74] Although having similarity with the MAX phase, this material has two 'A' atoms (Ga) layers between the carbide layers. Zhou *et al.* reported recent types of layered compounds $Zr_3Al_3C_5$ and $Hf_3[Al(Si)]_4C_6$, which can be used as the precursor for $Zr_3C_2T_x$ and $Hf_3C_2T_x$ MXenes by eliminating aluminum carbide (Al_3C_3) and $[Al(Si)C]_4$ rather than just A layers (Fig. 8b–e).[55,75]

Another possible method of MXene synthesis is a bottom-up synthesis process like chemical vapor deposition (CVD).[76] In 2015, ultrathin 2D orthorhombic α-Mo_2C crystals having lateral sizes up to 100 μm, were fabricated from methane on a bilayer substrate of a Cu foil kept on a Mo foil by CVD. MXenes prepared using this method are associated with large surface areas and fewer defects.

Currently, a solvothermal method was reported for the fabrication of Nb_2CT_x and $Ti_3C_2T_x$ with a five times larger surface area than that by the HF-method.[77] As HF and LiF–HCl methods are unsuccessful in synthesizing nitride-based MXene, MAX phase precursor was reacted with molten salt at high temperature to fabricate the first nitride-based MXene in 2016.[56] Then, a salt-template method was employed by reducing the oxide precursors in ammonia to prepare V_2NT_x and W_2NT_x.[78] Most recently, Yang *et al.* reported a fluoride-free electrochemical synthesis of Ti_3C_2 MXene using NH_4Cl and tetramethylammonium hydroxide (TMAOH).[79] Few newly synthesized MXenes are summarized in Table 1.

As multilayered MXene has 2 to 6 fold interlayer interaction, which is stronger than that of MoS_2 and graphite, typical mechanical exfoliation results in the low yield of single layers. Generally, multilayered MXene can be delaminated into single layers through intercalation with different polar organic molecules like urea, hydrazine, isopropylamine, dimethyl sulphoxide (DMSO), and bigger organic base molecules such as chlorine hydroxide, tetrabutylammonium hydroxide (TBAOH), *n*-butylamine.[22]

2.5 Structural features of MXenes

2.5.1 Structural property of MXene sheets. Similar to the MAX phase precursors, 'X' atoms in MXene occupy an octahedral interstitial position, and 'M' atoms are in a closely packed structure. MXenes also has a hexagonal close-packed crystal structure. Fig. 9 shows three possible crystal structures of MXenes: BαCβAγB–BγAβCαB (M_4X_3–M_4X_3), BγAβC–CβAγB (M_3X_2–M_3X_2), and BγA–AγB (M_2X–M_2X), where capital Roman and Greek letters represent positions of M and X elements. As a whole, MXene is associated with a hexagonal close-packed crystal structure. The arrangement of the 'M' atom changes from M_2X to M_3X_2 to M_4X_3. In M_3X_2 and M_4X_3, M atoms follow the ABCABC arrangement, which is a face-centered cubic stacking, whereas M atoms in M_2X follow the ABABAB arrangement, which is a hexagonal close-packed stacking.

As the fluoride-containing acidic solution is used for MXene synthesis, the MXene surface is functionalized with –OH, –O, and –F groups. However, the most stable and effective surface termination of such functionalities has not been well-established yet, and it depends on different synthesis pathways and corresponding MAX phases. According to the theoretical study, in some MXenes such as M_2CT_x (where M = Ti, Zr and Hf),[89] $Ti_3C_2T_x$, $Ti_4N_3T_x$,[56] $Nb_4C_3T_x$,[90] the surface functionalization stability follows the trend –O > –F > –OH. The –OH functional group having the lowest stability is due to the substitution of

Table 1 Different synthesis conditions are summarised for the preparation of different MXenes from their precursor MAX phases

MXenes	MAX phase precursors	Etchants	Time (h)	Temperature (°C)	Ref.
Ti_2CT_x	Ti_2AlC	10% HF	10	RT	80
$Ti_3C_2T_x$	Ti_3AlC_2	50% HF	2	RT	14
Ti_2NT_x	Ti_2AlN	5% HF	24	RT	57
Ti_3CNT_x	Ti_3AlCN	30% HF	18	RT	15
V_2CT_x	V_2AlC	50% HF	90	RT	81
$(V_{0.5}Cr_{0.5})_3C_2T_x$	$(V_{0.5}Cr_{0.5})_3AlC_2$	50% HF	69	RT	15
$V_4C_3T_x$	V_4AlC_3	40% HF	165	RT	59
Nb_2AlC	Nb_2CT_x	50% HF	90	RT	53
$Nb_4C_3T_x$	Nb_4AlC_3	50% HF	96	RT	82
$Nb_{4/3}CT_x$	$(Nb_{2/3}Sc_{1/3})_2AlC$	48% HF	30	RT	83
$(Ti_{0.5}Nb_{0.5})_2CT_x$	$(Ti_{0.5}Nb_{0.5})_2AlC$	51% HF	28	RT	15
$Mo_2TiC_2T_x$	Mo_2TiAlC_2	50% HF	48	RT	41
$Mo_{4/3}CT_x$	$(Mo_{2/3}Y_{1/3})_2AlC$	48% HF	60	RT	61
$Zr_3C_2T_x$	$Zr_3Al_3C_5$	50% HF	60	RT	55
$W_{4/3}CT_x$	$(W_{2/3}Sc_{1/3})_2AlC$	48% HF	30	RT	84
$Hf_3C_2T_x$	$Hf_3[Al(Si)]_4C_6$	35% HF	60	RT	75
Ti_2CT_x	Ti_2AlC	0.9 M LiF + 6 M HCl	15	40	85
$Ti_3C_2T_x$	Ti_3AlC_2	1 M NH_4HF_2	12	80	86
Ti_3CNT_x	Ti_3AlCN	0.66 g LiF + 6 M HCl	12	35	71
$Ti_3C_2T_x$	Ti_3AlC_2	NH_3F	150	24	73
V_2CT_x	V_2AlC	2 g LiF + 40 M HCl	48	90	87
$Ti_4N_3T_x$	Ti_4AlN_3	59% KF + 29% LiF + 12% NaF	0.5	550	58
Mo_2CT_x	Mo_2Ga_2C	3 M LiF + 12 M HCl	384	35	88
$Cr_2TiC_2T_x$	Cr_2TiAlC_2	5 M LiF + 6 M HCl	42	55	42
$(Nb_{0.8}Zr_{0.2})_4C_3T_x$	$(Nb_{0.8}Zr_{0.2})_4AlC_3$	LiF + 12 M HCl	168	50	60

RT-Room temperature.

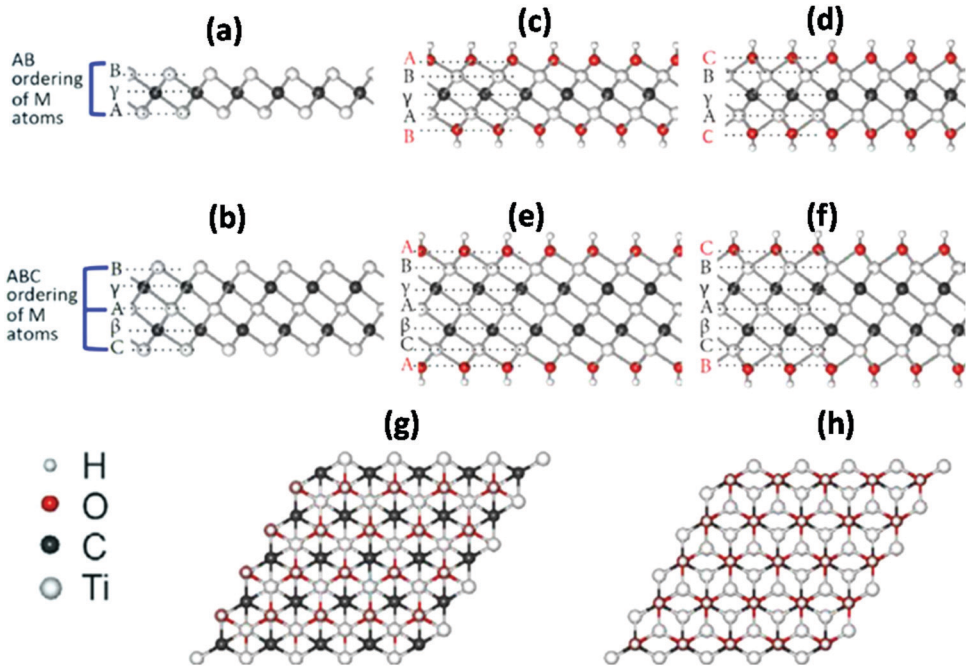

Fig. 9 Atomic structures of freestanding (a) Ti_2C, (b) Ti_3C_2, (c and d) $Ti_2C(OH)_2$ and (e and f) $Ti_3C_2(OH)_2$. (c, e and g) –OH groups remain at the hollow position between three neighbouring carbon atoms and (d, f and h) OH groups remain at the top position of the carbon atoms. (g and h) are top view. Reproduced with permission from ref. 22.

H-atoms by transition or alkali metals, and even at a higher temperature, it is converted to –O group.[91] According to the experimental report, for HF treatment, the functional group stability order is –F > –O > –OH, and for the thermal or LiF–HCl method, the stability order is –O > –F > –OH.[66,92] According to a recent study, the surface terminations of $Ti_3C_2T_x$ and V_2CT_x are randomly distributed on the MXene surface without forming any particular region for a specific functional group.[66] From the neutron scattering study, it was observed that the interaction between two MXene layers is due to the hydrogen bonding between F/O atoms of one sheet with OH of another sheet of $Ti_3C_2T_x$ and the van der Waals interaction between O and F atoms present in opposite sheets.[93]

2.5.2 Physical properties. Generally, bare MXenes like $Ti_{n+1}X_n$ are metallic in nature. But the metallic property decreases with increasing '*n*' value due to the addition of Ti–N bonds.[94] On the other hand, metallic property changes upon varying the 'X' atoms. For example, titanium carbide has lower metallic properties than titanium nitride because nitrogen is associated with more electrons than carbon. However, functionalized MXene sheets are metals or narrow band gap semiconductors, based on the type and inclination of the surface groups.[95,96] Some functionalized MXenes possessing band gaps are Zr_2CO_2, Sc_2CO_2, Ti_2CO_2, Hf_2CO_2, Sc_2CF_2, and $Sc_2C(OH)_2$. A comparative diagram of predicted band gaps of –O functionalized MXenes and the effect of the different termination groups on bandgap *via* DFT using HSE06 hybrid functional is shown in Fig. 10.[97]

In recent studies, it was observed that the bandgap of MXene also depends on the material doping[98] and modulation strain.[99] For example, the band gap of Sc_2CO_2 decreases from 2.0 to 1.8 eV after doping with niobium atoms. Moreover, under 3% uniaxial strain, the bandgap can be further reduced to 1.4 eV. Additionally, few MXenes are topological insulators such as $Sc_2C(OH)_2$, which can be transformed under an applied electric field from trivial to the topological insulator to metal.[100] Also, by changing the C/N ratio, MXene band gaps can be tuned, which was confirmed with $Sc_3(CN)F_2$ carbonitride.[101]

Additionally, the sample synthesis process also affects the electrical conductivity of MXenes. Usually, higher conductivity

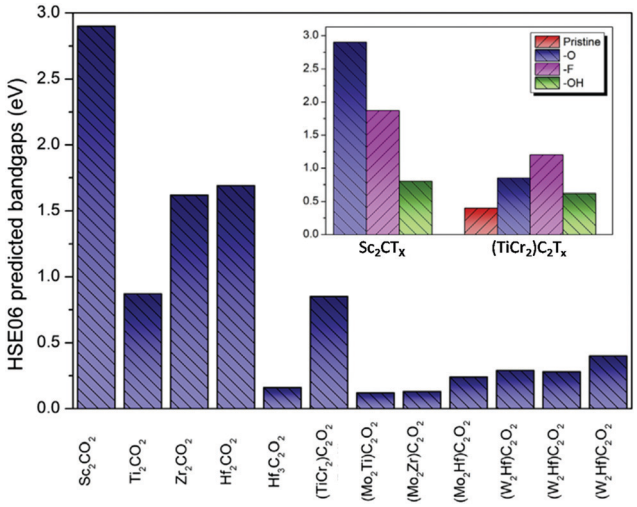

Fig. 10 A comparison of band gaps of oxygen functionalized MXenes. In the inset, the influence of different functional groups on specific compounds. Reused with permission from ref. 97.

is associated with large flake size and low defect concentration, which can be obtained with proper contact between each flake through coplanar alignment,[23] milder etching conditions and sonication-free delaminations,[102] and elimination of the intercalated species between the layers by drying.[103] For example, the conductivity of $Ti_3C_2T_x$ is less than 1000 S cm^{-1} for cold-pressed disks consisting of HF-etched highly defective products.[103] However, for spin-cast films[23] and milder etched, delaminated vacuum-filtered products,[102] the conductivity reaches 6500 and 4600 S cm^{-1}, respectively. Most interestingly, such electrical conductivity values of $Ti_3C_2T_x$ exceed graphene, too.[104]

While estimating the magnetic properties, ferromagnetism and anti-ferromagnetism have been estimated for a few functionalization-free MXenes.[16,97,105] Among all MXenes, only Cr_2NT_x and Cr_2CT_x have been estimated to have magnetic moments, despite having surface functionalization.[16,106] Functionalized Cr-MXenes were assumed to be ferromagnetic; on the other hand, Cr_2NT_x and Cr_2CT_x were predicted to be anti-ferromagnetic. However, their magnetic properties are not precise and yet to be characterized.

In general, thin films of MXene and hybrid composites are transparent. More specifically, per nanometer thickness, Ti_3C_2 MXene transmits >97% of visible light[23] (Fig. 11(e and f)), and the optoelectronic characteristics can be monitored by electrochemical or chemical cation intercalation.

Applying the theoretical calculations, the mechanical properties of MXene were investigated considering its composition, layer thickness, and surface functionalization. Fig. 11a and b shows in-plane stiffness and out-of-plane rigidity of different MXenes with different surface terminations describing their flexibility and elasticity.[107] The flexibility of $Ti_3C_2T_x$ MXene paper was also demonstrated by folding in the shape of the airplane (Fig. 11c). Fig. 11d shows a cylinder of $Ti_3C_2T_x$ paper with thickness 5 μm, which is capable of supporting ~4000 times its own weight.[22,108] Researchers further strengthened these MXene papers by incorporating 10 wt% polyvinyl alcohol (PVA) with $Ti_3C_2T_x$ to hold ~15000 times its weight.

2.5.3 Stability. Individual MXene sheets are not adequately durable in the atmosphere containing oxygen and water.[109] However, MXene flakes are relatively steady in dry air or degassed oxygen-free water. Additionally, the oxidation of colloidal MXene solution gets accelerated in the presence of light. Thus, it is suggested to store MXene in a dark, oxygen-free environment under refrigeration. Usually, the oxidation of MXene flakes initiated from the edges results in nanocrystals of metal oxide (for example, TiO_2) at the flake edges initially and then by nucleation and growth, they developed throughout the entire surface of MXene.[110–112]

The stability of MXene at high temperatures is based on the composition and environment. The phase stability of MXene can be predicted from the phase diagrams of non-stoichiometric transition metal carbides and nitrides.[113] Currently, it has been observed that in Ar atmosphere, $Ti_3C_2T_x$ is quite stable at 500 °C but, few TiO_2 nanocrystals generate on edges.[110] Under Ar atmosphere, Ti_3C_2 structure remains intact even at 1200 °C, and annealing defect generated. Under He atmosphere, a considerable weight loss of $Ti_3C_2T_x$ over 800 °C is observed from mass spectroscopy with temperature-programmed

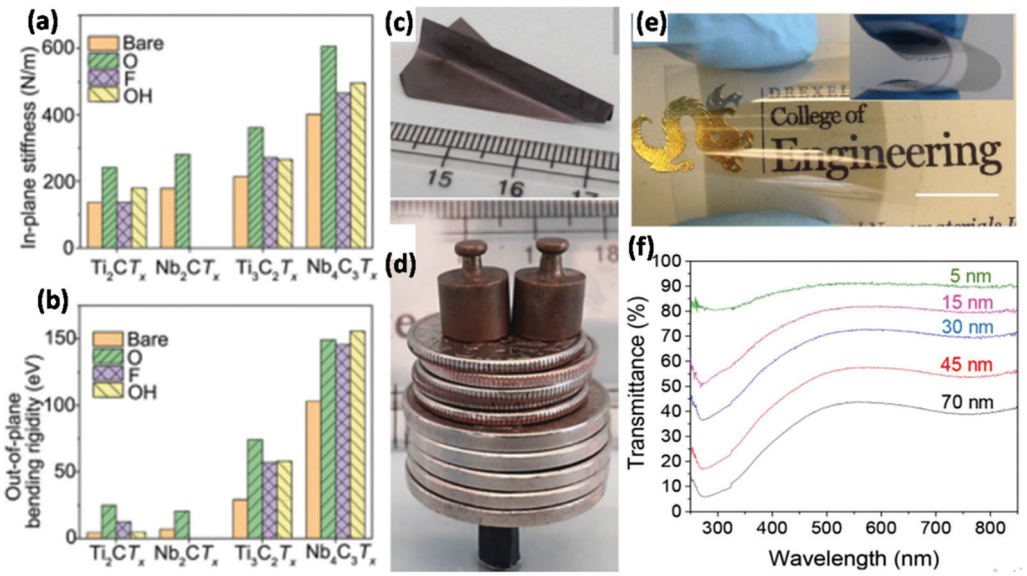

Fig. 11 (a) The in-plane stiffness and (b) the out-of-plane rigidity of different MXenes with different surface terminations, (c) a paper airplane made up by folding a $Ti_3C_2T_x$ film to illustrate its flexibility, (d) a 3.9 μm-thick strip of $Ti_3C_2T_x$/PVA composite (90 wt%) was folded into a hollow cylinder, which can tolerate about 15 000 times its own weight. The loads used were 2.0 g weights, dimes (2.27 g) and nickels (5 g), (e) photograph of $Ti_3C_2T_x$ film, spray-coated on a flexible polyester substrate and the inset exhibits the bending capacity of a $Ti_3C_2T_x$ film on the flexible substrate. The scale bar is 1 cm. (f) UV-visible spectra of spray-coated $Ti_3C_2T_x$ films with changing thicknesses. (a and b) reproduced with permission from ref.,107 (c and d) reused with permission from ref. 22 and (e and f) reproduced with permission from ref. 23.

desorption.[114] It was confirmed from another study that under a different inert atmosphere, Ti_2CT_x is stable at 250 °C.[112] In Ar or H_2 atmosphere, Ti_2CT_x was observed to be quite stable at 1100 °C.[115] In contrast to $Ti_3C_2T_x$ that converts to cubic carbide at high temperature, $Zr_3C_2T_x$ exhibited sufficient thermal stability and preserved its 2D nature even at 1000 °C temperature. The superior thermal stability of $Zr_3C_2T_x$ can be attributed to its structure, which is energetically more beneficial than bulk ZrC. On the other hand, $Ti_3C_2T_x$ is metastable compared with the bulk cubic TiC.

3. Applications of MXene materials

The versatility of MXene-based materials has gained huge attention in several fields of applications. Their tunable surface properties, electrical conductivity, and high Young's modulus are attractive to composites, and on the other hand, in ion intercalation, tunable bandgap, and chemical stability indicates energy storage and catalysis applications like fuel cell, supercapacitors, batteries, sensing, EMI shielding, OLED, and hydrogen storage.[22,39,116,117] Among these fields, MXenes have attracted maximum attention in supercapacitor and battery applications. In some of these applications, the performance of MXene is similar or even better than other available materials, such as energy storage systems[36,117] and EMI shielding in electronic components and aerospace.[101,118]

3.1 Supercapacitor

Supercapacitors (SCs) are an alternative to batteries as an energy storage device with a high charging/discharging rate and longer cyclic stability. As per the energy storage mechanism, SCs are categorized into two groups, one is electrical double-layer capacitors (EDLCs), and the other is pseudocapacitors. EDLCs store energy through the generation of an electrical double layer on the electrode surface. Pseudocapacitors reserve energy through redox reactions that take place at or near the electrode surface by specific materials. MXenes, having unique geometry and electronic properties have gained sufficient attention as electrode material for supercapacitors.[119,120]

3.1.1 Elemental MXene. Recently, Gogotsi *et al.* fabricated two different $Ti_3C_2T_x$ architectures, one is macroporous $Ti_3C_2T_x$, and the other is hydrogel $Ti_3C_2T_x$ for SC applications using H_2SO_4 electrolyte.[24] The schematic representation of MXene for electrochemical energy storage application is shown in Fig. 12a, in which a 2D structure with pre-intercalated water ensures quick ion transfer, a conducting transition metal carbide layer enables quick electron transport, and a transition metal oxide-type surface provides a redox activity. The hydrogel $Ti_3C_2T_x$ film (Fig. 12b), having a thickness of 13 μm, provided a volumetric capacitance of 1500 F cm^{-3} at 2 mV s^{-1} (Fig. 12d),

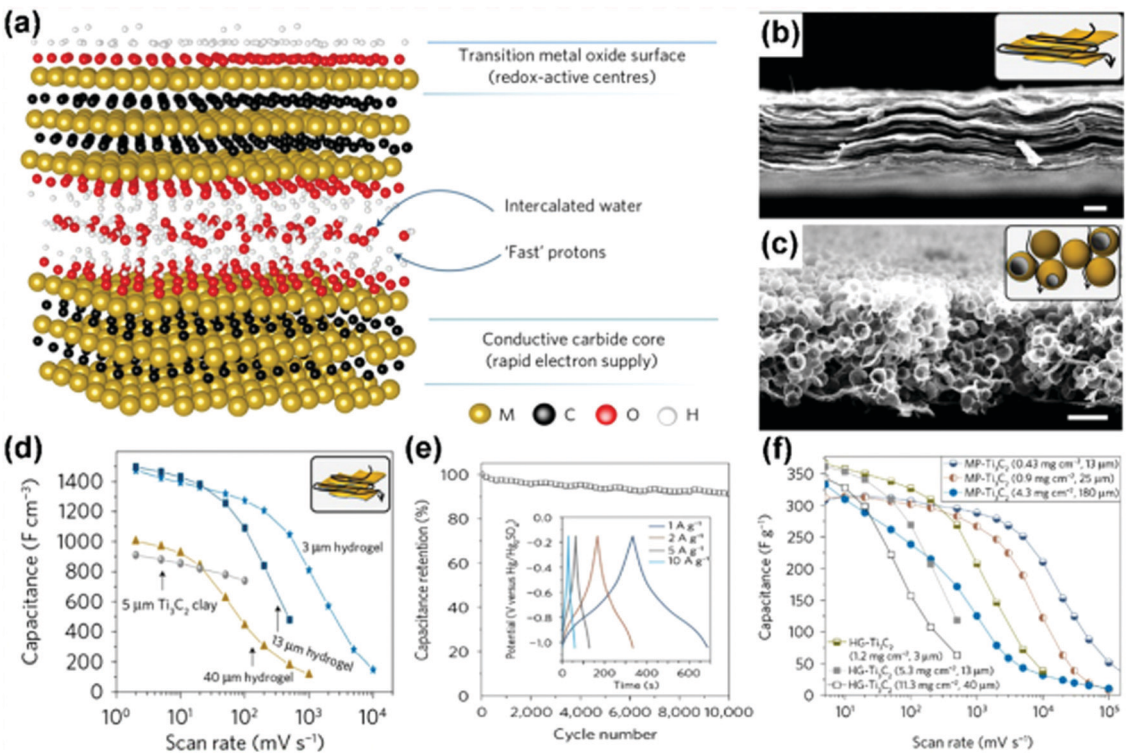

Fig. 12 (a) Diagrammatic representation of MXene configuration, (b) and (c) SEM images of $Ti_3C_2T_x$ hydrogel and macroporous $Ti_3C_2T_x$. Scale bars 5 μm, (d) volumetric capacitance of 3 μm-thick, 13 μm-thick and 40 μm-thick hydrogel film electrode in 3 M H_2SO_4 (mass loadings of 1.2 mg cm^{-2}, 5.3 mg cm^{-2} and 11.3 mg cm^{-2} respectively) comparing the efficiency with the reference of 5 μm-thick 'clay' electrode in 1 M H_2SO_4, (e) cycling behaviour of a 13 μm hydrogel film at 10 A g^{-1} and (f) rate capability of MXene films varying the synthesis processes and mass loadings. Reused with permission from ref. 24.

with outstanding capacitance retention of 90% after 10 000 cycles (Fig. 12e). Additionally, the macroporous $Ti_3C_2T_x$ film (Fig. 12c) displayed a gravimetric capacitance of 210 F g^{-1} at 10 V s^{-1} (Fig. 12f), surpassing the best-reported carbon material for SCs. It is also important to mention that the capacitive mechanism of MXene is dependent on the choice of the electrolyte. For instance, in acidic electrolytes such as H_2SO_4, MXene stores the charge *via* surface redox behaviour.[24] In organic or aqueous electrolytes, it stores charge *via* the cation (such as Na^+, K^+, Li^+, NH^{4+}, Al^{3+}, Mg^{2+}) intercalation reaction.[36,121,122]

A 2D V_2CT_x MXene was fabricated as an electrode material for a supercapacitor and its performance was studied in seawater electrolytes. The V_2CT_x MXene electrode delivered a good specific volumetric capacitance of 317.8 F cm^{-3} and gravimetric capacitance of 181.1 F g^{-1} with excellent capacitance retention of 89.1% after 5000 cycles.[123] The electrochemical behavior of the V_2CT_x MXene electrode is shown in Fig. 13.

2D tantalum carbide (Ta_4C_3) MXene was prepared by Syamsai *et al.*, which allowed the path for electrolyte ions inside the electrode leading to the enhancement in the electrochemical performance.[120] In 0.1 M H_2SO_4 electrolyte, the fabricated electrode exhibited a specific capacitance of 481 F g^{-1} at 5 mV s^{-1} with capacitance retention of 89% after 2000 cycles.

3.1.2 MXene composited with carbon materials. Though MXene is associated with several advantages, the self-restacking of MXene sheets limits its electrochemical utilization ratio.[124] To successfully prevent self-restacking and enhance the electrochemical performance, different materials such as carbonaceous materials, polymers and metal oxides have been used to form a hybrid composite with MXene.[125,126] Gogotsi *et al.* fabricated a flexible SC electrode with MXene/RGO composite in which nanosheets of RGO were inserted into MXene layers through electrostatic interaction.[125] The limitation of self-restacking was effectively prevented, leading to a higher number of electrochemical active positions. The flexible freestanding MXene/RGO-5 wt% electrode displayed a volumetric capacitance of 1040 F cm^{-3} at 2 mV s^{-1}. Additionally, in aqueous electrolytes, the assembled symmetric SC showed an outstanding energy density of 32.6 W h L^{-1}, and that was the largest reported value of MXene and carbon materials.

The electrochemical performance of Nb_2CT_x was studied for the first time in an aqueous electrolyte, and after incorporation of CNTs as conducting material, the rate performance of the composite electrode enhanced significantly.[24] The asymmetric supercapacitor fabricated with activated carbon as a positive electrode and Nb_2CT_x–CNT as a negative electrode delivered the highest energy and power density of 154.1 μW h cm^{-2} and 74843.1 μW cm^{-2}, respectively. In a three-electrode electrochemical setup, Nb_2CT_x–CNT provided a specific capacitance of 202 F g^{-1}, in an aqueous electrolyte, while in another study, $Ti_3C_2T_x$–CNT showed capacitance of 245 F cm^{-3}, in an organic electrolyte.[126] In a recent study, a stretchable supercapacitor electrode was fabricated with $Ti_3C_2T_x$-reduced graphene oxide

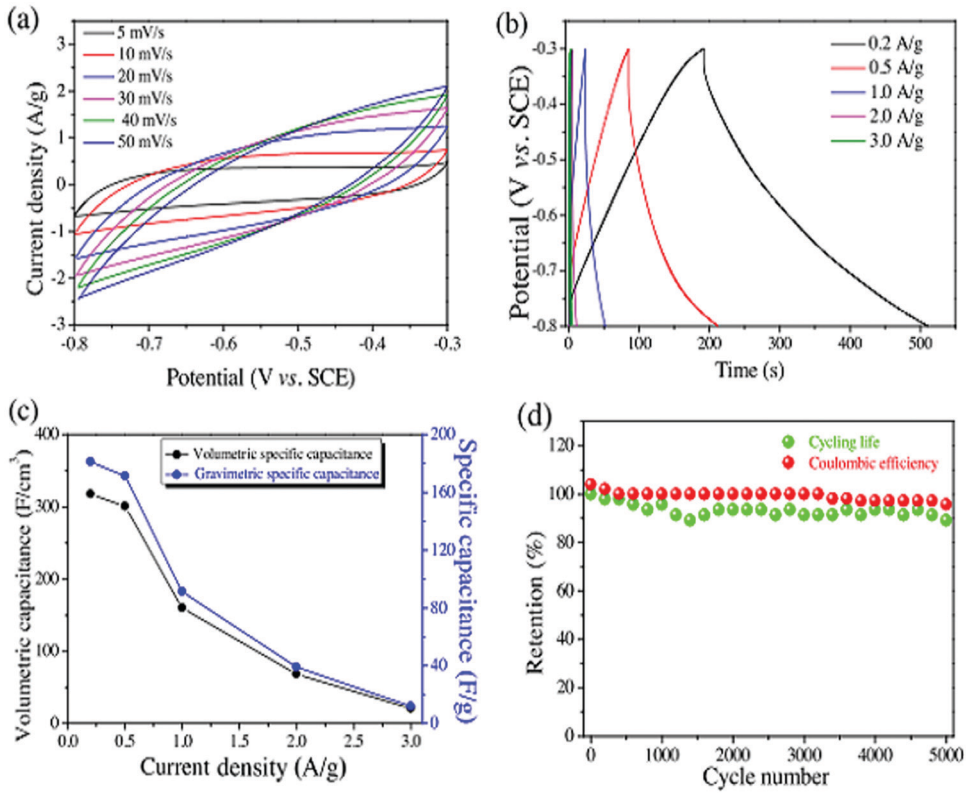

Fig. 13 Electrochemical performance of V_2CT_x electrode (a) cyclic voltammetry, (b) gravimetric charging–discharging, (c) a comparison of specific volumetric and gravimetric capacitance and (d) coulombic efficiency and cyclic stability at 2 A g^{-1}. Reproduced with permission from ref. 123.

nanocomposite and the assembled symmetric supercapacitor device delivered a specific capacitance of 18.6 mF cm^{-2} as well as up to 300% stretchability.[127]

3.1.3 MXene composited with polymers. To increase the efficiency of MXene, polymers, including polyaniline (PANI) or polypyrrole (PPy) have also been incorporated. A freestanding hybrid $Ti_3C_2T_x$/PANI electrode displayed an enhanced pseudocapacitive behaviour than pristine $Ti_3C_2T_x$ with a large specific capacitance of 503 F g^{-1}.[128] In another study, Wu *et al.* revealed that the insertion of PPy chains inside the Ti_3C_2 MXene layers increases interlayer spacing and facilitates the diffusion for electrolyte ions and the charge transfer, resulting in an enhancement in specific capacitance.[25] The electrochemical performance of a novel organ-like Ti_3C_2/PPy composite electrode with different mass ratios of Ti_3C_2 and PPy is illustrated in Fig. 14. The highest specific capacitance of 184.36 F g^{-1} was delivered by the nanocomposite electrode at a 2 mV s^{-1} scan rate with 83.33% retention of specific capacitance after 4000 cycles at 1 A g^{-1}.

3.1.4 MXene composited with metal oxides. The hybrid composites of MXene with mixed metal sulfide[26] and layered double hydroxide (LDH)[27] provided excellent performance as supercapacitor electrode materials. A homogeneous deposition of $NiCo_2S_4$ over the $Ti_3C_2T_x$ sheets on nickel foam was fabricated as a binder-free electrode material for a supercapacitor and delivered around six times enhancement of the specific capacity from 106.34 C g^{-1} to 596.69 C g^{-1} at 1 A g^{-1} than $NiCo_2S_4$ nanoflakes.[26] Fig. 15(a) shows the schematic diagram of the assembled asymmetric supercapacitor (ASC) device, and Fig. 15(b–e) shows the ASC cell lighting up a red LED. In another study, porous 3D NiFe–LDH/MXene electrode delivered enhanced specific capacitance of 720.2 F g^{-1} than NiFe–LDH nanosheets (465 F g^{-1}).[27] At different current densities, the specific capacitances of 60 mg loaded NiFe–LDH/MXene ASC device are exhibited in Fig. 15(f), and the digital photograph of powering up a green LED by the ASC device is shown in Fig. 15(g). A few applications of MXene-based materials for supercapacitor are summarized in Table 2.

3.2 Secondary batteries

3.2.1 Li-ion battery. Li-ion batteries (LIBs) have been extensively utilized in transportable electronic gadgets because of their large energy density and sufficient cyclic life. For advanced development in efficiency, it is crucial to introduce the latest and efficient electrode materials for LIBs.

3.2.1.1 Elemental MXene. After the discovery of MXene, it was first studied as an anode material in LIBs. For example, the theoretical capacity of Li intercalated bare Ti_3C_2 was predicted as 320 mA h g^{-1} by Xie *et al.*[138] But, the existence of –F or –OH surface terminations reduces the Li-ion storage capability. Tang *et al.* had shown the capacity for $Ti_3C_2(OH)_2$ was only 67 mA h g^{-1} and for $Ti_3C_2F_2$ was 130 mA h g^{-1}.[95] A novel, H_2O_2 assisted, oxidized V_2CT_x was studied as an anode material for Li-ion batteries, and the oxidized V_2CT_x displayed enhanced electrochemical behavior with 125 mA h g^{-1} at 1000 mA g^{-1}

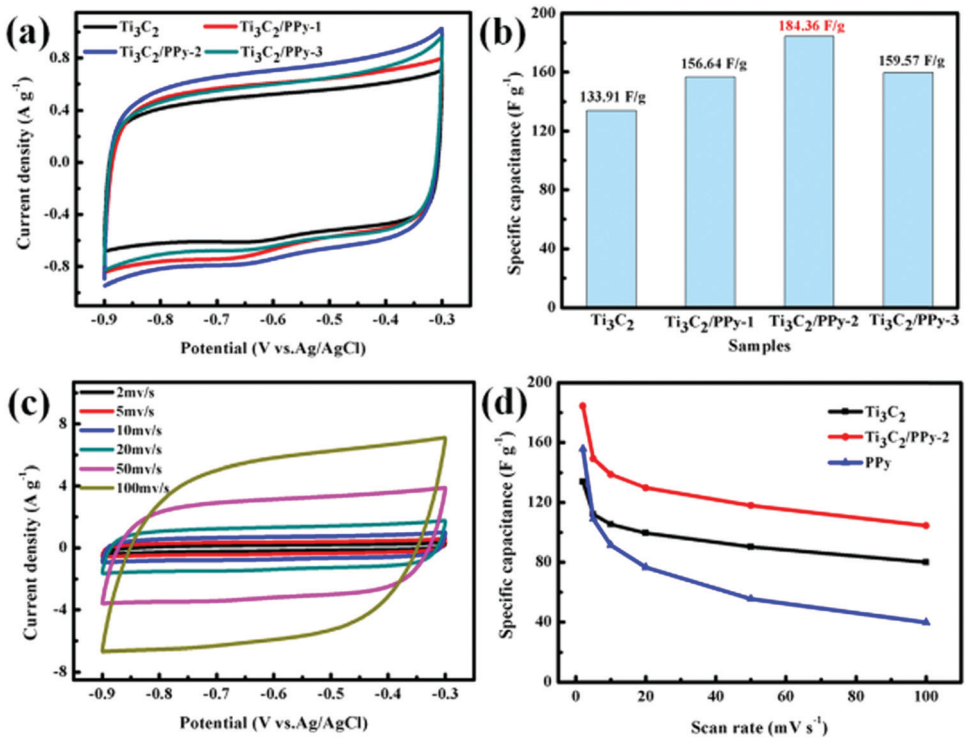

Fig. 14 (a) Cyclic voltammogram curves of Ti_3C_2 and Ti_3C_2/PPy composites were compared at 10 mV s^{-1} scan rate, (b) specific capacitance of Ti_3C_2 and Ti_3C_2/PPy composites were compared at 2 mV s^{-1} scan rate, (c) CV curves of Ti_3C_2/PPy-2 composite electrode with varying scan rates and (d) specific capacitance of Ti_3C_2, Ti_3C_2/PPy-2 and PPy electrode at scan rates from 2–100 mV s^{-1}. Reused with permission from ref. 25.

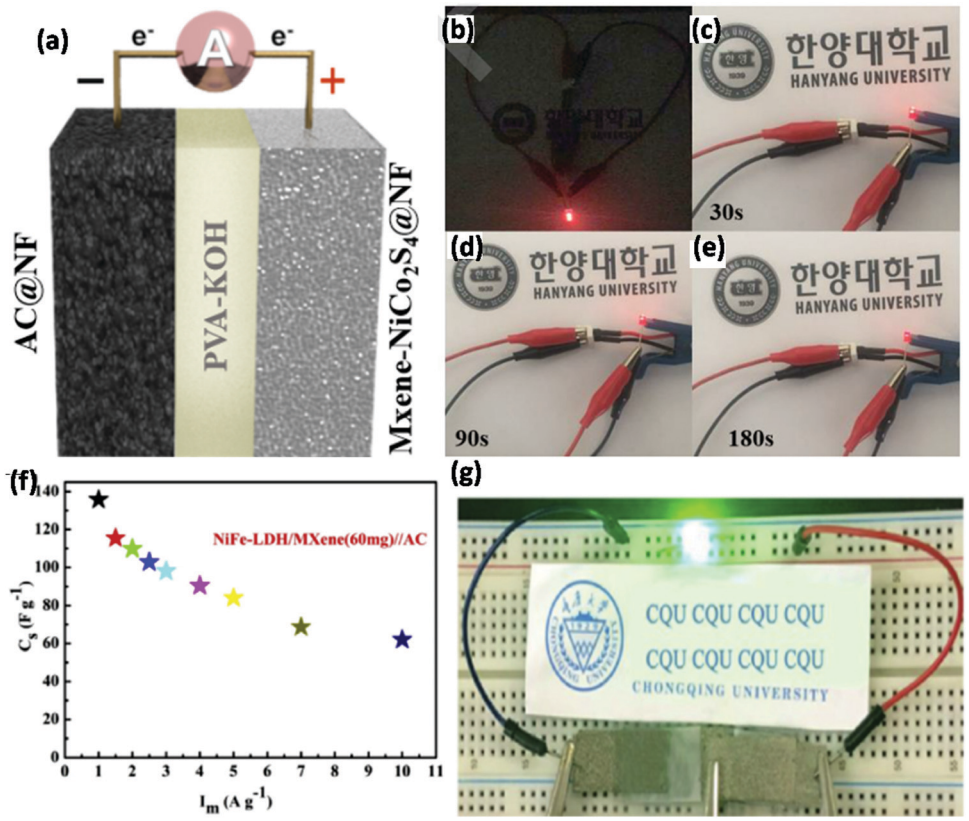

Fig. 15 Asymmetric device performance of $Ti_3C_2T_x$-$NiCo_2S_4$@NF (a) schematic representation of the assembled asymmetric device, (b–e) digital photograph of the cell lighting up a red LED. Asymmetric device performance of NiFe–LDH/MXene (f) at various current densities the specific capacitance of the assembled device and (g) photograph of lighting up a green LED by the device. (a–e) reused with permission from ref. 26 and (f and g) reused with permission from ref. 27.

after 1000 cycles and 318 mA h g^{-1} at 100 mA g^{-1} after 100 cycles with a superior rate performance as well as excellent cyclic stability.[139]

Other types of MXene materials, in addition to the most studied titanium carbides, have also shown promising performances in LIBs. Yu *et al.* used a complex MXene Ta_xC_y (x = 2 and y = 1, or x = 1 and y = 1–4) as an anode material in LIBs and also explored their stabilities and frameworks.[140] A new type of nitrogen-incorporated Nb_2CT_x MXene was prepared by Liu *et al.* as an efficient anode material for Li-ion batteries through the hydrothermal treatment with urea (Fig. 16a), leading to the increment in the d-spacing in Nb_2CT_x MXene.[141] The N-doped Nb_2CT_x displayed excellent cyclic stability of 288 mA h g^{-1} at 0.5 C after 1500 cycles and a much higher reversible capacity of 360 mA h g^{-1} at 0.2 C than Nb_2CT_x without doping (Fig. 16b and c). Another type of MXene $Hf_3C_2T_x$ used for LIBs, which was fabricated from $Hf_3[Al(Si)]_4C_6$ showed an excellent reversible volumetric capacity of 1567 mA h cm^{-3} at 200 mA g^{-1} after 200 cycles.[75]

3.2.1.2 MXene composited with carbon materials. A systematic study of the electrochemical characteristics of Ti_2CT_x/graphene heterostructure using first-principles theory revealed that the incorporation of graphene eliminates the restacking problems of MXene as well as increases the Li adsorption capability, electrical conductivity and mechanical strength.[142] It was proposed that Ti_2CO_2/graphene composite could be the most favorable member with excellent performance for future MXene based materials. Later, Li *et al.* experimentally fabricated a 3D spring-roll like Ti_3C_2/carbon wrapped Fe_3O_4 hybrid composite for Li-ion batteries as the anode material to achieve a long cyclic performance of Fe_3O_4 and get rid of intrinsic limits.[143] The hybrid composite provided 997 mA h g^{-1} reversible capacity at 1 A g^{-1} after 2000 cycles and the capacity retention was 543 mA h g^{-1} at 5 A g^{-1}.

Currently, Wu *et al.* used an east carbon nanoplating method to fabricate MoS_2/Ti_3C_2–MXene@C composite and this nanocomposite exhibited an enhanced discharge capacity of 1750 mA h g^{-1} at 0.2 A g^{-1}.[144] The MoS_2/Ti_3C_2–MXene@C composite showed adequate rate performance and reversible capacity of 1200 mA h g^{-1} at 1 A g^{-1} after 700 cycles. To enhance the battery potential, Gogotsi *et al.* introduced $Ti_3C_2T_x$–CNT paper electrode as a cathode, dendrite-free Mg metal as an anode and a duel-salt electrolyte containing Mg^{2+} and Li^+.[145] This flexible $Ti_3C_2T_x$–CNT free-standing electrode displayed around 100 mA h g^{-1} at 0.1 C and around 50 mA h g^{-1} at 10 C.

3.2.1.3 MXene composited with metal or metal oxides. The fabrication of nanocomposites with interrelated characteristics

Table 2 Summary of the applications of MXene-based materials for supercapacitor applications

MXene-based electrode material	Specific capacitance	Electrolyte	Cyclic life	Device	Specific capacitance	Cyclic life	Energy density	Ref.
Nb_2CT_x/CNT	202 F g^{-1} at 2 mV s^{-1}	1 M H_2SO_4	80.3% after 5000 cycles	AC//Nb_2CT_x/CNT	462.0 mF cm^{-2} at 2 mV s^{-1}	73.3% after 2000 cycles	154.1 μW h cm^{-2}	124
Modified-$Ti_3C_2T_x$ by annealing	442 F g^{-1} at 0.5 A g^{-1}	1 M H_2SO_4	95.4% after 5000 cycles	Modified-$Ti_3C_2T_x$// Modified-$Ti_3C_2T_x$	223 F g^{-1} at 0.5 A g^{-1}		15.2 W h L^{-1}	119
V_4C_3	330 F g^{-1} at 5 mV s^{-1}	1 M H_2SO_4	90% after 3000 cycles					129
$Ti_3C_2T_x$-$NiCo_2S_4$@Nickel Foam	596.69 C g^{-1} at 1 A g^{-1}	3 M KOH	80.4% after 3000 cycles	$Ti_3C_2T_x$-$NiCo_2S_4$@NF// AC@NF			27.24 Wh kg^{-1}	26
$Ni_{1.5}Co_{1.5}S_4$@Ti_3C_2	166 mA h g^{-1} at 1 A g^{-1}	2 M KOH		$Ni_{1.5}Co_{1.5}S_4$@Ti_3C//AC	140 F g^{-1} at 1 A g^{-1}	90% after 8000 cycles	49.8 W h kg^{-1}	130
NiFe–LDH/MXene	720.2 F g^{-1} at 1 A g^{-1}	1 M KOH	86% after 1000 cycles	NiFe–LDH/MXene//AC	135.7 F g^{-1} at 1 A g^{-1}		42.4 W h kg^{-1}	27
$Ti_3C_2T_x$-RGO	140 F g^{-1} at 0.5 A g^{-1}	1 M H_2SO_4	-	$Ti_3C_2T_x$-RGO//$Ti_3C_2T_x$-RGO	29 F g^{-1} at 0.1 A g^{-1}	85% after 10000 cycles		127
Ti_3C_2/CuS	169.5 C g^{-1} at 1 A g^{-1}	1 M KOH	90.5% after 5000 cycles	Ti_3C_2/CuS//Ti_3C_2	49.3 F g^{-1} at 1 A g^{-1}	82.4% after 5000 cycles	15.4 W h kg^{-1}	131
MXene/CoS_2	1320 F g^{-1} at 1 A g^{-1}	2 M KOH	78.4% after 3000 cycles	MXene/CoS_2//rGO	80.6 F g^{-1} at 1 A g^{-1}	98% after 5000 cycles	28.8 W h kg^{-1}	132
rGO/$Ti_3C_2T_x$	405 F g^{-1}	60 M KOH		rGO/$Ti_3C_2T_x$//rGO/ $Ti_3C_2T_x$	148.5 F g^{-1} at 0.2 A g^{-1}	100% after 10000 cycles	63 mWh cm^{-3}	133
$Ti_3C_2T_x$/PANI	503 F g^{-1} at 2 mV s^{-1}	3 M H_2SO_4	98.3% after 10000 cycles	$Ti_3C_2T_x$/PANI//$Ti_3C_2T_x$/ PANI	575 F cm^{-3} at 2 mV s^{-1}		79.8 W h L^{-1}	128
$Ti_3C_2T_x$/CF	401 F g^{-1} at 10 mV s^{-1}	1 M H_2SO_4	98% after 20000 cycles	RuO_2/CF//$Ti_3C_2T_x$/CF	93 F g^{-1} at 10 mV s^{-1}	86% after 20000 cycles	29 W h kg^{-1}	134
N-$Ti_3C_2T_x$	192 F g^{-1} at 1 mV s^{-1}	1 M H_2SO_4	92% after 10000 cycles.					135
BiOCl/$Ti_3C_2T_x$	396.5 F cm^{-3} at 1 A g^{-1}	1 M KOH	95.2% after 5000 cycles.	BiOCl/$Ti_3C_2T_x$//BiOCl/ $Ti_3C_2T_x$	64.3 F cm^{-3} at 0.5 A g^{-1}	85% after 5000 cycles	15.2 W h kg^{-1}	136
NiO/derived-TiO_2/C-$Ti_3C_2T_x$	92.0 mA h cm^{-3} at 1 A g^{-1}	1 M KOH	70.4% after 5000 cycles	NiO/derived-TiO_2/C-$Ti_3C_2T_x$//$Ti_3C_2T_x$	4.7 mA h g^{-1} at 0.1 A g^{-1}	72.1% after 5000 cycles	1.04×10^{-2} W h cm^{-3}	137

AC-activated carbon; CNT-carbon nanotube; NF-nickel foam; rGO-reduced graphene oxide; PANI-polyaniline; CF-carbon fabric.

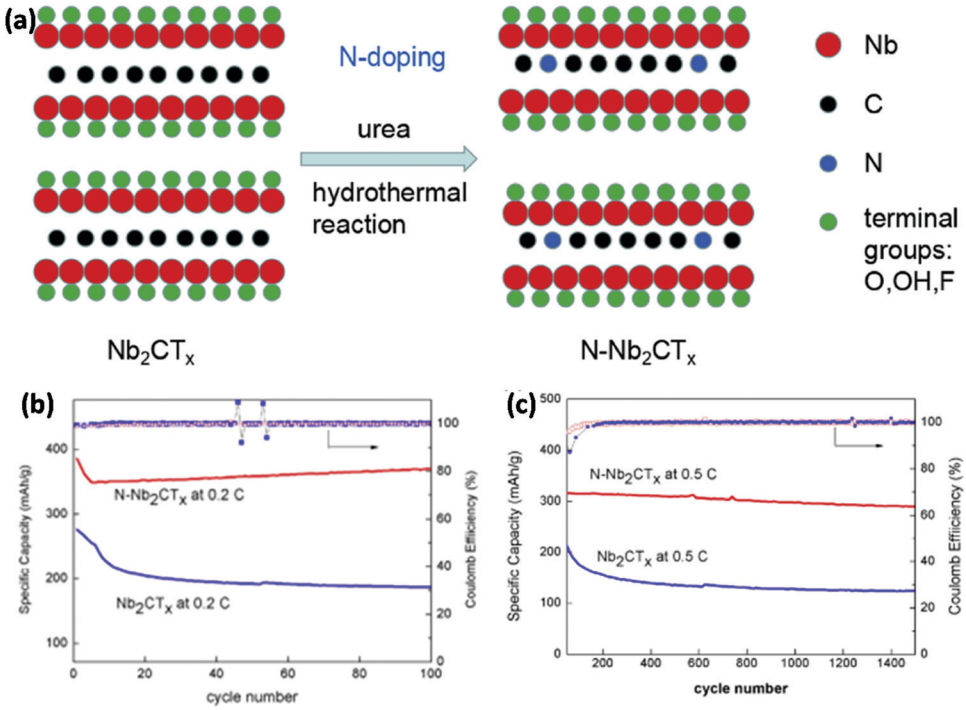

Fig. 16 (a) Diagrammatic representation of the synthesis of N-Nb_2CT_x by hydrothermal reaction, (b) cycling performance of Nb_2CT_x and N-Nb_2CT_x at 0.2 C up to 100 cycles and (c) cyclic stability of Nb_2CT_x and N-Nb_2CT_x electrodes at 0.5 C up to 1500 cycles. Reused with permission from ref. 141.

and well-fashioned conformation is a promising prospect to prepare multi-functional, efficient materials for LIBs. Sun *et al.* prepared SnO_x@Ti_3C_2 nanocomposite through the hydrothermal method in which ultrathin nanosheets of SnO_x were uniformly decorated over the Ti_3C_2 matrix leading to efficient lithium storage (Fig. 17a–c).[146] The metallic conductivity of Ti_3C_2, the huge capacity of SnO_x nanosheets, and strong interaction between Ti_3C_2 and SnO_x contributed to superb rate performance and prolonged cyclic life. The composite delivered a large reversible capacitance of 540 mA h g^{-1} at 500 mA g^{-1} current density after 1000 cycles (Fig. 17d and e).

The incorporation of metal oxides with MXene results in high capacity with improved electrochemical performance. Ahmed *et al.* synthesized SnO_2/$Ti_3C_2T_x$ composites for anode materials in LIBs *via* the atomic layer deposition method.[147] Further, the HfO_2 layer was coated on the surface of SnO_2 to enhance the electrochemical performance and the HfO_2 coated SnO_2/$Ti_3C_2T_x$ composites showed a discharge-specific capacity

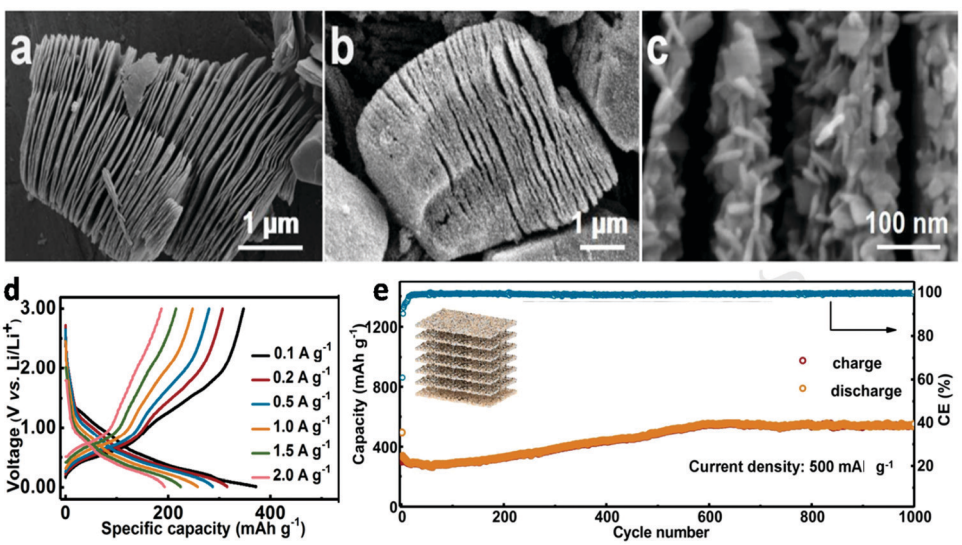

Fig. 17 FESEM images of (a) $Ti_3C_2T_x$, (b and c) SnO_x@Ti_3C_2, (d) charging–discharging curves of SnO_x@Ti_3C_2 anode at various current densities and (e) cyclic life and Coulombic efficiency (CE) of SnO_x@Ti_3C_2 at 500 mA g^{-1} current density. Reproduced with permission from ref. 146.

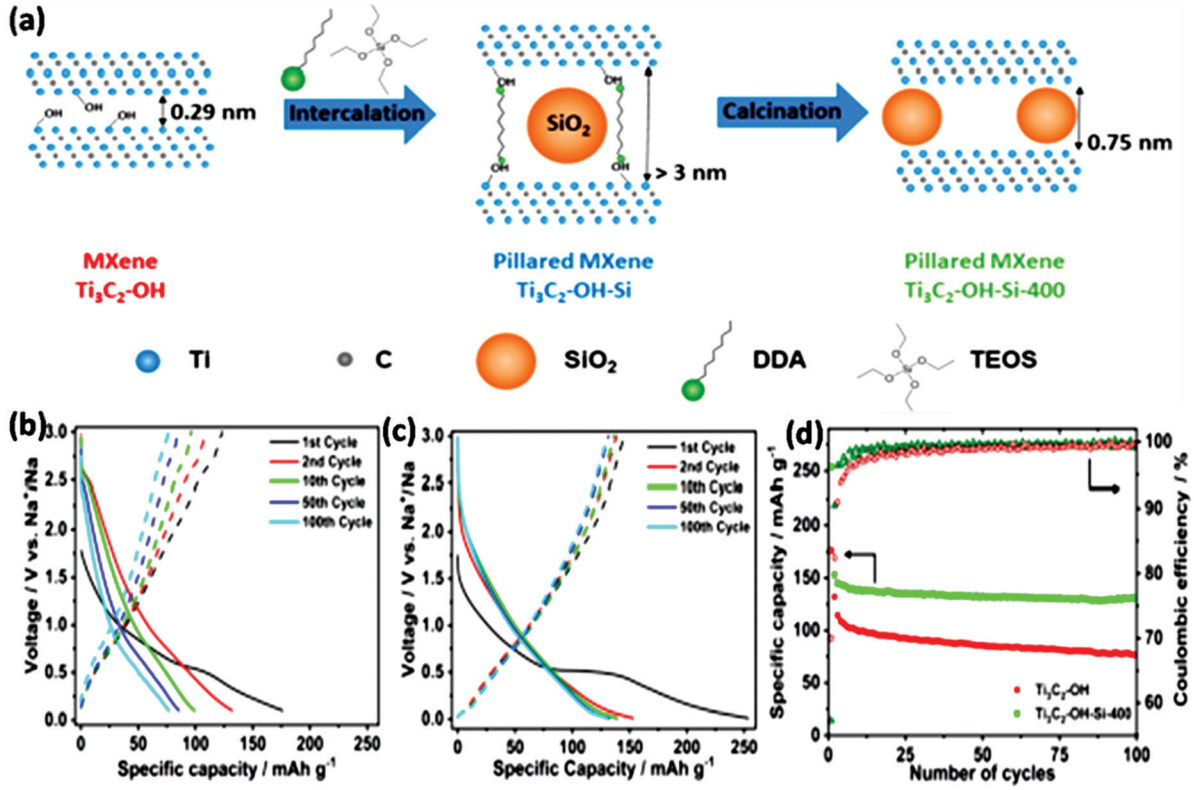

Fig. 18 (a) Diagrammatic representation of the pillaring method of MXene, galvanostatic charging–discharging curves of (b) Ti_3C_2–OH and (c) Ti_3C_2–OH–Si, discharge capacities and Coulombic efficiency of Ti_3C_2–OH and Ti_3C_2–OH–Si over 100 cycles. Reused with permission from ref. 149. Copyright (2020) American Chemical Society.

of 843 mA h g^{-1} at 500 mA g^{-1} over 50 cycles. A unique Fe_3O_4@Ti_3C_2 composite with well-anchored Fe_3O_4 nanoparticles inside Ti_3C_2 layers was fabricated by Xu *et al.* and the charge polarization due to covalent Ti-O–Fe bonds effectively enhanced the electron transfer as well as lithium storage mechanism.[148] The hybrid composite exhibited an ultrahigh capacity of 1172 mA h g^{-1} with 90% retention of capacity at 5 A g^{-1} after 1000 cycles.

3.2.2 Na-ion battery. Though LIBs have been extensively used in various areas, the limited supply of lithium has failed to meet the increasing requirement of the global market. So, the evolution of new categories of batteries has become mandatory and in this context, sodium-ion batteries (NIBs) are associated with comparable working principles with LIBs. Also, sodium resources are very abundant on the earth. Thus, NIBs could be a better option for large-scale energy storage for wind and solar energy. MXenes were also studied widely as an electrode material for NIBs due to their unique structure and properties.

3.2.2.1 Elemental MXene. A new amine-supported pillaring method was effectively demonstrated using silica-based pillars intercalating inside the Ti_3C_2 layers (Fig. 18a) for NIB applications, which eliminated the difficulty in ion accessibility inside the closely stacked multilayered MXene sheets.[149] In this process, the interlayer distance of MXene can be adjusted by opting for specific amine and temperature of calcination and there was a huge increment in the surface area of 235 m^2 g^{-1} that is six-fold higher than the unpillared one. The porous MXene material exhibited excellent rate capability, specific capacity and superb cyclic stability than the unpillared MXene with 98.5% capacity retention between 50th and 100th cycles (Fig. 18b–d).

The charge storage mechanism of V_2CT_x was studied by Bak *et al.* during Na^+ ion intercalation/deintercalation.[150] The XRD pattern of V_2CT_x showed the shifting of (002) diffraction peak from 9.3 to 8.1 during the initial sodiation process from open-circuit voltage to 0.1 V state correspondents to the increment of the c-lattice parameter from 19.0 to 21.8 Å. As well as Na^+ adsorption on the surface of V_2CT_x, leading to double-layer storage, energy stored *via* Na^+ intercalation in the interlayer spacing of V_2CT_x. This mechanism was similar to Ti_2CT_x and $Ti_3C_2T_x$ MXene materials.[39,151] Recently, Zhao *et al.* reported a template method to fabricate macroporous $Ti_3C_2T_x$ 3D film, which was used as a freestanding, flexible and highly conducting electrode.[152] This macroporous 3D MXene film showed a reversible capacity of 330 mA h g^{-1} at 0.25 C and after 1000 cycles, the $Ti_3C_2T_x$ 3D film exhibited a reversible capacity of 295 mA h g^{-1} at 2.5 C.

3.2.2.2 MXene-based composites. An easy solution-phase technique was employed to prepare Sb_2O_3/$Ti_3C_2T_x$ composites by Guo *et al.*, wherein, Sb_2O_3 nanoparticles were uniformly distributed over the 3D $Ti_3C_2T_x$ network.[153] The discharge capacity of this nanocomposite was 472 mA h g^{-1} after 100 cycles at 100 mA g^{-1} while used as the anode material for NIBs. The hybrid composite showed better rate performance than the

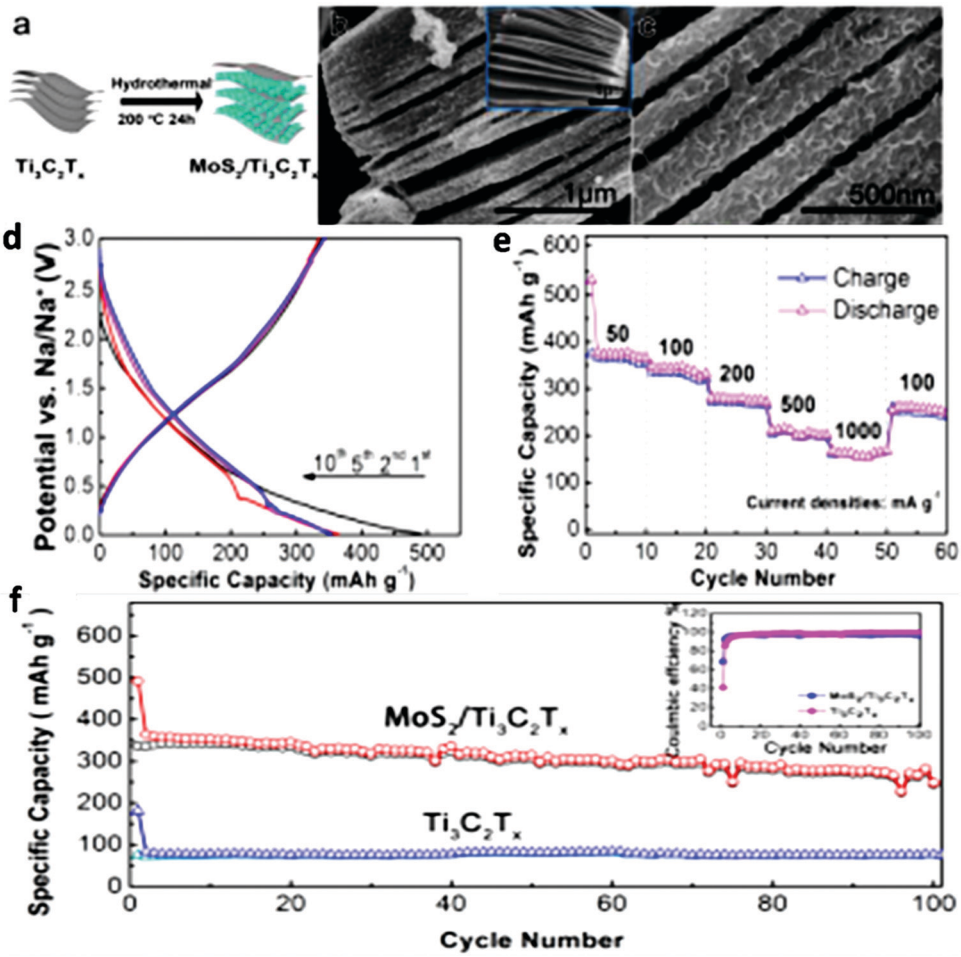

Fig. 19 (a) Schematic representation displaying the preparation of $MoS_2/Ti_3C_2T_x$ composite hydrothermally, (b and c) SEM images of $Ti_3C_2T_x$ (inset b) and $MoS_2/Ti_3C_2T_x$ composite, The electrochemical properties of the $MoS_2/Ti_3C_2T_x$ composite in a two-electrode sodium-ion cell with Na foil as the counter and reference electrode: (d) charge/discharge curve of $MoS_2/Ti_3C_2T_x$ composite at 100 mA g^{-1} in the voltage range of 0.01–3.0 V, (e) rate capability of $MoS_2/Ti_3C_2T_x$ composite and (f) cycling performance of pure $Ti_3C_2T_x$ and $MoS_2/Ti_3C_2T_x$ composite at 100 mA g^{-1}, the Coulombic efficiencies of $MoS_2/Ti_3C_2T_x$ composite and pure $Ti_3C_2T_x$ are also shown. Reused with permission from ref. 154.

pure Sb_2O_3 anode and that can be ascribed to the distinctive structure and synergistic effects of $Ti_3C_2T_x$ sheets and Sb_2O_3 nanoparticles. To enhance the ion accessibilities in MXene sheets, recently Wu *et al.* prepared $MoS_2/Ti_3C_2T_x$ hybrid composite *via* the hydrothermal method, in which MoS_2 nanosheets remain intercalated between $Ti_3C_2T_x$ layers (Fig. 19a–c).[154] This composite exhibited a discharge capacity of 250.9 mA h g^{-1} at 100 mA g^{-1} after 100 cycles with a reasonable rate performance of 162.7 mA h g^{-1} at 1 A g^{-1}, while used as an anode for NIBs (Fig. 19d–f).

A high-performance $MoSe_2/Ti_3C_2T_x$ heterostructure electrode as anode material for NIBs was fabricated through a facile hydrothermal reaction followed by annealing by Xu *et al.*[155] The van der Waals force of attraction between $MoSe_2$ and $Ti_3C_2T_x$ prevented the volume change that occurs during sodium ion intercalation/deintercalation and enhanced the reaction kinetics resulting in a potential sodium storage application. The fabricated cells delivered an impressive reversible capacity of 490 mA h g^{-1} at 1 A g^{-1} current density and 250 mA h g^{-1} at 10 A g^{-1} current density with 99.8% Coulombic efficiency.

3.2.3 Li–S battery. Li–S batteries have gained considerable attention because of their vast energy density, but some issues limit their practical applications. The discharge products Li_2S and 'S', both are insulators. Additionally, the resultant intermediate groups get dissolved in many organic electrolytes and are transferred to the anode by the shuttle effect and react to form Li_2S, causing the reduction of the Coulombic efficiency and cyclic life. The multilayered $Ti_3C_2T_x$ nanosheets were also utilized as a separator for Li–S batteries and $Ti_3C_2T_x$/CNT modified polypropylene (PP) separator maintained a capacity of 650 mA h g^{-1} at 1 C after 200 cycles.[28] Fig. 20(a and b) shows the capacities obtained during self-discharge of Li–S batteries with different separators after 120 h rest and cyclic stability after the rest time of 120 h. Fig. 20(c) shows the digital photograph of the assembled Li–S batteries using $Ti_3C_2T_x$/CNT modified PP (10%) powering the LEDs.

A unique strategy of coupling MXene-based cathode with an antifouling separator to increase the rate performance and sulfur loading of Li–S batteries through an easy electrostatic self-assembly procedure was proposed by Guo *et al.*[156] MXene

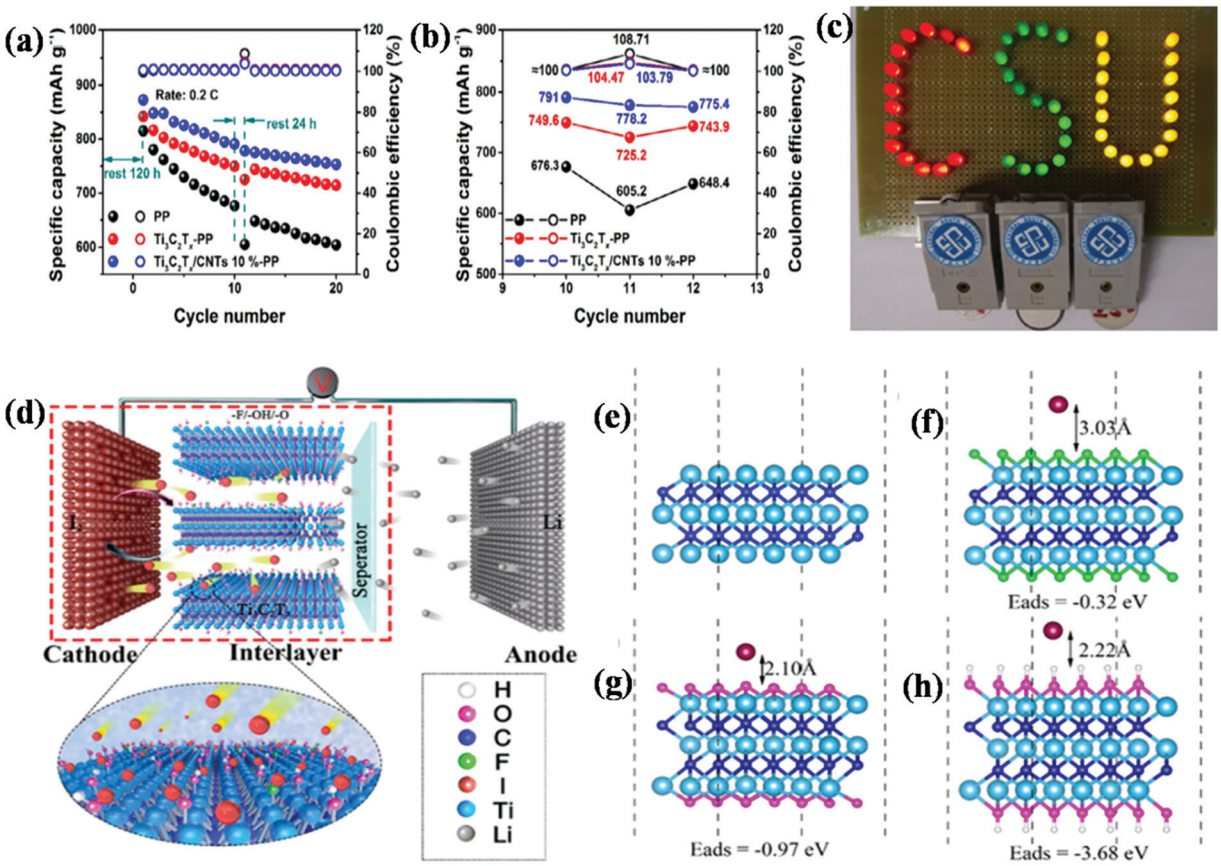

Fig. 20 (a) Self-discharge of Li–S batteries with different separators after 120 h rest, (b) cyclic stability after the rest time of 120 h, (c) photograph of Li–S battery using $Ti_3C_2T_x$/CNT modified PP (10%) powering up LEDs. (d) Schematic diagram of the reaction mechanism of lithium–iodine battery using MXene interface layer and molecular models of (e) Ti_3C_2, binding energies of iodine with (f) $Ti_3C_2F_x$, (g) $Ti_3C_2O_x$ and (h) $Ti_3C_2(OH)_x$. (a–c) reused with permission from ref. 28 and (d–h) reproduced with permission from ref. 29. Copyright (2020) American Chemical Society.

composite with CNT-polyethyleneimine delivered an ultrahigh capacity of 980 mA h g^{-1} at 5 mA cm^{-2} after 500 cycles. Liang *et al.* investigated the surface-responsive nature of Ti_2C, Ti_3C_2 and Ti_3CN with polysulfide species through DFT calculations and X-ray photoelectron spectroscopy (XPS) analysis.[157] For further improvement of conductivity and check the restacking of MXene sheets, CNTs were combined with MXenes and this S/CNT-MXene composite displayed excellent cyclic life up to 1200 cycles.

Table 3 Summary of the efficiency of MXene-based materials in battery applications

Material	Application	Current density	Reversible capacity//Cycle number	Ref.
Carbon coated Fe_3O_4/Ti_3C_2	Li-ion battery	1 A g^{-1}	997 mA h g^{-1}//2000	143
N-Nb_2CT_x	Li-ion battery	0.5 C	288 mA h g^{-1}//1500	141
Oxidized V_2CT_x	Li-ion battery	1000 mA g^{-1}	125 mA h g^{-1}//1000	139
Fe_3O_4@Ti_3C_2	Li-ion battery	1.6 mA cm^{-2}	592 mA h g^{-1}//500	148
SnO_x@Ti_3C_2	Li-ion battery	500 mA g^{-1}	~540 mA h g^{-1}//1000	146
$Hf_3C_2T_x$	Li-ion battery	200 mA g^{-1}	1567 mA h cm^{-3}//200	75
MoS_2/Ti_3C_2–MXene@C	Li-ion battery	1 A g^{-1}	1200 mA h g^{-1}//700	144
HfO_2 coated $SnO_2/Ti_3C_2T_x$	Li-ion battery	500 mA g^{-1}	843 mA h g^{-1}//50	147
Macroporous 3D $Ti_3C_2T_x$ film	Na-ion battery	0.25 C	330 mA h g^{-1}//1000	152
$Sb_2O_3/Ti_3C_2T_x$	Na-ion battery	100 mA g^{-1}	472 mA h g^{-1}//100	153
$MoS_2/Ti_3C_2T_x$	Na-ion battery	100 mA g^{-1}	250.9 mA h g^{-1}//100	154
$MoSe_2/Ti_3C_2T_x$	Na-ion battery	1 A g^{-1}	434 mA h g^{-1}//200	155
$Ti_3C_2T_x$–CNT modified PP	Li–S battery	1 C	640 mA h g^{-1}//200	28
MXene/CNT-polyethyleneimine	Li–S battery	5 mA cm^{-2}	980 mA h g^{-1}//500	156
S/CNT-MXene	Li–S battery	C/2	~450 mA h g^{-1}//1200	157
$Ti_3C_2T_x$/rGO/S	Li–S battery	0.5 C	878.4 mA h g^{-1}//300	158
N-Ti_3C_2@CNT/S	Li–S battery	1 C	775 mA h g^{-1}//1000	160

CNT-Carbon nanotube; PP-Polypropylene; rGO-Reduced graphene oxide.

Bao *et al.* fabricated reduced graphene oxide (rGO)/$Ti_3C_2T_x$ hybrid composite as a host material for Li–S batteries.[158] The $Ti_3C_2T_x$/rGO/S composite exhibited a large initial capacity of 1144 mA h g^{-1} and after 300 cycles the capacity retention was 878 mA h g^{-1} due to the effective interaction of sulfur and polysulphide with –OH decorated MXene phase. Recently, the capability of MXene as a host material for polysulphides in Li–S batteries was explored by DFT calculations and it was observed that both $Ti_3C_2O_2$ and Ti_2CO_2 single-layers could allow outstanding trapping with polysulphide species, preventing the shuttling effect.[159] In another study, N-Ti_3C_2@CNT microspheres were prepared as an efficient sulfur host, as well as allowed proper chemical immobilizations of polysulphides and capture them inside the porous microspheres.[160] The N-Ti_3C_2@CNT/S cathode exhibited an initial specific capacity of 927 mA h g^{-1} at 1 C and 775 mA h g^{-1} after 1000 cycles with only 0.016% degradation rate per cycle.

Recently, MXene was introduced as a potential material for lithium iodine batteries. A porous, 3D MXene foam was introduced as a cathode-electrolyte interface in lithium-iodine batteries, which provided long cyclic life and high rate performance.[29] Fig. 20d shows a schematic representation of the reaction mechanism of lithium-iodine batteries using the MXene interface layer and Fig. 20(e–h) shows the theoretical model of Ti_3C_2 and the binding energies of iodine with MXenes. The electrochemical performance of some MXene-based materials in battery applications are summarized in Table 3.

3.3 Electrocatalyst for water splitting

Electrolytic/solar water splitting is a green and sustainable energy field, which includes oxygen evolution reaction (OER) and hydrogen evolution reaction (HER). Generally, expensive noble metal electrocatalysts have been used for water splitting reactions. The 2D MXene materials having excellent efficiency and stability have become a promising alternative to costly noble metals.

Wang *et al.* fabricated $Ti_3C_2T_x$ MXene composited with TiO_2 and studied the effect of $Ti_3C_2T_x$ loading on the catalytic performance of the composite (shown in Fig. 21a).[161] The optimized $TiO_2/Ti_3C_2T_x$ composite with 5 wt% $Ti_3C_2T_x$ loading displayed an improvement of around 400% in photocatalytic HER reaction than that of pure TiO_2. The constructive decoration of TiO_2 over $Ti_3C_2T_x$ sheets leads to adequate light absorption, which accelerates the effective charge transport from TiO_2 to $Ti_3C_2T_x$, developing a Schottky barrier at the interface of TiO_2–$Ti_3C_2T_x$ (Fig. 21b) that indicates the superior photocatalytic activity. This research group also synthesized TiO_2/Ti_2CT_x and

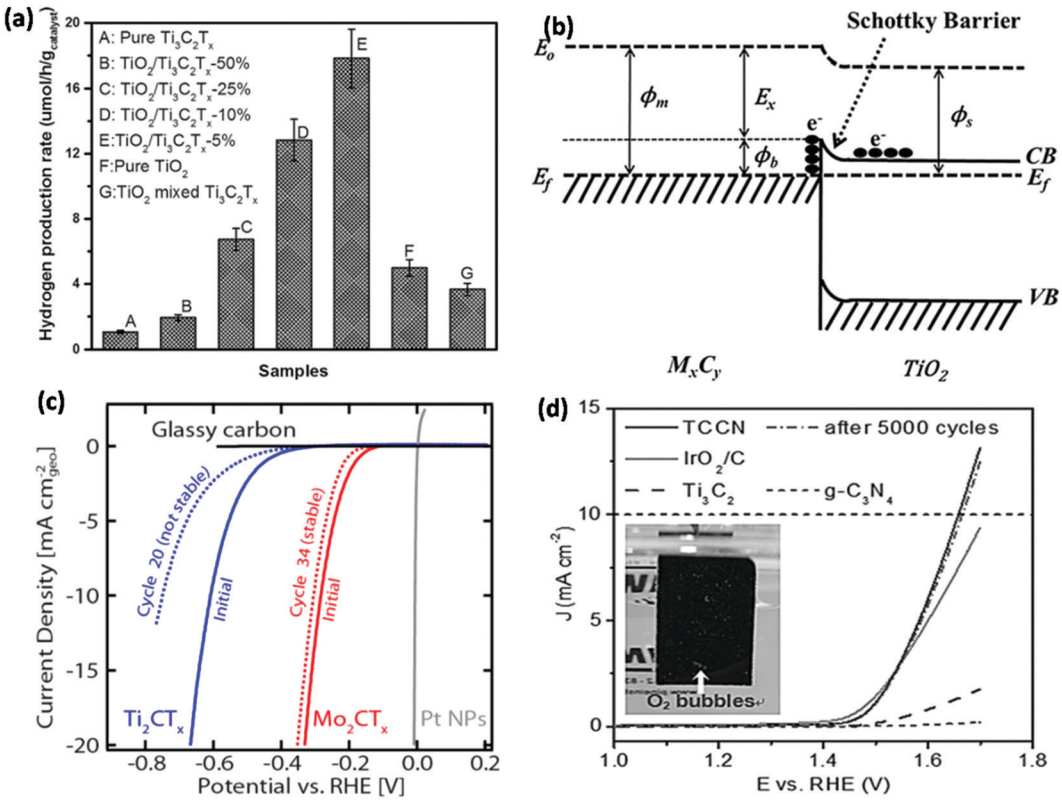

Fig. 21 (a) The effect of $Ti_3C_2T_x$ loading on photocatalytic hydrogen production rates. (b) A schematic diagram of the Schottky barrier formation at TiO_2–$Ti_3C_2T_x$ interface, (c) HER performance of MXene showing LSV of Mo_2CT_x and Ti_2CT_x with commercial Pt for comparison and (d) polarization curve, inset optical image of O_2 bubble generation on the electrode surface at 1.7 V using TCCN (Ti_3C_2 and g-C_3N_4 hybrid composite film) as OER electrode, dotted lines are polarization curve of samples after 5000 cycles at 100 mV s^{-1} scan rate. (a and b) Reused with permission from ref,161 (c) reused with permission from ref. 35 (Copyright (2016) American Chemical Society) and (d) reused with permission from ref. 21.

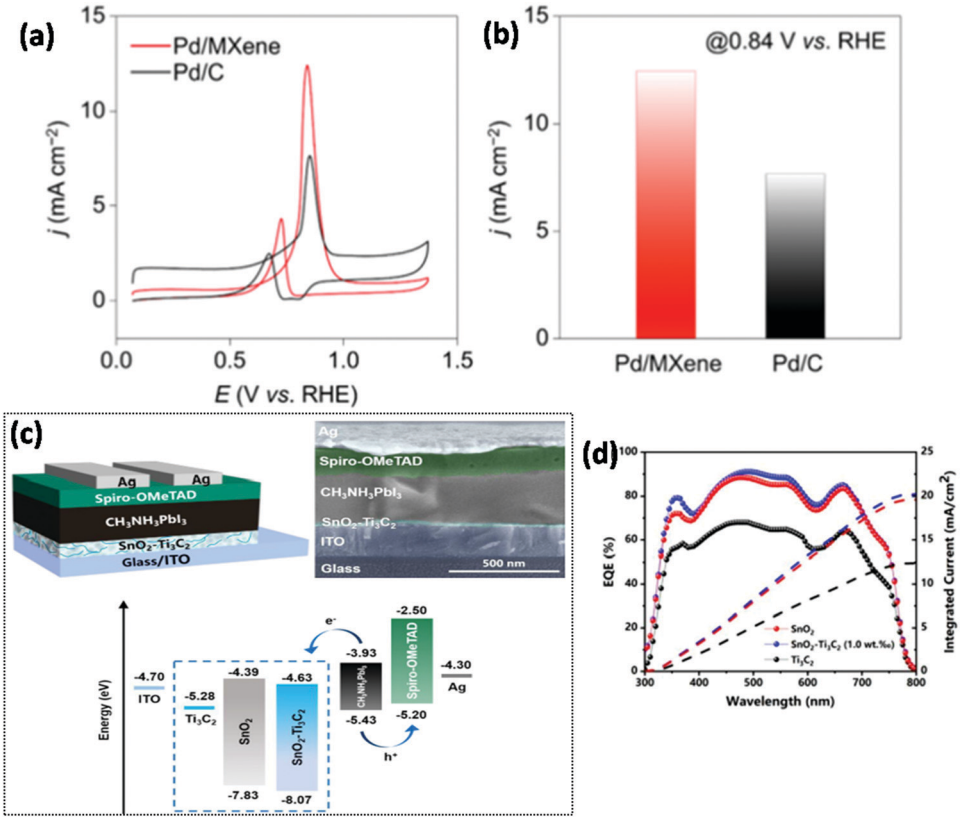

Fig. 22 Fuel cell performance (a) CV plots of Pd/MXene and Pd/C in 1 M KOH and 1 M methanol solution mixture and (b) comparison of current densities of Pd/MXene and Pd/C at 0.84 V vs RHE. (c) Schematic diagram and SEM image of cross-sectional PSC device assembly and energy diagram of individual PSC layers, (d) external quantum efficiency (EQE) and integrated current of the fabricated PSC device with SnO_2, SnO_2–Ti_3C_2 (1.0 wt%) and Ti_3C_2. (a and b) redrawn with permission from ref. 162 (Copyright (2020) American Chemical Society.) and (c and d) reused with permission from ref. 30.

TiO_2/Nb_2CT_x composite with 5 wt% MXene packing and TiO_2/Nb_2CT_x exhibited the best HER performance.

A combination of theoretical and experimental investigation of Mo_2CT_x and Ti_2CT_x as electrocatalysts for HER was reported by Seh *et al.*[35] From the computational study, they confirmed that Mo_2CT_x is a better HER catalyst than Ti_2CT_x because of the catalytically active basal planes of Mo_2CT_x towards HER. According to the experimental study, the HER activity of Mo_2CT_x after 30 cycles remained almost stable, attaining a current density of 10 mA cm_{geo}^{-2} with 305 mV overpotential (Fig. 21c). On the other hand, Ti_2CT_x exhibited a deteriorated cyclic life and attained 10 mA cm_{geo}^{-2} current density at 609 mV overpotential.

A freestanding $Ti_3C_2T_x$ MXene film composited with graphitic C_3N_4 (g-C_3N_4) was studied by Ma *et al.* as electroactive material for OER.[21] The hybrid composite displayed an onset potential of 1.44 V *vs.* RHE (reversible hydrogen electrode) and a lesser operating potential of 1.65 V in 0.1 M KOH to attain 10 mA cm^{-2} current density (Fig. 21d). They also fabricated a rechargeable Zn–air battery using MXene composite as an efficient cathode.

3.4 Fuel cell

In fuel cells, the cathode reaction, known as the oxygen reduction reaction (ORR) generally requires costly Pt group metals as a catalyst. MXenes having interesting characteristics emerged as a useful replacement of noble metals as a catalyst in fuel cells.

Lang *et al.* used 2D $Ti_3C_2T_x$ MXene as a productive catalyst for methanol oxidation reaction and attained above 60% performance improvement over conventional Pd catalyst.[162] Here, MXene was used as support for Pd catalyst and the Pd/MXene catalyst exhibited a superior current density of 12.4 mA cm^{-2} for methanol oxidation reaction than that shown by a conventionally used Pd/C catalyst, which displayed a current density of 7.6 mA cm^{-2} (Fig. 22a and b). In another study, $Ti_3C_2T_x$ was used as a support material for the Pt catalyst used in proton exchange membrane fuel cell.[19] The introduction of $Ti_3C_2T_x$ enhances the homogeneous dispersion and proper attachment of Pt nanoparticles due to the existence of surface terminal groups (–OH, –F, –O) in $Ti_3C_2T_x$ and this superior $Ti_3C_2T_x$–Pt interaction led to reduced oxidation and degradation of the catalyst.

An urchin-like bimetallic nanowire composite of Ti_3C_2/Ag/$Ag_{0.9}Ti_{0.1}$ was prepared by Zhang *et al.* by combining alkali (NaOH) treated $Ti_3C_2T_x$, $AgNO_3$ and PVP.[163] The hybrid composite displayed an outstanding efficiency towards ORR with and V half-wave potential and onset potential, respectively. Ti doping on Ag nanowire expanded the defect concentration leading to avail increased oxygen adsorption sites and conductive $Ti_3C_2T_x$ layers facilitated the electron transfer from Ti to Ag

or different oxygen adsorption sites. T_3C_2 was used in a microbial fuel cell as an efficient anode material by Liu *et al.* after being inoculated with the bacterial mixture for 1 day.[164] The 2D T_3C_2 MXene provided an output voltage of around 640 ± 8 mV and external resistance of 1000 Ω with the highest power density of 3.74 W m^{-2} that was better than that of commercial carbon cloth, which exhibited an output voltage of 550 ± 8 and power density of 2.05 W m^{-2}.

3.5 Solar cell

Due to the novel fusion of metallic conductivity and hydrophilicity, MXene materials have been explored in different types of solar cells. Yang *et al.* fabricated SnO_2/T_3C_2 hybrid composites with varying T_3C_2 concentrations for low-temperature working planner perovskite solar cells (PSC) as electron transport layers (ETLs).[30] The fabricated PSC device was assembled as indium tin oxide (ITO)/ETL/$CH_3NH_3PbI_3$/2,2′,7,7′-tetrakis-(*N*,*N*-di-*p*-methoxyphenylamino)-9,9′-spirobifluoren (Spiro-OMe TAD)/Ag (Fig. 22c). T_3C_2 (1 wt%) was composited with SnO_2 and provided the best result with power conversion efficiency (PCE) of 18.34%, while pure showed PCE of 5.28% (Fig. 22d). Layered MXene sheets facilitate electron mobility and electron extraction, allow charge transfer by decreasing resistance at the interface and lead to superior photocurrents.

A flexible, transparent $Ti_3C_2T_x$/Ag nanowire conductive hybrid nanocomposite film was prepared by Tang *et al.*, which exhibited an excellent figure of merit of 162.49.[165] The assembled organic photovoltaics resulted in PCE of 8.30% with 84.65% retention of initial PCE after 1000 cycles of bending/unbending to a bending radius of 5 mm. T_3C_2 nanosheets were utilized as an electrode material for dye-sensitized solar cells after converting into porous TiO_2 through oxidization.[166] The influence of oxidation time and temperature on the device efficiency with varying thickness was studied. The best device performance with PCE of 2.66% was obtained at 450 °C temperature with a 30 min duration time and 6.4 μm film thickness.

3.6 EMI shielding

$Ti_3C_2T_x$ was first studied by Qing *et al.* as fillers with epoxy composites having a thickness of 1.4 mm and the surface terminal groups and defects present in the MXene sheets facilitate polarization and influence the dielectric loss.[167] They achieved a superb microwave absorption efficiency (above 92%) with less reflection loss of −11 decibels (dB) at the frequency region of 12.4–18 GHz. In another study, a composite was prepared with varying Ti_3C_2 concentrations over the frequency region of 2.0 to 18.0 GHz.[118] It was observed that EMI shielding effectiveness was enhanced with increasing T_3C_2 concentration and the best result (39.1 dB) was achieved at 60 wt% of T_3C_2 with a thickness of 2.0 mm (shown in Fig. 23a and b).

A $Ti_3C_2T_x$–ZnO composite having urchin-like morphology was fabricated by Qian *et al. via* a co-precipitation method for the application of electromagnetic absorber due to the generation of wider interface and novel semiconductive networks.[168] The synthesized composite provided a superior electromagnetic absorbing efficiency with much less reflection loss (−26.30 dB) than pure pristine $Ti_3C_2T_x$ (−6.70 dB). They studied that by varying the formation time of ZnO, the absorption performance of the nanocomposite was significantly influenced within the region of 14.0–18.0 bands. In another report, delaminated $Ti_3C_2T_x$ composited with sodium alginate (10 wt%) provided superb EMI shielding performance of 92 dB with 45 μm thickness and 57 dB with 8 μm thickness.[102] It is evident that EMI shielding and absorption application of MXenes are limited with only $Ti_3C_2T_x$ by varying the synthesis pathway or composite formation.

3.7 Energy harvesting

Electrically conductive MXene ($Ti_3C_2T_x$), which is triboelectrically much negative compared with Teflon or polytetrafluorethylene, was used as a triboelectric nanogenerator, which transforms the useless mechanical energy that comes from human motion into electrical energy.[31] The flexible $Ti_3C_2T_x$ nanogenerator can assist large open-circuit voltage within the region of 500–600 V as well as power-up instantly ∼0.5 to 0.65 mW, which would light up above 60 light-emitting diodes (LEDs) or 1 μF capacitor could be instantly charged up to 50 V. Additionally, this powerful MXene nanogenerator can generate electrical energy from general body movements like texting or typing and become attractive for wearable electronics (Fig. 23c–h).

Hong *et al.* reported $Ti_3C_2T_x$ lamellar membranes with ion-selective nanochannels for osmotic power generation.[169] In the presence of a salinity gradient, the $Ti_3C_2T_x$ membranes allow a cation-selective pathway with the help of surface terminal groups. Under a 1000-fold salinity gradient, a very high power density of 21.0 W m^{-2} and power conversion efficiency of 40.6% was achieved at room temperature. It was observed that a very high thermal increment at 331 K was obtained due to thermal control of ionic mobility and surface charges, leading to the enhancement of power density up to 54 W m^{-2}.

3.8 Sensors: biosensors and electrochemical sensors

The use of MXenes in the field of sensing attain interest due to their biocompatibility, metallic conductivity, a huge number of absorption sites and homogeneous dispersion in the aqueous medium, resulting in high signal, lower detection limit as well as lower electrical noise, which are prominent criteria for efficient sensors.[170,171] MXenes were introduced as sensors in a variety of applications in biomedical, electrochemical and environmental detection like enzymes, NH_3,[172,173] N_2 gases,[174] humidity,[175,176] encapsulating haemoglobin,[20] phenol,[170] SO_2,[172] cancer biomarkers,[177] adrenalin,[178] macromolecules and cell adsorption.[179]

According to the theoretical calculation, V_2CO_2 and Mo_2CO_2 exhibited superior selectivity towards NO; on the other hand, Ti_2CO_2 and Nb_2CO_2 showed selectivity towards NH_3.[172,173] It was also confirmed that MXenes have efficient characteristics for the selective adsorption or storage of methane,[180] hydrogen,[181] CO_2[182] at environmental conditions. Theoretical as well as experimental studies displayed that CO_2 uptakes

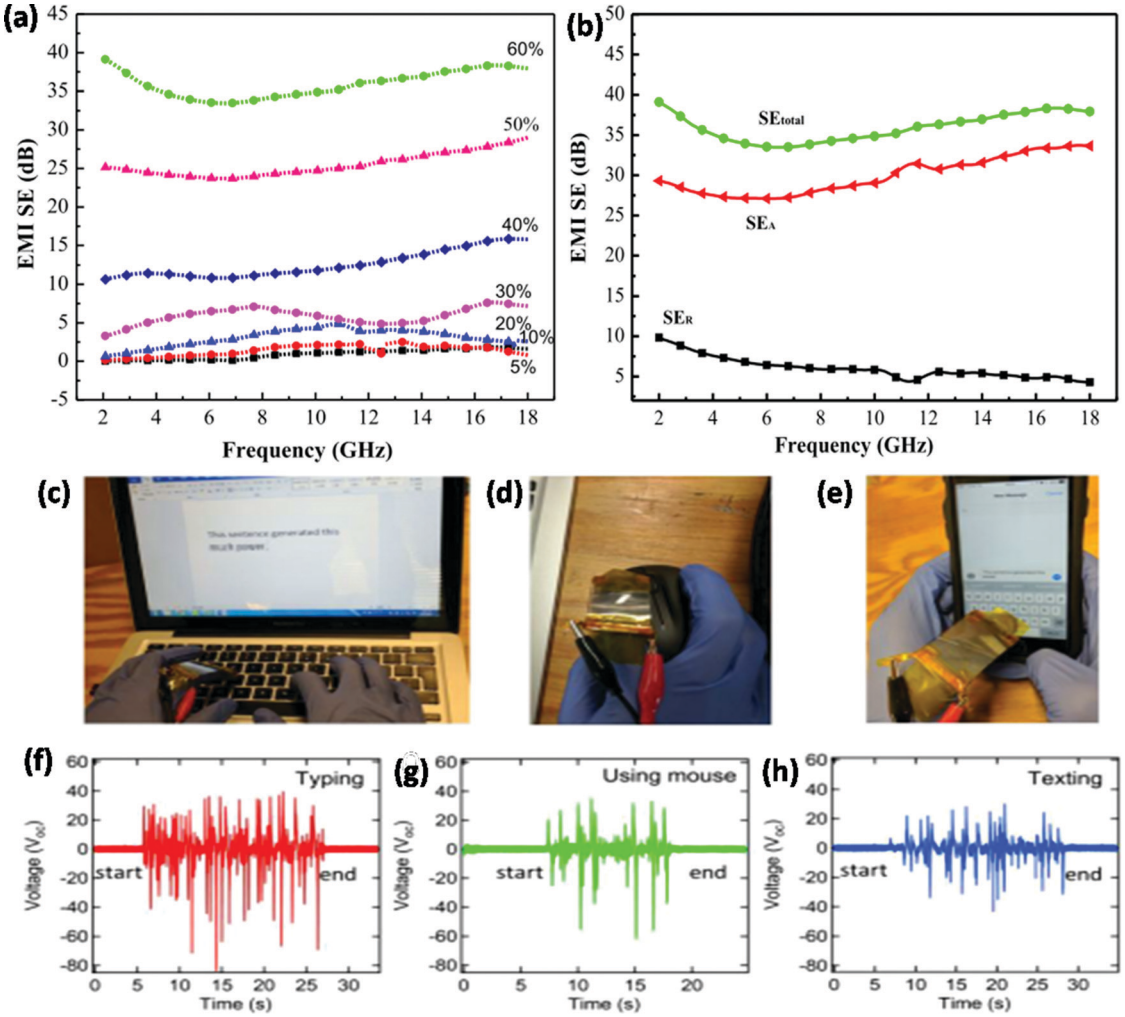

Fig. 23 (a) EMI shielding (EMI SE) of the nanocomposite with varying Ti_3C_2 loading (5–60 wt%) within the frequency window of 2.0–18.0 GHz with 2.0 mm thickness, (b) comparison of SE_{total}, SE_A and SE_R of the Ti_3C_2/paraffin composite at 60 wt% Ti_3C_2 loading (SE_{total} is the sum of absorption SE_A and reflection SE_R contributions). A flexible nanogenerator assembled with $Ti_3C_2T_x$/polyethylene terephthalate (PET)-indium tin oxide (ITO): PET-ITO triboelectric nanogenerator mounted on the index finger harvesting waste mechanical energy from the human body motion (c) typing, (d) clicking a mouse, (e) texting, (f–h) voltage produced due to the actions in (a–c) respectively. (a and b) Reused with permission from ref. 118 and (c–h) reused with permission ref. 31.

using MXene materials were up to around 12 mol CO_2/kg,[183] which is much better than recently studied materials in this field. Junkaew *et al.* reported that oxygen functionalized MXene materials provide more efficient gas sensing than bare MXenes.[172]

Currently, MXene materials used as strain sensors like piezoresistive[184] and hydrogel[185] provide superior efficiency than the earlier reported MoS_2 or hydrogels. While incorporated in electronic skin and wearable devices, MXene materials displayed superb sensitivity, superior stability, quick response and impressive accuracy with delicate human movement detection, such as handwriting, throat swallowing, or eye blinking.[32,184,185] In anti-counterfeiting applications, they could be used and allowed the possibility of the vocally damaged people to hear. For example, strain sensors consisting $Ti_3C_2T_x$/CNT composite provided a sensing region of 30 to 130% and a gauge factor of 4.4 to 772.6 (Fig. 24a), which is far more superior than the conventional semiconductor or metal-based strain sensors.[32] Fig. 24b shows a digital photograph of this $Ti_3C_2T_x$/CNT sensor before and after stretching up to 200%. It is important to mention that multilayered MXenes exhibited more sensitivity compared with partly exfoliated MXenes.

3.9 Blends and composites: mechanical properties

One of the chief benefits of MXene materials is their metallic conductivity with hydrophilicity that allows greater interaction with polymeric matrices, making them favorable in the field of blends and composite materials.[108,186–188] Also, these composites can be prepared by a facile cost-effective process like solution mixing and a variety of shapes like fibers, 3D structures, films are obtained.[189–191] Variety of polymer matrices composite with MXenes were reported, including polyvinyl alcohol (PVA),[108,192,193] polyethylene,[188] polyacrylamide (PAM),[194] polydiallyl dimethylammonium chloride (PDDA),[108] polyurethane (PU),[195] epoxy,[196] polyfluorenes[187] and poly(vinylidene fluoride).[197]

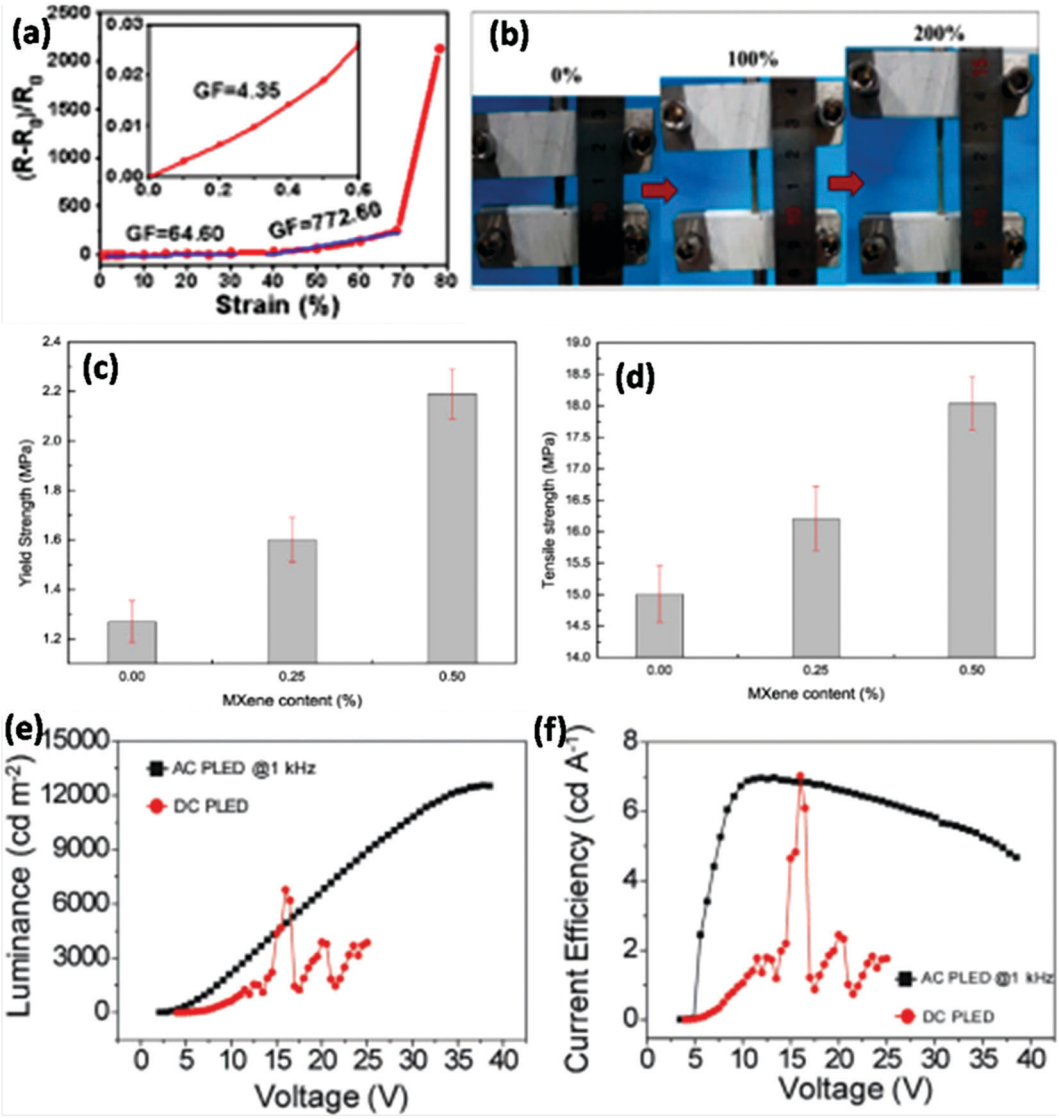

Fig. 24 (a) Relative resistance *vs.* the strain curve $Ti_3C_2T_x$/CNT/latex strain sensor at the stretching rate 5% min^{-1}. Inset is the curve at strain 0.6%, (b) digital photograph of a strain sensor before and after stretching up to 100% and 200%, (c) yield strength and (d) tensile strength of MXene/PU composite, (e) luminance *vs.* voltage plot and (f) current efficiency *vs.* voltage plot of AC MXene PLED under AC and DC condition at 1 KHz AC frequency. (a and b) Reused with permission from ref. 32 (Copyright (2018) American Chemical Society), (c and d) redrawn with permission from ref,195 (e and f) reused with permission from ref. 200.

Actually, MXenes are introduced to enhance the mechanical properties as well as the electrical conductivity of polymer materials. The Ti_2CT_x-epoxy composite provided impact strength and storage modulus increments by 76% and 38%, respectively[196] and $Ti_3C_2T_x$/PVA/cellulose nanocrystals (CNC) composite fibers enhanced the Young Modulus from 392 to 855 MPa.[192] Further, the incorporation of $Ti_3C_2T_x$ (0.5 wt%) in the PU polymer matrix enhanced the stress yield by around 70%[195] (Fig. 24c and d). Regarding electrical conductivities, $Ti_3C_2T_x$-PAM,[166] PVA, PDDA[108] composites showed superb electrical conductivity and V_2C-based polymer composites enhanced electrical conductivity by tenfold with increasing temperature from 15 to 45 °C.[186]

A recent experimental study on MXene-polyfluorenes with various functional groups, including polar, non-polar or charged end alkyl chains, showed that the polymer intercalation inside the MXene ($Ti_3C_2T_x$) layer is favorable for the nitrogen-containing functional groups due to the polarity.[187]

3.10 Organic light-emitting diodes (OLED)

MXene (Ti_3C_2) as a solution-processed electrode was used as OLED due to its huge work function of 5.1 eV, the large electrical conductivity of 11670 S cm^{-1} and excellent optical transmittance up to 85%.[198] A flexible transparent conducting electrode (TCE) of single-layered Ti_3C_2 was fabricated *via* a single-step spin-coating technique and to prevent damaging surface oxidation, as well as deterioration of electrode film; a hole-injection layer of conducting polymer was used. MXene TCE provided an external quantum efficiency of 28.5% ph/el and current efficiency of 102.0 cd A^{-1},

which was well in accordance with the theoretical highest values from optical simulations.

In another study, MXene was treated solvothermally in dimethylformamide (DMF) to prepare carbon-derived, amphiphilic, graphene quantum dots (GQDs), which showed promising performance as light-emitting composite and fluorescent ink due to its excellent photo-stability and tunable photoluminescence.[199] Recently, Lee *et al.* demonstrated transparent MXene electrodes as polymer light-emitting diodes (PLED) due to their superb electrical stability under alternating current (AC).[200] The PLED using MXene electrode performed under AC at 1 kHz frequency, displayed current efficiency of 7 cd A^{-1}, the turn-on voltage of 2.1 V and brightness of 12 547 cd m^{-2} (Fig. 24e and f).

3.11 Actuators and robotics

It was established from *in situ* atomic force microscopy, X-ray diffraction and morphology that different cations can be intercalated into the MXene layers electrochemically, leading to the volume change, which is beneficial for the actuators with electrical stimulants.[33,123,201,202] The intercalation occurs due to the polar terminal groups and the negative surface of MXene.[203] Fig. 25 shows the electroactive MXene-based actuators used as electroactive, photothermal and moisture actuators that were established as the best performer regarding actuation efficiency and promising application.[204] Umrao *et al.* reported a flexible $Ti_3C_2T_x$/poly(3,4-ethylene dioxythiophene) polystyrene sulfonate (PEDOT:PSS) nanocomposite electrode in which PEDOT:PSS was intercalated inside $Ti_3C_2T_x$ layers and displayed excellent conductivity and high capacitance leading to a potential member for soft robotics.[33] The composite electrode displayed a huge volumetric capacitance of 932 F cm^{-3} with excellent durability and cyclic stability of 97% retention after constant actuation up to 18 000 cycles.

In another study, MXene/cellulose/polycarbonate (PC) composite was employed as photothermal actuators with high light to heat conversion ability and good repeatability. Under near-infrared (NIR) light irradiation at 80 mW cm^{-2} intensity, the reported composite was capable of bending at an angle of 11° from flat 108° state to 169° within 6.5 s. Due to the presence of polar terminal groups and huge free spacing between layers, MXenes also became a potential humidity-responsive actuator.[204] Depending on the relative humidity, the surface terminal groups absorb water molecules through H-bonding and the *d*-spacing of MXene sheets increases without changing the crystal structure. Cai *et al.* reported a humidity-responsive bilayer actuator using $Ti_3C_2T_x$/cellulose hygroscopic nanocomposite as an active part and PC as an inert layer.[34] At 70% relative humidity, the actuator was almost flat and with decreasing humidity at 10%, it became bent.

MXenes as electroactive ionic actuators have become promising candidates for soft-robotics such as a human hand, worm, lobsters, flower and fish due to their ability to self-sensing.[204] MXene based soft ionic actuators are used to power up to three kinetic art pieces (shown in Fig. 26a–c).[33] In Fig. 26a, an artificial flower was prepared, which bloomed, and the petals were closed by changing the stimulation in two reverse directions. As shown in Fig. 26b, a tree branch was designed, which hosted many art butterflies. As shown in

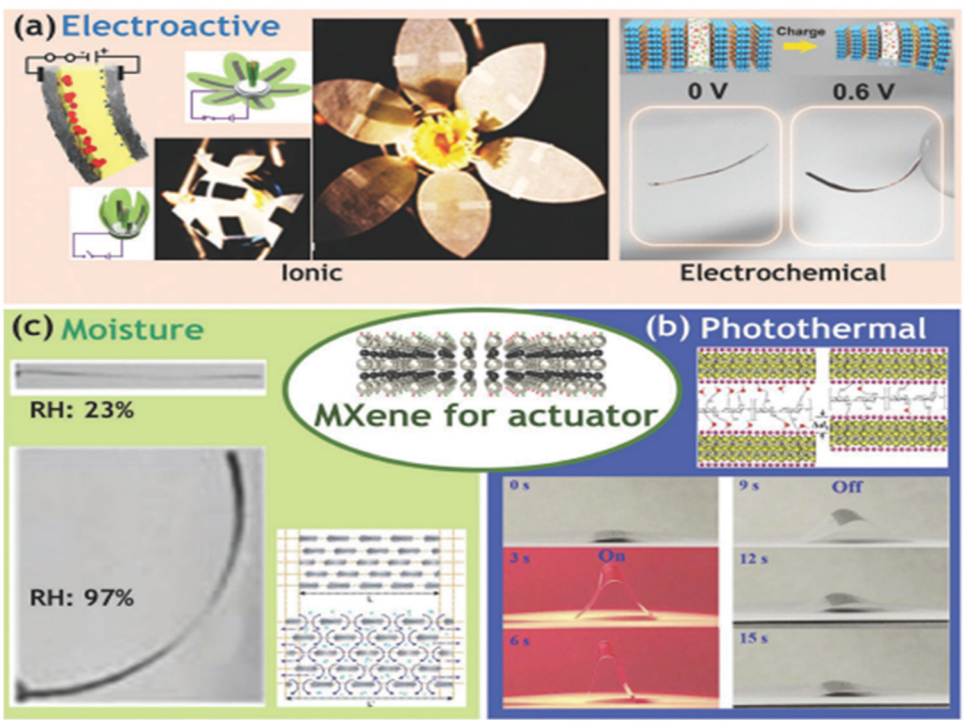

Fig. 25 MXene used in stimuli-responsive actuators (a) electroactive, (b) photothermal and (c) moisture-responsive actuators. Reused with permission from ref. 204.

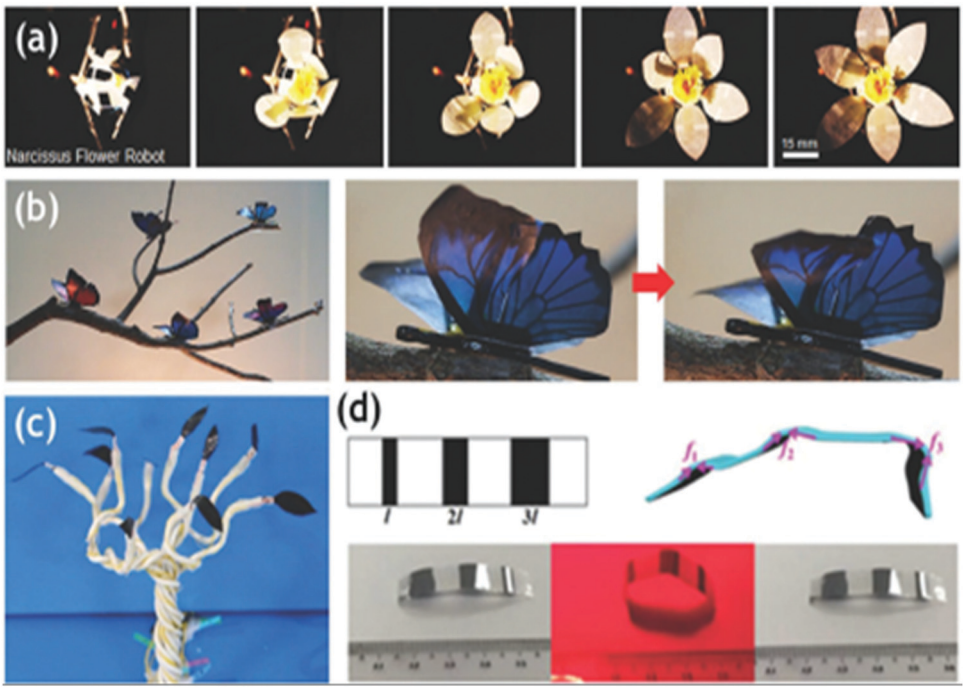

Fig. 26 MXene-based actuators used in soft robotics (a) narcissus flower robot, (b) butterflies on the tree branches, (c) leaves on the tree and (d) worm-like robot. (a–c) reused with permission from ref. 33 and (d) adapted with permission from ref. 34.

Table 4 Some other applications of MXene

Application	MXene based Material	Details	Ref.
Water purification	GO/MXene membrane	Rejection of organic dyes (MB, NR, CV, BB) and natural organic matter in raw water (HA and BSA)	205
	$Ti_3C_2(OH)_2$	Heavy metal (lead) adsorption	206
	$Ti_3C_2T_x$-Iron oxide	Phosphate sequestration	207
	$Ti_3C_2T_x$	Charge and size-selective rejection of molecules and ions.	208
	$Ti_3C_2T_x$-rGO	Heavy metal adsorption (chromate and arsenic)	209
	$Ti_3C_2T_x$/cellulose membrane	Solar driven interfacial water evaporation	210
Dye adsorption	Phytic acid/MXene	Adsorption of MB	211
	NaOH-$Ti_3C_2T_x$	Adsorption of MB	212
	MXene and Al-based metal–organic framework	Adsorption of MB and AB	213
	$Ti_3C_2T_x$	Adsorption and photocatalytic decomposition of AB and MB	109
Lubricant	$Ti_3C_2T_x$-nanosheets	Solid lubricant in machine elements	214
	$Ti_3C_2T_x$-nanoparticles	Solid lubricant under dry friction and reduced adhesive, abrasive and tribo-chemical wear	215
Antibacterial activity	Ti_3C_2	Antibacterial activity towards Gram-negative *Escherichia coli* bacteria	216
	$Ti_3C_2T_x$-nanosheets	Resistance against *Escherichia coli* and *Bacillus subtilis* bacteria	217
Photothermal therapy	PEG-coated Ti_2C	Biocompatible, high photothermal conversion efficacy and NIR-induced capability for cancer cells' ablation	218
Nuclear waste management	Carboxyl functionalized $Ti_3C_2T_x$ MXene	Superior adsorption capacity of U(VI) and Eu(III)	219

GO-graphene oxide; MB-methylene blue; NR-neutral red; CV-crystal violet; BB-Coomassie brilliant blue; HA-humic acid; BSA-bovine serum albumin; rGO-reduced graphene oxide; AB-acid blue; PEG-polyethylene glycol.

Fig. 26c, an artificial tree of thick wires was designed, and the wires were moved slowly in various directions by changing AC input stimulation. So also, kinetic artificial soft robots, as shown in Fig. 26d are made using a Mxene-based photothermal actuator in the shape of a worm by arranging the MXene-cellulose composite on a PC membrane.[34] In the presence of NIR irradiation, the robot bent upward and shrunk.

Some other applications of MXene beyond the above-discussed topics are summarised in Table 4.

4. Conclusions

MXenes are 2D layered carbonitrides, carbides, or nitrides, which are generally prepared by selective etching and delamination of

layered hexagonal MAX phase precursors. During the synthesis process, the surface of MXene layers is functionalized with –F, –OH and –O groups that are responsible for the hydrophilic nature of MXenes. They can form a stable colloidal solution with an aqueous medium without any surfactant due to the surface-negative charge and hydrophilicity, leading to the easy formation of MXene film and paper electrodes.

Theoretical studies revealed the promising properties of MXene-like thermo-electronic, electronic, and optical properties. Specifically, in the existence of terminal groups and water intercalation inside the sheets, $Ti_3C_2T_x$ exhibits metallic conductivity. On the other hand, some MXenes (Mo_2CT_x and $Mo_2TiC_2T_x$) also exhibit semiconductor characteristics. Further, polymer composites with MXene and films of MXenes have excellent mechanical characteristics, and many theoretical predictions about properties are yet to be confirmed experimentally.

Additionally, MXenes allow the intercalation of a variety of cations, long polar organic molecules inside the layers that facilitate energy storage application as well as water purification, soft actuators, and robotics. The metallic conductivity and electronic properties make them potential candidates for solar cells, OLED, and electrochemical sensors. All these exceptional properties establish MXenes as one of the ''hot topics'' of modern science and technology.

5. Future prospects

After nine years of discovery, tremendous progress has been made on the fabrication methods, structural properties, and variety of applications, as well as continuous discovery of the latest types of MXenes. However, similar to other 2D materials, a range of limitations has to be overcome for further developments as well as further progress. Few drawbacks of this material are discussed below –

1. Regarding the extension of the MXene family, till now, only 1/8th portion of discovered MAX phases has been exfoliated experimentally, and another 37 are expected to be feasible.[220] Among the 44 predicted MAX quaternary phases, only nine are prepared so far mainly because of the restricted production of nitride precursors, and MAX phase synthesis is mostly restricted with aluminum. The development of synthesis pathways to get proper control on surface termination groups, controlled morphology, lateral size, and design to tune the properties for a particular application are required to the explored.[221] It is also important to highlight that the characterization of surface terminal groups experimentally or their exact image viewing is still challenging.[222]

2. It has been observed that the theoretical studies are much higher in number than experimental confirmations. Finite element modeling and conventional molecular dynamics are still infrequent in the case of the MXene simulation survey. A few characteristics of MXenes are only described by theoretical calculations like mechanical and magnetic properties, which are not confirmed experimentally yet.[223] In addition, some applications like EMI shielding, actuators and robotics, OLED, and energy harvesting are only limited to $Ti_3C_2T_x$ and needed to explore with other MXenes.

3. Finally, for industrial applications, high cost and environmental stability are the two main factors that hinder the practical utilization of MXenes. The high cost of MXene is associated with costly MAX phase precursors (Y-Carbon, Ukraine, ~$550 per 150 g MAX phase) as well as synthesis, delamination, and device manufacturing cost of MXene.[224] So, a cheaper synthesis process, including the MAX phase and device manufacturing, is needed. Due to the oxidation tendency during the storage and degradation during the applications urge expansion of stability characterizations in various solvents and explore for different applications for interest. Future research should be directed to overcome such obstacles.

Overall, the current material MXene has been considered as one of the magical 2D materials of the current century. However, further research is required, mainly in the synthesis and application parts for the progress of the MXene family in order to make them commercially viable.

Conflicts of interest

There are no conflicts to declare.

References

1 K. S. Novoselov, A. K. Geim, S. V. Morozov, D. Jiang, Y. Zhang, S. V. Dubonos, I. V. Grigorieva and A. A. Firsov, Electric field effect in atomically thin carbon films, *Science*, 2004, **306**(5696), 666–669.
2 Z. S. Wu, K. Parvez, A. Winter, H. Vieker, X. Liu, S. Han, A. Turchanin, X. Feng and K. Müllen, Layer-by-layer assembled heteroatom-doped graphene films with ultrahigh volumetric capacitance and rate capability for micro-supercapacitors, *Adv. Mater.*, 2014, **26**(26), 4552–4558.
3 M. Deng, X. Yang, M. Silke, W. Qiu, M. Xu, G. Borghs and H. Chen, Electrochemical deposition of polypyrrole/graphene oxide composite on microelectrodes towards tuning the electrochemical properties of neural probes, *Sens. Actuators, B*, 2011, **158**(1), 176–184.
4 Y.-M. Lin, C. Dimitrakopoulos, K. A. Jenkins, D. B. Farmer, H.-Y. Chiu, A. Grill and P. Avouris, 100 GHz transistors from wafer-scale epitaxial graphene, *Science*, 2010, **327**(5966), 662.
5 M. Liu, X. Yin, E. Ulin-Avila, B. Geng, T. Zentgraf, L. Ju, F. Wang and X. Zhang, A graphene-based broadband optical modulator, *Nature*, 2011, **474**(7349), 64–67.
6 S. Garaj, W. Hubbard, A. Reina, J. Kong, D. Branton and J. Golovchenko, Graphene as a subnanometre *trans*-electrode membrane, *Nature*, 2010, **467**(7312), 190–193.
7 Z. S. Wu, Y. Zheng, S. Zheng, S. Wang, C. Sun, K. Parvez, T. Ikeda, X. Bao, K. Müllen and X. Feng, Stacked-layer heterostructure films of 2D thiophene nanosheets and graphene for high-rate all-solid-state pseudocapacitors with enhanced volumetric capacitance, *Adv. Mater.*, 2017, **29**(3), 1602960.

8 R. Kumar, S. Sahoo, E. Joanni, R. K. Singh, K. Maegawa, W. K. Tan, G. Kawamura, K. K. Kar and A. Matsuda, Heteroatom doped graphene engineering for energy storage and conversion, *Mater. Today*, 2020, **39**, 47–65.

9 S. K. Tiwari, S. Sahoo, N. Wang and A. Huczko, Graphene research and their outputs: Status and prospect, *J. Sci.: Adv. Mater. Devices*, 2020, **5**(1), 10–29.

10 R. Kumar, S. Sahoo, E. Joanni, R. K. Singh, R. M. Yadav, R. K. Verma, D. P. Singh, W. K. Tan, A. P. del Pino and S. A. Moshkalev, A review on synthesis of graphene, h-BN and MoS_2 for energy storage applications: Recent progress and perspectives, *Nano Res.*, 2019, 1–40.

11 C.-C. Yang, W.-C. Sun, A. Kumar, B. Pattanayak and T.-Y. Tseng, Templating synthesis of nickel cobaltite nanoflakes and their nanocomposites for making high-performance symmetric supercapacitors, *Mater. Today Energy*, 2019, **14**, 100356, DOI: 10.1016/j.mtener.2019.100356.

12 S. Sahoo and G. C. Nayak, Present Status and Prospect of Graphene Research. *Surface Engineering of Graphene*, Springer: 2019, pp. 1–29.

13 K. Parvez, Two-Dimensional Nanomaterials: Crystal Structure and Synthesis. *Biomedical Applications of Graphene and 2D Nanomaterials*, Elsevier, 2019, pp. 1–25.

14 M. Naguib, M. Kurtoglu, V. Presser, J. Lu, J. Niu, M. Heon, L. Hultman, Y. Gogotsi and M. W. Barsoum, Two-dimensional nanocrystals produced by exfoliation of Ti_3AlC_2, *Adv. Mater.*, 2011, **23**(37), 4248–4253.

15 M. Naguib, O. Mashtalir, J. Carle, V. Presser, J. Lu, L. Hultman, Y. Gogotsi and M. W. Barsoum, Two-dimensional transition metal carbides, *ACS Nano*, 2012, **6**(2), 1322–1331.

16 M. Khazaei, M. Arai, T. Sasaki, C. Y. Chung, N. S. Venkataramanan, M. Estili, Y. Sakka and Y. Kawazoe, Novel electronic and magnetic properties of two-dimensional transition metal carbides and nitrides, *Adv. Funct. Mater.*, 2013, **23**(17), 2185–2192.

17 M. Kurtoglu, M. Naguib, Y. Gogotsi and M. W. Barsoum, First principles study of two-dimensional early transition metal carbides, *MRS Commun.*, 2012, **2**(4), 133.

18 J. Come, M. Naguib, P. Rozier, M. W. Barsoum, Y. Gogotsi, P.-L. Taberna, M. Morcrette and P. Simon, A non-aqueous asymmetric cell with a Ti_2C-based two-dimensional negative electrode, *J. Electrochem. Soc.*, 2012, **159**(8), A1368.

19 X. Xie, S. Chen, W. Ding, Y. Nie and Z. Wei, An extraordinarily stable catalyst: Pt NPs supported on two-dimensional $Ti_3C_2X_2$ (X = OH, F) nanosheets for oxygen reduction reaction, *Chem. Commun.*, 2013, **49**(86), 10112–10114.

20 F. Wang, C. Yang, C. Duan, D. Xiao, Y. Tang and J. Zhu, An organ-like titanium carbide material (MXene) with multilayer structure encapsulating hemoglobin for a mediator-free biosensor, *J. Electrochem. Soc.*, 2014, **162**(1), B16.

21 T. Y. Ma, J. L. Cao, M. Jaroniec and S. Z. Qiao, Interacting carbon nitride and titanium carbide nanosheets for high-performance oxygen evolution, *Angew. Chem.*, 2016, **128**(3), 1150–1154.

22 B. Anasori, M. R. Lukatskaya and Y. Gogotsi, 2D metal carbides and nitrides (MXenes) for energy storage, *Nat. Rev. Mater.*, 2017, **2**(2), 1–17.

23 K. Hantanasirisakul, M. Q. Zhao, P. Urbankowski, J. Halim, B. Anasori, S. Kota, C. E. Ren, M. W. Barsoum and Y. Gogotsi, Fabrication of $Ti_3C_2T_x$ MXene transparent thin films with tunable optoelectronic properties, *Adv. Electron. Mater.*, 2016, **2**(6), 1600050.

24 M. R. Lukatskaya, S. Kota, Z. Lin, M.-Q. Zhao, N. Shpigel, M. D. Levi, J. Halim, P.-L. Taberna, M. W. Barsoum and P. Simon, Ultra-high-rate pseudocapacitive energy storage in two-dimensional transition metal carbides, *Nat. Energy*, 2017, **2**(8), 1–6.

25 W. Wu, D. Wei, J. Zhu, D. Niu, F. Wang, L. Wang, L. Yang, P. Yang and C. Wang, Enhanced electrochemical performances of organ-like Ti_3C_2 MXenes/polypyrrole composites as supercapacitors electrode materials, *Ceram. Int.*, 2019, **45**(6), 7328–7337.

26 H. Li, X. Chen, E. Zalnezhad, K. Hui, K. Hui and M. J. Ko, 3D hierarchical transition-metal sulfides deposited on MXene as binder-free electrode for high-performance supercapacitors, *J. Ind. Eng. Chem.*, 2020, **82**, 309–316.

27 H. Zhou, F. Wu, L. Fang, J. Hu, H. Luo, T. Guan, B. Hu and M. Zhou, Layered NiFe–LDH/MXene nanocomposite electrode for high-performance supercapacitor, *Int. J. Hydrogen Energy*, 2020, **45**(23), 13080–13089.

28 N. Li, Y. Xie, S. Peng, X. Xiong and K. Han, Ultra-lightweight $Ti_3C_2T_x$ MXene modified separator for Li–S batteries: Thickness regulation enabled polysulfide inhibition and lithium ion transportation, *J. Energy Chem.*, 2020, **42**, 116–125.

29 C. Sun, X. Shi, Y. Zhang, J. Liang, J. Qu and C. Lai, $Ti_3C_2T_x$ MXene Interface Layer Driving Ultra-Stable Lithium-Iodine Batteries with Both High Iodine Content and Mass Loading, *ACS Nano*, 2020, **14**(1), 1176–1184.

30 L. Yang, Y. Dall'Agnese, K. Hantanasirisakul, C. E. Shuck, K. Maleski, M. Alhabeb, G. Chen, Y. Gao, Y. Sanehira and A. K. Jena, SnO_2–Ti_3C_2 MXene electron transport layers for perovskite solar cells, *J. Mater. Chem. A*, 2019, **7**(10), 5635–5642.

31 Y. Dong, S. S. K. Mallineni, K. Maleski, H. Behlow, V. N. Mochalin, A. M. Rao, Y. Gogotsi and R. Podila, Metallic MXenes: a new family of materials for flexible triboelectric nanogenerators, *Nano Energy*, 2018, **44**, 103–110.

32 Y. Cai, J. Shen, G. Ge, Y. Zhang, W. Jin, W. Huang, J. Shao, J. Yang and X. Dong, Stretchable $Ti_3C_2T_x$ MXene/carbon nanotube composite based strain sensor with ultrahigh sensitivity and tunable sensing range, *ACS Nano*, 2018, **12**(1), 56–62.

33 S. Umrao, R. Tabassian, J. Kim, Q. Zhou, S. Nam and I.-K. Oh, MXene artificial muscles based on ionically cross-linked $Ti_3C_2T_x$ electrode for kinetic soft robotics, *Sci. Rob.*, 2019, **4**, 33.

34 G. Cai, J.-H. Ciou, Y. Liu, Y. Jiang and P. S. Lee, Leaf-inspired multiresponsive MXene-based actuator for programmable smart devices, *Sci. Adv.*, 2019, **5**(7), eaaw7956.

35 Z. W. Seh, K. D. Fredrickson, B. Anasori, J. Kibsgaard, A. L. Strickler, M. R. Lukatskaya, Y. Gogotsi, T. F. Jaramillo and A. Vojvodic, Two-dimensional molybdenum carbide (MXene) as an efficient electrocatalyst for hydrogen evolution, *ACS Energy Lett.*, 2016, **1**(3), 589–594.
36 M. Ghidiu, M. R. Lukatskaya, M.-Q. Zhao, Y. Gogotsi and M. W. Barsoum, Conductive two-dimensional titanium carbide 'clay'with high volumetric capacitance, *Nature*, 2014, **516**(7529), 78–81.
37 M. Khazaei, M. Arai, T. Sasaki, M. Estili and Y. Sakka, Two-dimensional molybdenum carbides: potential thermoelectric materials of the MXene family, *Phys. Chem. Chem. Phys.*, 2014, **16**(17), 7841–7849.
38 Y. Gogotsi and B. Anasori, *The rise of MXenes*. ACS Publications, 2019.
39 M. Naguib, V. N. Mochalin, M. W. Barsoum and Y. Gogotsi, 25th anniversary article: MXenes: a new family of two-dimensional materials, *Adv. Mater.*, 2014, **26**(7), 992–1005.
40 M. Khazaei, A. Mishra, N. S. Venkataramanan, A. K. Singh and S. Yunoki, Recent advances in MXenes: From fundamentals to applications, *Curr. Opin. Solid State Mater. Sci.*, 2019, **23**(3), 164–178.
41 B. Anasori, Y. Xie, M. Beidaghi, J. Lu, B. C. Hosler, L. Hultman, P. R. Kent, Y. Gogotsi and M. W. Barsoum, Two-dimensional, ordered, double transition metals carbides (MXenes), *ACS Nano*, 2015, **9**(10), 9507–9516.
42 Q. Tao, J. Lu, M. Dahlqvist, A. Mockute, S. Calder, A. Petruhins, R. Meshkian, O. Rivin, D. Potashnikov and E. A. N. Caspi, Atomically layered and ordered rare-earth i-MAX phases: a new class of magnetic quaternary compounds, *Chem. Mater.*, 2019, **31**(7), 2476–2485.
43 A. Petruhins, J. Lu, L. Hultman and J. Rosen, Synthesis of atomically layered and chemically ordered rare-earth (RE) i-MAX phases;(Mo2/3RE1/3) 2GaC with RE= Gd, Tb, Dy, Ho, Er, Tm, Yb, and Lu, *Mater. Res. Lett.*, 2019, **7**(11), 446–452.
44 M. Dahlqvist, J. Lu, R. Meshkian, Q. Tao, L. Hultman and J. Rosen, Prediction and synthesis of a family of atomic laminate phases with Kagomé-like and in-plane chemical ordering, *Sci. Adv.*, 2017, **3**(7), e1700642.
45 M. Ashton, R. G. Hennig, S. R. Broderick, K. Rajan and S. B. Sinnott, Computational discovery of stable M_2AX phases, *Phys. Rev. B*, 2016, **94**(5), 054116.
46 M. Dahlqvist, A. Petruhins, J. Lu, L. Hultman and J. Rosen, Origin of chemically ordered atomic laminates (i-MAX): expanding the elemental space by a theoretical/experimental approach, *ACS Nano*, 2018, **12**(8), 7761–7770.
47 A. C. Rajan, A. Mishra, S. Satsangi, R. Vaish, H. Mizuseki, K.-R. Lee and A. K. Singh, Machine-learning-assisted accurate band gap predictions of functionalized MXene, *Chem. Mater.*, 2018, **30**(12), 4031–4038.
48 N. C. Frey, J. Wang, G. I. Vega Bellido, B. Anasori, Y. Gogotsi and V. B. Shenoy, Prediction of synthesis of 2D metal carbides and nitrides (MXenes) and their precursors with positive and unlabeled machine learning, *ACS Nano*, 2019, **13**(3), 3031–3041.
49 W. Sun, S. Shah, Y. Chen, Z. Tan, H. Gao, T. Habib, M. Radovic and M. Green, Electrochemical etching of Ti_2AlC to Ti_2CT_x (MXene) in low-concentration hydrochloric acid solution, *J. Mater. Chem. A*, 2017, **5**(41), 21663–21668.
50 M. Li, J. Lu, K. Luo, Y. Li, K. Chang, K. Chen, J. Zhou, J. Rosen, L. Hultman and P. Eklund, Element replacement approach by reaction with Lewis acidic molten salts to synthesize nanolaminated MAX phases and MXenes, *J. Am. Chem. Soc.*, 2019, **141**(11), 4730–4737.
51 L. Cheng, X. Wang, F. Gong, T. Liu and Z. Liu, 2D nanomaterials for cancer theranostic applications, *Adv. Mater.*, 2020, **32**(13), 1902333.
52 A. Sarycheva, A. Polemi, Y. Liu, K. Dandekar, B. Anasori and Y. Gogotsi, 2D titanium carbide (MXene) for wireless communication, *Sci. Adv.*, 2018, **4**(9), eaau0920.
53 M. Naguib, J. Halim, J. Lu, K. M. Cook, L. Hultman, Y. Gogotsi and M. W. Barsoum, New two-dimensional niobium and vanadium carbides as promising materials for Li-ion batteries, *J. Am. Chem. Soc.*, 2013, **135**(43), 15966–15969.
54 M. Ghidiu, M. Naguib, C. Shi, O. Mashtalir, L. Pan, B. Zhang, J. Yang, Y. Gogotsi, S. J. Billinge and M. W. Barsoum, Synthesis and characterization of two-dimensional Nb_4C_3 (MXene), *Chem. Commun.*, 2014, **50**(67), 9517–9520.
55 J. Zhou, X. Zha, F. Y. Chen, Q. Ye, P. Eklund, S. Du and Q. Huang, A two-dimensional zirconium carbide by selective etching of Al_3C_3 from nanolaminated $Zr_3Al_3C_5$, *Angew. Chem., Int. Ed.*, 2016, **55**(16), 5008–5013.
56 P. Urbankowski, B. Anasori, T. Makaryan, D. Er, S. Kota, P. L. Walsh, M. Zhao, V. B. Shenoy, M. W. Barsoum and Y. Gogotsi, Synthesis of two-dimensional titanium nitride Ti_4N_3 (MXene), *Nanoscale*, 2016, **8**(22), 11385–11391.
57 B. Soundiraraju and B. K. George, Two-dimensional titanium nitride (Ti_2N) MXene: synthesis, characterization, and potential application as surface-enhanced Raman scattering substrate, *ACS Nano*, 2017, **11**(9), 8892–8900.
58 M. Alhabeb, K. Maleski, T. S. Mathis, A. Sarycheva, C. B. Hatter, S. Uzun, A. Levitt and Y. Gogotsi, Selective etching of silicon from Ti_3SiC_2 (MAX) to obtain 2D titanium carbide (MXene), *Angew. Chem.*, 2018, **130**(19), 5542–5546.
59 M. H. Tran, T. Schäfer, A. Shahraei, M. Dürrschnabel, L. Molina-Luna, U. I. Kramm and C. S. Birkel, Adding a New Member to the MXene Family: Synthesis, Structure, and Electrocatalytic Activity for the Hydrogen Evolution Reaction of $V_4C_3T_x$, *ACS Appl. Energy Mater.*, 2018, **1**(8), 3908–3914.
60 J. Yang, M. Naguib, M. Ghidiu, L. M. Pan, J. Gu, J. Nanda, J. Halim, Y. Gogotsi and M. W. Barsoum, Two-Dimensional Nb-Based M_4C_3 Solid Solutions (MXenes), *J. Am. Ceram. Soc.*, 2016, **99**(2), 660–666.
61 Q. Tao, M. Dahlqvist, J. Lu, S. Kota, R. Meshkian, J. Halim, J. Palisaitis, L. Hultman, M. W. Barsoum and P. O. Persson, Two-dimensional Mo 1.33 C MXene with divacancy

ordering prepared from parent 3D laminate with in-plane chemical ordering, *Nat. Commun.*, 2017, **8**(1), 1–7.

62 J. Lu, A. Thore, R. Meshkian, Q. Tao, L. Hultman and J. Rosén, Theoretical and experimental exploration of a novel in-plane chemically ordered (Cr2/3M1/3) 2AlC i-MAX phase with M = Sc and Y, *Cryst. Growth Des.*, 2017, **17**(11), 5704–5711.

63 B. Anasori, M. Dahlqvist, J. Halim, E. J. Moon, J. Lu, B. C. Hosler, E. A. N. Caspi, S. J. May, L. Hultman and P. Eklund, Experimental and theoretical characterization of ordered MAX phases Mo_2TiAlC_2 and $Mo_2Ti_2AlC_3$, *J. Appl. Phys.*, 2015, **118**(9), 094304.

64 R. Meshkian, Q. Tao, M. Dahlqvist, J. Lu, L. Hultman and J. Rosen, Theoretical stability and materials synthesis of a chemically ordered MAX phase, Mo_2ScAlC_2, and its two-dimensional derivate Mo_2ScC_2 MXene, *Acta Mater.*, 2017, **125**, 476–480.

65 J. Zhou, S. Gao, Z. Guo and Z. Sun, Ti-enhanced exfoliation of V_2AlC into V_2C MXene for lithium-ion battery anodes, *Ceram. Int.*, 2017, **43**(14), 11450–11454.

66 M. A. Hope, A. C. Forse, K. J. Griffith, M. R. Lukatskaya, M. Ghidiu, Y. Gogotsi and C. P. Grey, NMR reveals the surface functionalisation of Ti_3C_2 MXene, *Phys. Chem. Chem. Phys.*, 2016, **18**(7), 5099–5102.

67 L. H. Karlsson, J. Birch, J. Halim, M. W. Barsoum and P. O. Persson, Atomically resolved structural and chemical investigation of single MXene sheets, *Nano Lett.*, 2015, **15**(8), 4955–4960.

68 J. Pang, R. G. Mendes, A. Bachmatiuk, L. Zhao, H. Q. Ta, T. Gemming, H. Liu, Z. Liu and M. H. Rummeli, Applications of 2D MXenes in energy conversion and storage systems, *Chem. Soc. Rev.*, 2019, **48**(1), 72–133.

69 P. Srivastava, A. Mishra, H. Mizuseki, K.-R. Lee and A. K. Singh, Mechanistic insight into the chemical exfoliation and functionalization of Ti_3C_2 MXene, *ACS Appl. Mater. Interfaces*, 2016, **8**(36), 24256–24264.

70 Q. Wan, S. Li and J.-B. Liu, First-principle study of Li-ion storage of functionalized Ti_2C monolayer with vacancies, *ACS Appl. Mater. Interfaces*, 2018, **10**(7), 6369–6377.

71 F. Du, H. Tang, L. Pan, T. Zhang, H. Lu, J. Xiong, J. Yang and C. J. Zhang, Environmental friendly scalable production of colloidal 2D titanium carbonitride MXene with minimized nanosheets restacking for excellent cycle life lithium-ion batteries, *Electrochim. Acta*, 2017, **235**, 690–699.

72 X. Sang, Y. Xie, M.-W. Lin, M. Alhabeb, K. L. Van Aken, Y. Gogotsi, P. R. Kent, K. Xiao and R. R. Unocic, Atomic Defects in Monolayer Titanium Carbide ($Ti_3C_2T_x$) MXene, *ACS Nano*, 2016, **10**(10), 9193–9200.

73 L. Wang, H. Zhang, B. Wang, C. Shen, C. Zhang, Q. Hu, A. Zhou and B. Liu, Synthesis and electrochemical performance of $Ti_3C_2T_x$ with hydrothermal process, *Electron. Mater. Lett.*, 2016, **12**(5), 702–710.

74 R. Meshkian, L.-Å. Näslund, J. Halim, J. Lu, M. W. Barsoum and J. Rosen, Synthesis of two-dimensional molybdenum carbide, Mo_2C, from the gallium based atomic laminate Mo_2Ga_2C, *Scr. Mater.*, 2015, **108**, 147–150.

75 J. Zhou, X. Zha, X. Zhou, F. Chen, G. Gao, S. Wang, C. Shen, T. Chen, C. Zhi and P. Eklund, Synthesis and electrochemical properties of two-dimensional hafnium carbide, *ACS Nano*, 2017, **11**(4), 3841–3850.

76 C. Xu, L. Wang, Z. Liu, L. Chen, J. Guo, N. Kang, X.-L. Ma, H.-M. Cheng and W. Ren, Large-area high-quality 2D ultrathin Mo_2C superconducting crystals, *Nat. Mater.*, 2015, **14**(11), 1135–1141.

77 C. Peng, P. Wei, X. Chen, Y. Zhang, F. Zhu, Y. Cao, H. Wang, H. Yu and F. Peng, A hydrothermal etching route to synthesis of 2D MXene (Ti_3C_2, Nb_2C): enhanced exfoliation and improved adsorption performance, *Ceram. Int.*, 2018, **44**(15), 18886–18893.

78 X. Xiao, H. Yu, H. Jin, M. Wu, Y. Fang, J. Sun, Z. Hu, T. Li, J. Wu and L. Huang, Salt-templated synthesis of 2D metallic MoN and other nitrides, *ACS Nano*, 2017, **11**(2), 2180–2186.

79 S. Yang, P. Zhang, F. Wang, A. G. Ricciardulli, M. R. Lohe, P. W. Blom and X. Feng, Fluoride-free synthesis of two-dimensional titanium carbide (MXene) using a binary aqueous system, *Angew. Chem.*, 2018, **130**(47), 15717–15721.

80 K. Zhu, Y. Jin, F. Du, S. Gao, Z. Gao, X. Meng, G. Chen, Y. Wei and Y. Gao, Synthesis of Ti_2CT_x MXene as electrode materials for symmetric supercapacitor with capable volumetric capacitance, *J. Energy Chem.*, 2019, **31**, 11–18.

81 A. VahidMohammadi, A. Hadjikhani, S. Shahbazmohamadi and M. Beidaghi, Two-dimensional vanadium carbide (MXene) as a high-capacity cathode material for rechargeable aluminum batteries, *ACS Nano*, 2017, **11**(11), 11135–11144.

82 S. Zhao, X. Meng, K. Zhu, F. Du, G. Chen, Y. Wei, Y. Gogotsi and Y. Gao, Li-ion uptake and increase in interlayer spacing of Nb_4C_3 MXene, *Energy Storage Mater.*, 2017, **8**, 42–48.

83 J. Halim, J. Palisaitis, J. Lu, J. Thörnberg, E. Moon, M. Precner, P. Eklund, P. Å. Persson, M. Barsoum and J. Rosen, Synthesis of two-dimensional Nb1. 33C (MXene) with randomly distributed vacancies by etching of the quaternary solid solution (Nb2/3Sc1/3) 2AlC MAX phase, *ACS Appl. Nano Mater.*, 2018, **1**(6), 2455–2460.

84 R. Meshkian, M. Dahlqvist, J. Lu, B. Wickman, J. Halim, J. Thörnberg, Q. Tao, S. Li, S. Intikhab and J. Snyder, W-based atomic laminates and their 2D derivative W1. 33C MXene with vacancy ordering, *Adv. Mater.*, 2018, **30**(21), 1706409.

85 S. Kajiyama, L. Szabova, H. Iinuma, A. Sugahara, K. Gotoh, K. Sodeyama, Y. Tateyama, M. Okubo and A. Yamada, Enhanced Li-ion accessibility in MXene titanium carbide by steric chloride termination, *Adv. Energy Mater.*, 2017, 7(9), 1601873.

86 J. Halim, M. R. Lukatskaya, K. M. Cook, J. Lu, C. R. Smith, L.-Å. Näslund, S. J. May, L. Hultman, Y. Gogotsi and P. Eklund, Transparent conductive two-dimensional titanium carbide epitaxial thin films, *Chem. Mater.*, 2014, **26**(7), 2374–2381.

87 F. Liu, J. Zhou, S. Wang, B. Wang, C. Shen, L. Wang, Q. Hu, Q. Huang and A. Zhou, Preparation of high-purity V_2C

MXene and electrochemical properties as Li-ion batteries, *J. Electrochem. Soc.*, 2017, **164**(4), A709.

88 J. Halim, S. Kota, M. R. Lukatskaya, M. Naguib, M. Q. Zhao, E. J. Moon, J. Pitock, J. Nanda, S. J. May and Y. Gogotsi, Synthesis and characterization of 2D molybdenum carbide (MXene), *Adv. Funct. Mater.*, 2016, **26**(18), 3118–3127.

89 H. Zhang, G. Yang, X. Zuo, H. Tang, Q. Yang and G. Li, Computational studies on the structural, electronic and optical properties of graphene-like MXenes (M_2CT_2, M = Ti, Zr, Hf; T = O, F, OH) and their potential applications as visible-light driven photocatalysts, *J. Mater. Chem. A*, 2016, **4**(33), 12913–12920.

90 T. Hu, M. Hu, B. Gao, W. Li and X. Wang, Screening surface structure of MXenes by high-throughput computation and vibrational spectroscopic confirmation, *J. Phys. Chem. C*, 2018, **122**(32), 18501–18509.

91 X. Tang, X. Guo, W. Wu and G. Wang, 2D Metal Carbides and Nitrides (MXenes) as High-Performance Electrode Materials for Lithium-Based Batteries, *Adv. Energy Mater.*, 2018, **8**(33), 1801897.

92 I. Persson, L.-Å. Näslund, J. Halim, M. W. Barsoum, V. Darakchieva, J. Palisaitis, J. Rosen and P. O. Å. Persson, On the organization and thermal behavior of functional groups on Ti_3C_2 MXene surfaces in vacuum, *2D Mater.*, 2017, **5**(1), 015002.

93 H.-W. Wang, M. Naguib, K. Page, D. J. Wesolowski and Y. Gogotsi, Resolving the structure of $Ti_3C_2T_x$ mxenes through multilevel structural modeling of the atomic pair distribution function, *Chem. Mater.*, 2016, **28**(1), 349–359.

94 H. Lashgari, M. Abolhassani, A. Boochani, S. Elahi and J. Khodadadi, Electronic and optical properties of 2D graphene-like compounds titanium carbides and nitrides: DFT calculations, *Solid State Commun.*, 2014, **195**, 61–69.

95 Q. Tang, Z. Zhou and P. Shen, Are MXenes promising anode materials for Li ion batteries? Computational studies on electronic properties and Li storage capability of Ti_3C_2 and $Ti_3C_2X_2$ (X = F, OH) monolayer, *J. Am. Chem. Soc.*, 2012, **134**(40), 16909–16916.

96 A. N. Enyashin and A. L. Ivanovskii, Structural and electronic properties and stability of MX enes Ti_2C and Ti_3C_2 functionalized by methoxy groups, *J. Phys. Chem. C*, 2013, **117**(26), 13637–13643.

97 R. M. Ronchi, J. T. Arantes and S. F. Santos, Synthesis, structure, properties and applications of MXenes: current status and perspectives, *Ceram. Int.*, 2019, **45**(15), 18167–18188.

98 Z. M. Wong, T. L. Tan, S.-W. Yang and G. Q. Xu, Enhancing the photocatalytic performance of MXenes via stoichiometry engineering of their electronic and optical properties, *ACS Appl. Mater. Interfaces*, 2018, **10**(46), 39879–39889.

99 J. Guo, Y. Sun, B. Liu, Q. Zhang and Q. Peng, Two-dimensional scandium-based carbides (MXene): band gap modulation and optical properties, *J. Alloys Compd.*, 2017, **712**, 752–759.

100 E. Balcı, Ü. Ö. Akkuş and S. Berber, Controlling topological electronic structure of multifunctional MXene layer, *Appl. Phys. Lett.*, 2018, **113**(8), 083107.

101 K. Luo, X.-H. Zha, Y. Zhou, Z. Guo, C.-T. Lin, Q. Huang, S. Zhou, R. Zhang and S. Du, First-principles study on the electrical and thermal properties of the semiconducting $Sc_3(CN)F_2$ MXene, *RSC Adv.*, 2018, **8**(40), 22452–22459.

102 F. Shahzad, M. Alhabeb, C. B. Hatter, B. Anasori, S. M. Hong, C. M. Koo and Y. Gogotsi, Electromagnetic interference shielding with 2D transition metal carbides (MXenes), *Science*, 2016, **353**(6304), 1137–1140.

103 H. Wang, Y. Wu, J. Zhang, G. Li, H. Huang, X. Zhang and Q. Jiang, Enhancement of the electrical properties of MXene Ti_3C_2 nanosheets by post-treatments of alkalization and calcination, *Mater. Lett.*, 2015, **160**, 537–540.

104 K. R. Paton, E. Varrla, C. Backes, R. J. Smith, U. Khan, A. O'Neill, C. Boland, M. Lotya, O. M. Istrate and P. King, Scalable production of large quantities of defect-free few-layer graphene by shear exfoliation in liquids, *Nat. Mater.*, 2014, **13**(6), 624–630.

105 I. Shein and A. Ivanovskii, Graphene-like titanium carbides and nitrides $Ti_{n+1}C_n$, $Ti_{n+1}N_n$ (n = 1, 2, and 3) from de-intercalated MAX phases: First-principles probing of their structural, electronic properties and relative stability, *Comput. Mater. Sci.*, 2012, **65**, 104–114.

106 C. Si, J. Zhou and Z. Sun, Half-metallic ferromagnetism and surface functionalization-induced metal–insulator transition in graphene-like two-dimensional Cr_2C crystals, *ACS Appl. Mater. Interfaces*, 2015, **7**(31), 17510–17515.

107 T. Hu, J. Yang and X. Wang, Carbon vacancies in Ti_2CT_2 MXenes: defects or a new opportunity?, *Phys. Chem. Chem. Phys.*, 2017, **19**(47), 31773–31780.

108 Z. Ling, C. E. Ren, M.-Q. Zhao, J. Yang, J. M. Giammarco, J. Qiu, M. W. Barsoum and Y. Gogotsi, Flexible and conductive MXene films and nanocomposites with high capacitance, *Proc. Natl. Acad. Sci. U. S. A.*, 2014, **111**(47), 16676–16681.

109 O. Mashtalir, K. M. Cook, V. N. Mochalin, M. Crowe, M. W. Barsoum and Y. Gogotsi, Dye adsorption and decomposition on two-dimensional titanium carbide in aqueous media, *J. Mater. Chem. A*, 2014, **2**(35), 14334–14338.

110 K. Wang, Y. Zhou, W. Xu, D. Huang, Z. Wang and M. Hong, Fabrication and thermal stability of two-dimensional carbide Ti_3C_2 nanosheets, *Ceram. Int.*, 2016, **42**(7), 8419–8424.

111 M. Naguib, O. Mashtalir, M. R. Lukatskaya, B. Dyatkin, C. Zhang, V. Presser, Y. Gogotsi and M. W. Barsoum, One-step synthesis of nanocrystalline transition metal oxides on thin sheets of disordered graphitic carbon by oxidation of MXenes, *Chem. Commun.*, 2014, **50**(56), 7420–7423.

112 R. B. Rakhi, B. Ahmed, M. N. Hedhili, D. H. Anjum and H. N. Alshareef, Effect of postetch annealing gas composition on the structural and electrochemical properties of Ti_2CT_x MXene electrodes for supercapacitor applications, *Chem. Mater.*, 2015, **27**(15), 5314–5323.

113 A. Gusev and A. Rempel, Atomic ordering and phase equilibria in strongly nonstoichiometric carbides and nitrides. *Materials science of carbides, nitrides and borides*, Springer, 1999, pp. 47–64.

114 O. Mashtalir, M. R. Lukatskaya, A. I. Kolesnikov, E. Raymundo-Pinero, M. Naguib, M. Barsoum and Y. Gogotsi, The effect of hydrazine intercalation on the structure and capacitance of 2D titanium carbide (MXene), *Nanoscale*, 2016, **8**(17), 9128–9133.

115 S. Lai, J. Jeon, S. K. Jang, J. Xu, Y. J. Choi, J.-H. Park, E. Hwang and S. Lee, Surface group modification and carrier transport properties of layered transition metal carbides (Ti_2CT_x, T: –OH,–F and–O), *Nanoscale*, 2015, **7**(46), 19390–19396.

116 J.-C. Lei, X. Zhang and Z. Zhou, Recent advances in MXene: Preparation, properties, and applications, *Front. Phys.*, 2015, **10**(3), 276–286.

117 Q. Hu, D. Sun, Q. Wu, H. Wang, L. Wang, B. Liu, A. Zhou and J. He, MXene: a new family of promising hydrogen storage medium, *J. Phys. Chem. A*, 2013, **117**(51), 14253–14260.

118 X. Liu, J. Wu, J. He and L. Zhang, Electromagnetic interference shielding effectiveness of titanium carbide sheets, *Mater. Lett.*, 2017, **205**, 261–263.

119 X. Zhao, Z. Wang, J. Dong, T. Huang, Q. Zhang and L. Zhang, Annealing modification of MXene films with mechanically strong structures and high electrochemical performance for supercapacitor applications, *J. Power Sources*, 2020, **470**, 228356.

120 R. Syamsai and A. N. Grace, Ta_4C_3 MXene as supercapacitor electrodes, *J. Alloys Compd.*, 2019, **792**, 1230–1238.

121 X. Wang, T. S. Mathis, K. Li, Z. Lin, L. Vlcek, T. Torita, N. C. Osti, C. Hatter, P. Urbankowski and A. Sarycheva, Influences from solvents on charge storage in titanium carbide MXenes, *Nat. Energy*, 2019, **4**(3), 241–248.

122 M. R. Lukatskaya, O. Mashtalir, C. E. Ren, Y. Dall'Agnese, P. Rozier, P. L. Taberna, M. Naguib, P. Simon, M. W. Barsoum and Y. Gogotsi, Cation intercalation and high volumetric capacitance of two-dimensional titanium carbide, *Science*, 2013, **341**(6153), 1502–1505.

123 H. He, Q. Xia, B. Wang, L. Wang, Q. Hu and A. Zhou, Two-dimensional vanadium carbide (V_2CT_x) MXene as supercapacitor electrode in seawater electrolyte, *Chin. Chem. Lett.*, 2020, **31**(4), 984–987.

124 J. Xiao, J. Wen, J. Zhao, X. Ma, H. Gao and X. Zhang, A safe etching route to synthesize highly crystalline Nb_2CT_x MXene for high performance asymmetric supercapacitor applications, *Electrochim. Acta*, 2020, **337**, 135803.

125 J. Yan, C. E. Ren, K. Maleski, C. B. Hatter, B. Anasori, P. Urbankowski, A. Sarycheva and Y. Gogotsi, Flexible MXene/graphene films for ultrafast supercapacitors with outstanding volumetric capacitance, *Adv. Funct. Mater.*, 2017, **27**(30), 1701264.

126 Y. Dall'Agnese, P. Rozier, P.-L. Taberna, Y. Gogotsi and P. Simon, Capacitance of two-dimensional titanium carbide (MXene) and MXene/carbon nanotube composites in organic electrolytes, *J. Power Sources*, 2016, **306**, 510–515.

127 Y. Zhou, K. Maleski, B. Anasori, J. O. Thostenson, Y. Pang, Y. Feng, K. Zeng, C. B. Parker, S. Zauscher and Y. Gogotsi, $Ti_3C_2T_x$ MXene-Reduced Graphene Oxide Composite Electrodes for Stretchable Supercapacitors, *ACS Nano*, 2020, **14**(3), 3576–3586.

128 A. VahidMohammadi, J. Moncada, H. Chen, E. Kayali, J. Orangi, C. A. Carrero and M. Beidaghi, Thick and free-standing MXene/PANI pseudocapacitive electrodes with ultrahigh specific capacitance, *J. Mater. Chem. A*, 2018, **6**(44), 22123–22133.

129 R. Syamsai and A. N. Grace, Synthesis, properties and performance evaluation of vanadium carbide MXene as supercapacitor electrodes, *Ceram. Int.*, 2020, **46**(4), 5323–5330.

130 X. He, T. Bi, X. Zheng, W. Zhu and J. Jiang, Nickel cobalt sulfide nanoparticles grown on titanium carbide MXenes for high-performance supercapacitor, *Electrochim. Acta*, 2020, **332**, 135514.

131 Z. Pan, F. Cao, X. Hu and X. Ji, A facile method for synthesizing CuS decorated Ti_3C_2 MXene with enhanced performance for asymmetric supercapacitors, *J. Mater. Chem. A*, 2019, **7**(15), 8984–8992.

132 H. Liu, R. Hu, J. Qi, Y. Sui, Y. He, Q. Meng, F. Wei, Y. Ren, Y. Zhao and W. Wei, One-Step Synthesis of Nanostructured CoS_2 Grown on Titanium Carbide MXene for High-Performance Asymmetrical Supercapacitors, *Adv. Mater. Interfaces*, 2020, **7**(6), 1901659.

133 S. Xu, G. Wei, J. Li, W. Han and Y. Gogotsi, Flexible MXene–graphene electrodes with high volumetric capacitance for integrated co-cathode energy conversion/storage devices, *J. Mater. Chem. A*, 2017, **5**(33), 17442–17451.

134 Q. Jiang, N. Kurra, M. Alhabeb, Y. Gogotsi and H. N. Alshareef, All pseudocapacitive MXene-RuO_2 asymmetric supercapacitors, *Adv. Energy Mater.*, 2018, **8**(13), 1703043.

135 Y. Wen, T. E. Rufford, X. Chen, N. Li, M. Lyu, L. Dai and L. Wang, Nitrogen-doped $Ti_3C_2T_x$ MXene electrodes for high-performance supercapacitors, *Nano Energy*, 2017, **38**, 368–376.

136 Q. X. Xia, N. M. Shinde, J. M. Yun, T. Zhang, R. S. Mane, S. Mathur and K. H. Kim, Bismuth oxychloride/MXene symmetric supercapacitor with high volumetric energy density, *Electrochim. Acta*, 2018, **271**, 351–360.

137 Q. X. Xia, J. Fu, J. M. Yun, R. S. Mane and K. H. Kim, High volumetric energy density annealed-MXene-nickel oxide/MXene asymmetric supercapacitor, *RSC Adv.*, 2017, **7**(18), 11000–11011.

138 Y. Xie, M. Naguib, V. N. Mochalin, M. W. Barsoum, Y. Gogotsi, X. Yu, K.-W. Nam, X.-Q. Yang, A. I. Kolesnikov and P. R. Kent, Role of surface structure on Li-ion energy storage capacity of two-dimensional transition-metal carbides, *J. Am. Chem. Soc.*, 2014, **136**(17), 6385–6394.

139 W. Luo, Y. Liu, F. Li, J. Huo, D. Zhao, J. Zhu and S. Guo, H_2O_2 Assisted Hydrothermal Oxidation of Partially Etched Vanadium Carbides (MXene) and Their Electrochemical Properties as Anode for Li-ion Batteries, *Appl. Surf. Sci.*, 2020, 146387.

140 T. Yu, S. Zhang, F. Li, Z. Zhao, L. Liu, H. Xu and G. Yang, Stable and metallic two-dimensional TaC_2 as an anode

material for lithium-ion battery, *J. Mater. Chem. A*, 2017, **5**(35), 18698–18706.

141 R. Liu, W. Cao, D. Han, Y. Mo, H. Zeng, H. Yang and W. Li, Nitrogen-doped Nb_2CT_x MXene as anode materials for lithium ion batteries, *J. Alloys Compd.*, 2019, **793**, 505–511.

142 Y.-T. Du, X. Kan, F. Yang, L.-Y. Gan and U. Schwingenschlögl, MXene/graphene heterostructures as high-performance electrodes for Li-ion batteries, *ACS Appl. Mater. Interfaces*, 2018, **10**(38), 32867–32873.

143 Q. Li, J. Zhou, F. Li and Z. Sun, Spring-roll-like Ti_3C_2 MXene/carbon-coated Fe_3O_4 composite as a long-life Li-ion storage material, *Inorg. Chem. Front.*, 2020, **7**, 3491–3499.

144 X. Wu, Z. Wang, M. Yu, L. Xiu and J. Qiu, Stabilizing the MXenes by carbon nanoplating for developing hierarchical nanohybrids with efficient lithium storage and hydrogen evolution capability, *Adv. Mater.*, 2017, **29**(24), 1607017.

145 A. Byeon, M.-Q. Zhao, C. E. Ren, J. Halim, S. Kota, P. Urbankowski, B. Anasori, M. W. Barsoum and Y. Gogotsi, Two-dimensional titanium carbide MXene as a cathode material for hybrid magnesium/lithium-ion batteries, *ACS Appl. Mater. Interfaces*, 2017, **9**(5), 4296–4300.

146 X. Sun, Y. Liu, J. Zhang, L. Hou, J. Sun and C. Yuan, Facile construction of ultrathin SnO_x nanosheets decorated MXene (Ti_3C_2) nanocomposite towards Li-ion batteries as high performance anode materials, *Electrochim. Acta*, 2019, **295**, 237–245.

147 B. Ahmed, D. H. Anjum, Y. Gogotsi and H. N. Alshareef, Atomic layer deposition of SnO_2 on MXene for Li-ion battery anodes, *Nano Energy*, 2017, **34**, 249–256.

148 D. Xu, K. Ma, L. Chen, Y. Hu, H. Jiang and C. Li, MXene interlayer anchored Fe_3O_4 nanocrystals for ultrafast Li-ion batteries, *Chem. Eng. Sci.*, 2020, **212**, 115342.

149 P. A. Maughan, V. R. Seymour, R. Bernardo-Gavito, D. J. Kelly, S. Shao, S. Tantisriyanurak, R. Dawson, S. J. Haigh, R. J. Young and N. Tapia-Ruiz, Porous silica-pillared MXenes with controllable interlayer distances for long-life Na-ion batteries, *Langmuir*, 2020, **36**(16), 4370–4382.

150 S. M. Bak, R. Qiao, W. Yang, S. Lee, X. Yu, B. Anasori, H. Lee, Y. Gogotsi and X. Q. Yang, Na-Ion Intercalation and Charge Storage Mechanism in 2D Vanadium Carbide, *Adv. Energy Mater.*, 2017, **7**(20), 1700959.

151 X. Wang, S. Kajiyama, H. Iinuma, E. Hosono, S. Oro, I. Moriguchi, M. Okubo and A. Yamada, Pseudocapacitance of MXene nanosheets for high-power sodium-ion hybrid capacitors, *Nat. Commun.*, 2015, **6**(1), 1–6.

152 M. Q. Zhao, X. Xie, C. E. Ren, T. Makaryan, B. Anasori, G. Wang and Y. Gogotsi, Hollow MXene spheres and 3D macroporous MXene frameworks for Na-ion storage, *Adv. Mater.*, 2017, **29**(37), 1702410.

153 X. Guo, X. Xie, S. Choi, Y. Zhao, H. Liu, C. Wang, S. Chang and G. Wang, Sb_2O_3/MXene ($Ti_3C_2T_x$) hybrid anode materials with enhanced performance for sodium-ion batteries, *J. Mater. Chem. A*, 2017, **5**(24), 12445–12452.

154 Y. Wu, P. Nie, J. Jiang, B. Ding, H. Dou and X. Zhang, MoS_2-Nanosheet-Decorated 2D Titanium Carbide (MXene) as High-Performance Anodes for Sodium-Ion Batteries, *ChemElectroChem*, 2017, **4**(6), 1560–1565.

155 E. Xu, Y. Zhang, H. Wang, Z. Zhu, J. Quan, Y. Chang, P. Li, D. Yu and Y. Jiang, Ultrafast kinetics net electrode assembled via $MoSe_2$/MXene heterojunction for high-performance sodium-ion batteries, *Chem. Eng. J.*, 2020, **385**, 123839.

156 D. Guo, F. Ming, H. Su, Y. Wu, W. Wahyudi, M. Li, M. N. Hedhili, G. Sheng, L.-J. Li and H. N. Alshareef, MXene based self-assembled cathode and antifouling separator for high-rate and dendrite-inhibited Li–S battery, *Nano Energy*, 2019, **61**, 478–485.

157 X. Liang, Y. Rangom, C. Y. Kwok, Q. Pang and L. F. Nazar, Interwoven MXene nanosheet/carbon-nanotube composites as Li–S cathode hosts, *Adv. Mater.*, 2017, **29**(3), 1603040.

158 W. Bao, X. Xie, J. Xu, X. Guo, J. Song, W. Wu, D. Su and G. Wang, Confined sulfur in 3 D MXene/reduced graphene oxide hybrid nanosheets for lithium–sulfur battery, *Chem. – Eur. J.*, 2017, **23**(51), 12613–12619.

159 Y. Zhao and J. Zhao, Functional group-dependent anchoring effect of titanium carbide-based MXenes for lithium-sulfur batteries: A computational study, *Appl. Surf. Sci.*, 2017, **412**, 591–598.

160 J. Wang, Z. Zhang, X. Yan, S. Zhang, Z. Wu, Z. Zhuang and W.-Q. Han, Rational Design of Porous N-Ti_3C_2 MXene@CNT Microspheres for High Cycling Stability in Li–S Battery, *Nano-Micro Lett.*, 2020, **12**(1), 4.

161 H. Wang, R. Peng, Z. D. Hood, M. Naguib, S. P. Adhikari and Z. Wu, Titania Composites with 2 D Transition Metal Carbides as Photocatalysts for Hydrogen Production under Visible-Light Irradiation, *ChemSusChem*, 2016, **9**(12), 1490–1497.

162 Z. Lang, Z. Zhuang, S. Li, L. Xia, Y. Zhao, Y. Zhao, C. Han and L. Zhou, MXene surface terminations enable strong metal–support interactions for efficient methanol oxidation on palladium, *ACS Appl. Mater. Interfaces*, 2019, **12**(2), 2400–2406.

163 Z. Zhang, H. Li, G. Zou, C. Fernandez, B. Liu, Q. Zhang, J. Hu and Q. Peng, Self-reduction synthesis of new MXene/Ag composites with unexpected electrocatalytic activity, *ACS Sustainable Chem. Eng.*, 2016, **4**(12), 6763–6771.

164 D. Liu, R. Wang, W. Chang, L. Zhang, B. Peng, H. Li, S. Liu, M. Yan and C. Guo, Ti_3C_2 MXene as an excellent anode material for high-performance microbial fuel cells, *J. Mater. Chem. A*, 2018, **6**(42), 20887–20895.

165 H. Tang, H. Feng, H. Wang, X. Wan, J. Liang and Y. Chen, Highly Conducting MXene–Silver Nanowire Transparent Electrodes for Flexible Organic Solar Cells, *ACS Appl. Mater. Interfaces*, 2019, **11**(28), 25330–25337.

166 C. Dall'Agnese, Y. Dall'Agnese, B. Anasori, W. Sugimoto and S. Mori, Oxidized Ti_3C_2 MXene nanosheets for dye-sensitized solar cells, *New J. Chem.*, 2018, **42**(20), 16446–16450.

167 Y. Qing, W. Zhou, F. Luo and D. Zhu, Titanium carbide (MXene) nanosheets as promising microwave absorbers, *Ceram. Int.*, 2016, **42**(14), 16412–16416.

168 Y. Qian, H. Wei, J. Dong, Y. Du, X. Fang, W. Zheng, Y. Sun and Z. Jiang, Fabrication of urchin-like ZnO–MXene nanocomposites for high-performance electromagnetic absorption, *Ceram. Int.*, 2017, **43**(14), 10757–10762.

169 S. Hong, F. Ming, Y. Shi, R. Li, I. S. Kim, C. Y. Tang, H. N. Alshareef and P. Wang, Two-Dimensional $Ti_3C_2T_x$ MXene Membranes as Nanofluidic Osmotic Power Generators, *ACS Nano*, 2019, **13**(8), 8917–8925.

170 L. Wu, X. Lu, Z.-S. Wu, Y. Dong, X. Wang, S. Zheng and J. Chen, 2D transition metal carbide MXene as a robust biosensing platform for enzyme immobilization and ultrasensitive detection of phenol, *Biosens. Bioelectron.*, 2018, **107**, 69–75.

171 S. J. Kim, H.-J. Koh, C. E. Ren, O. Kwon, K. Maleski, S.-Y. Cho, B. Anasori, C.-K. Kim, Y.-K. Choi and J. Kim, Metallic $Ti_3C_2T_x$ MXene gas sensors with ultrahigh signal-to-noise ratio, *ACS Nano*, 2018, **12**(2), 986–993.

172 A. Junkaew and R. Arroyave, Enhancement of the selectivity of MXenes (M_2C, M = Ti, V, Nb, Mo) via oxygen-functionalization: promising materials for gas-sensing and-separation, *Phys. Chem. Chem. Phys.*, 2018, **20**(9), 6073–6082.

173 X.-F. Yu, Y.-C. Li, J.-B. Cheng, Z.-B. Liu, Q.-Z. Li, W.-Z. Li, X. Yang and B. Xiao, Monolayer Ti_2CO_2: a promising candidate for NH3 sensor or capturer with high sensitivity and selectivity, *ACS Appl. Mater. Interfaces*, 2015, **7**(24), 13707–13713.

174 L. M. Azofra, N. Li, D. R. MacFarlane and C. Sun, Promising prospects for 2D d_2–d_4 M_3C_2 transition metal carbides (MXenes) in N_2 capture and conversion into ammonia, *Energy Environ. Sci.*, 2016, **9**(8), 2545–2549.

175 E. S. Muckley, M. Naguib and I. N. Ivanov, Multi-modal, ultrasensitive, wide-range humidity sensing with Ti_3C_2 film, *Nanoscale*, 2018, **10**(46), 21689–21695.

176 E. S. Muckley, M. Naguib, H.-W. Wang, L. Vlcek, N. C. Osti, R. L. Sacci, X. Sang, R. R. Unocic, Y. Xie and M. Tyagi, Multimodality of structural, electrical, and gravimetric responses of intercalated MXenes to water, *ACS Nano*, 2017, **11**(11), 11118–11126.

177 S. Kumar, Y. Lei, N. H. Alshareef, M. Quevedo-Lopez and K. N. Salama, Biofunctionalized two-dimensional Ti_3C_2 MXenes for ultrasensitive detection of cancer biomarker, *Biosens. Bioelectron.*, 2018, **121**, 243–249.

178 S. S. Shankar, R. M. Shereema and R. Rakhi, Electrochemical determination of adrenaline using MXene/Graphite composite paste electrodes, *ACS Appl. Mater. Interfaces*, 2018, **10**(50), 43343–43351.

179 J. Zhu, E. Ha, G. Zhao, Y. Zhou, D. Huang, G. Yue, L. Hu, N. Sun, Y. Wang and L. Y. S. Lee, Recent advance in MXenes: a promising 2D material for catalysis, sensor and chemical adsorption, *Coord. Chem. Rev.*, 2017, **352**, 306–327.

180 F. Liu, A. Zhou, J. Chen, J. Jia, W. Zhou, L. Wang and Q. Hu, Preparation of Ti_3C_2 and Ti_2C MXenes by fluoride salts etching and methane adsorptive properties, *Appl. Surf. Sci.*, 2017, **416**, 781–789.

181 N. C. Osti, M. Naguib, M. Tyagi, Y. Gogotsi, A. I. Kolesnikov and E. Mamontov, Evidence of molecular hydrogen trapped in two-dimensional layered titanium carbide-based MXene, *Phys. Rev. Mater.*, 2017, **1**(2), 024004.

182 Á. Morales-García, A. Fernández-Fernández, F. Viñes and F. Illas, CO_2 abatement using two-dimensional MXene carbides, *J. Mater. Chem. A*, 2018, **6**(8), 3381–3385.

183 I. Persson, J. Halim, H. Lind, T. W. Hansen, J. B. Wagner, L. Å. Näslund, V. Darakchieva, J. Palisaitis, J. Rosen and P. O. Persson, 2D transition metal carbides (MXenes) for carbon capture, *Adv. Mater.*, 2019, **31**(2), 1805472.

184 Y. Ma, N. Liu, L. Li, X. Hu, Z. Zou, J. Wang, S. Luo and Y. Gao, A highly flexible and sensitive piezoresistive sensor based on MXene with greatly changed interlayer distances, *Nat. Commun.*, 2017, **8**(1), 1–8.

185 Y.-Z. Zhang, K. H. Lee, D. H. Anjum, R. Sougrat, Q. Jiang, H. Kim and H. N. Alshareef, MXenes stretch hydrogel sensor performance to new limits, *Sci. Adv.*, 2018, **4**(6), eaat0098.

186 J. Chen, K. Chen, D. Tong, Y. Huang, J. Zhang, J. Xue, Q. Huang and T. Chen, CO_2 and temperature dual responsive "Smart" MXene phases, *Chem. Commun.*, 2015, **51**(2), 314–317.

187 M. Boota, M. Pasini, F. Galeotti, W. Porzio, M.-Q. Zhao, J. Halim and Y. Gogotsi, Interaction of polar and nonpolar polyfluorenes with layers of two-dimensional titanium carbide (MXene): intercalation and pseudocapacitance, *Chem. Mater.*, 2017, **29**(7), 2731–2738.

188 H. Zhang, L. Wang, Q. Chen, P. Li, A. Zhou, X. Cao and Q. Hu, Preparation, mechanical and anti-friction performance of MXene/polymer composites, *Mater. Des.*, 2016, **92**, 682–689.

189 B. Anasori, A. Sarycheva, S. Buondonno, Z. Zhou, S. Yang and Y. Gogotsi, 2D metal carbides (MXenes) in fibers, *Mater. Today*, 2017, **20**(8), 481–482.

190 B. Akuzum, K. Maleski, B. Anasori, P. Lelyukh, N. J. Alvarez, E. C. Kumbur and Y. Gogotsi, Rheological characteristics of 2D titanium carbide (MXene) dispersions: a guide for processing MXenes, *ACS Nano*, 2018, **12**(3), 2685–2694.

191 C. Zhang, M. P. Kremer, A. Seral-Ascaso, S. H. Park, N. McEvoy, B. Anasori, Y. Gogotsi and V. Nicolosi, Stamping of flexible, coplanar micro-supercapacitors using MXene inks, *Adv. Funct. Mater.*, 2018, **28**(9), 1705506.

192 P. Sobolčiak, A. Ali, M. K. Hassan, M. I. Helal, A. Tanvir, A. Popelka, M. A. Al-Maadeed, I. Krupa and K. A. Mahmoud, 2D $Ti_3C_2T_x$ (MXene)-reinforced polyvinyl alcohol (PVA) nanofibers with enhanced mechanical and electrical properties, *PLoS One*, 2017, **12**(8), e0183705.

193 R. Liu and W. Li, High-Thermal-Stability and High-Thermal-Conductivity $Ti_3C_2T_x$ MXene/Poly(vinyl alcohol)(PVA) Composites, *ACS Omega*, 2018, **3**(3), 2609–2617.

194 M. Naguib, T. Saito, S. Lai, M. S. Rager, T. Aytug, M. P. Paranthaman, M.-Q. Zhao and Y. Gogotsi, $Ti_3C_2T_x$

(MXene)–polyacrylamide nanocomposite films, *RSC Adv.*, 2016, **6**(76), 72069–72073.

195 W. Zhi, S. Xiang, R. Bian, R. Lin, K. Wu, T. Wang and D. Cai, Study of MXene-filled polyurethane nanocomposites prepared via an emulsion method, *Compos. Sci. Technol.*, 2018, **168**, 404–411.

196 H. Zhang, L. Wang, A. Zhou, C. Shen, Y. Dai, F. Liu, J. Chen, P. Li and Q. Hu, Effects of 2-D transition metal carbide Ti_2CT_x on properties of epoxy composites, *RSC Adv.*, 2016, **6**(90), 87341–87352.

197 Y. Cao, Q. Deng, Z. Liu, D. Shen, T. Wang, Q. Huang, S. Du, N. Jiang, C.-T. Lin and J. Yu, Enhanced thermal properties of poly(vinylidene fluoride) composites with ultrathin nanosheets of MXene, *RSC Adv.*, 2017, **7**(33), 20494–20501.

198 S. Ahn, T. H. Han, K. Maleski, J. Song, Y. H. Kim, M. H. Park, H. Zhou, S. Yoo, Y. Gogotsi and T. W. Lee, A 2D Titanium Carbide MXene Flexible Electrode for High-Efficiency Light-Emitting Diodes, *Adv. Mater.*, 2020, **32**(23), 2000919.

199 L. Zhou, F. Wu, J. Yu, Q. Deng, F. Zhang and G. Wang, Titanium carbide ($Ti_3C_2T_x$) MXene: a novel precursor to amphiphilic carbide-derived graphene quantum dots for fluorescent ink, light-emitting composite and bioimaging, *Carbon*, 2017, **118**, 50–57.

200 S. Lee, E. H. Kim, S. Yu, H. Kim, C. Park, T. H. Park, H. Han, S. W. Lee, S. Baek and W. Jin, Alternating-Current MXene Polymer Light-Emitting Diodes, *Adv. Funct. Mater.*, 2020, **30**(32), 2001224.

201 D. Pang, M. Alhabeb, X. Mu, Y. Dall'Agnese, Y. Gogotsi and Y. Gao, Electrochemical Actuators Based on Two-Dimensional $Ti_3C_2T_x$ (MXene), *Nano Lett.*, 2019, **19**(10), 7443–7448.

202 Q. Gao, J. Come, M. Naguib, S. Jesse, Y. Gogotsi and N. Balke, Synergetic effects of K^+ and Mg^{2+} ion intercalation on the electrochemical and actuation properties of the two-dimensional Ti3C2 MXene, *Faraday Discuss.*, 2017, **199**, 393–403.

203 X. Xie, M.-Q. Zhao, B. Anasori, K. Maleski, C. E. Ren, J. Li, B. W. Byles, E. Pomerantseva, G. Wang and Y. Gogotsi, Porous heterostructured MXene/carbon nanotube composite paper with high volumetric capacity for sodium-based energy storage devices, *Nano Energy*, 2016, **26**, 513–523.

204 V. H. Nguyen, R. Tabassian, S. Oh, S. Nam, M. Mahato, P. Thangasamy, A. Rajabi-Abhari, W. J. Hwang, A. K. Taseer and I. K. Oh, Stimuli-Responsive MXene-Based Actuators, *Adv. Funct. Mater.*, 2020, 1909504.

205 T. Liu, X. Liu, N. Graham, W. Yu and K. Sun, Two-dimensional MXene incorporated graphene oxide composite membrane with enhanced water purification performance, *J. Membr. Sci.*, 2020, **593**, 117431.

206 J. Guo, Q. Peng, H. Fu, G. Zou and Q. Zhang, Heavy-metal adsorption behavior of two-dimensional alkalization-intercalated MXene by first-principles calculations, *J. Phys. Chem. C*, 2015, **119**(36), 20923–20930.

207 Q. Zhang, J. Teng, G. Zou, Q. Peng, Q. Du, T. Jiao and J. Xiang, Efficient phosphate sequestration for water purification by unique sandwich-like MXene/magnetic iron oxide nanocomposites, *Nanoscale*, 2016, **8**(13), 7085–7093.

208 C. E. Ren, K. B. Hatzell, M. Alhabeb, Z. Ling, K. A. Mahmoud and Y. Gogotsi, Charge-and size-selective ion sieving through $Ti_3C_2T_x$ MXene membranes, *J. Phys. Chem. Lett.*, 2015, **6**(20), 4026–4031.

209 X. Xie, C. Chen, N. Zhang, Z.-R. Tang, J. Jiang and Y.-J. Xu, Microstructure and surface control of MXene films for water purification, *Nat. Sustainability*, 2019, **2**(9), 856–862.

210 X.-J. Zha, X. Zhao, J.-H. Pu, L.-S. Tang, K. Ke, R.-Y. Bao, L. Bai, Z.-Y. Liu, M.-B. Yang and W. Yang, Flexible anti-biofouling MXene/cellulose fibrous membrane for sustainable solar-driven water purification, *ACS Appl. Mater. Interfaces*, 2019, **11**(40), 36589–36597.

211 C. Cai, R. Wang, S. Liu, X. Yan, L. Zhang, M. Wang, Q. Tong and T. Jiao, Synthesis of self-assembled phytic acid-MXene nanocomposites *via* a facile hydrothermal approach with elevated dye adsorption capacities, *Colloids Surf., A*, 2020, **589**, 124468.

212 Z. Wei, Z. Peigen, T. Wubian, Q. Xia, Z. Yamei and S. ZhengMing, Alkali treated $Ti_3C_2T_x$ MXenes and their dye adsorption performance, *Mater. Chem. Phys.*, 2018, **206**, 270–276.

213 B.-M. Jun, J. Heo, N. Taheri-Qazvini, C. M. Park and Y. Yoon, Adsorption of selected dyes on $Ti_3C_2T_x$ MXene and Al-based metal–organic framework, *Ceram. Int.*, 2020, **46**(3), 2960–2968.

214 M. Marian, S. Tremmel, S. Wartzack, G. Song, B. Wang, J. Yu and A. Rosenkranz, MXene nanosheets as an emerging solid lubricant for machine elements–Towards increased energy efficiency and service life, *Appl. Surf. Sci.*, 2020, 146503.

215 A. Rosenkranz, P. G. Grützmacher, R. Espinoza, V. M. Fuenzalida, E. Blanco, N. Escalona, F. J. Gracia, R. Villarroel, L. Guo and R. Kang, Multi-layer $Ti_3C_2T_x$-nanoparticles (MXenes) as solid lubricants–Role of surface terminations and intercalated water, *Appl. Surf. Sci.*, 2019, **494**, 13–21.

216 A. M. Jastrzębska, E. Karwowska, T. Wojciechowski, W. Ziemkowska, A. Rozmysłowska, L. Chlubny and A. Olszyna, The atomic structure of Ti_2C and Ti_3C_2 MXenes is responsible for their antibacterial activity toward *E. coli* bacteria, *J. Mater. Eng. Performance*, 2019, **28**(3), 1272–1277.

217 A. Arabi Shamsabadi, Gh, M. Sharifian, B. Anasori and M. Soroush, Antimicrobial Mode-of-Action of Colloidal $Ti_3C_2T_x$ MXene Nanosheets, *ACS Sustainable Chem. Eng.*, 2018, **6**(12), 16586–16596.

218 A. Szuplewska, D. Kulpińska, A. Dybko, A. M. Jastrzębska, T. Wojciechowski, A. Rozmysłowska, M. Chudy, I. Grabowska-Jadach, W. Ziemkowska and Z. Brzózka, 2D Ti2C (MXene) as a novel highly efficient and selective agent for photothermal therapy, *Mater. Sci. Eng., C*, 2019, **98**, 874–886.

219 P. Zhang, L. Wang, K. Du, S. Wang, Z. Huang, L. Yuan, Z. Li, H. Wang, L. Zheng and Z. Chai, Effective removal of U(VI) and Eu(III) by carboxyl functionalized MXene nanosheets, *J. Hazard. Mater.*, 2020, 122731.

220 M. Khazaei, A. Ranjbar, K. Esfarjani, D. Bogdanovski, R. Dronskowski and S. Yunoki, Insights into exfoliation possibility of MAX phases to MXenes, *Phys. Chem. Chem. Phys.*, 2018, **20**(13), 8579–8592.

221 Z. Wang, J. Xuan, Z. Zhao, Q. Li and F. Geng, Versatile cutting method for producing fluorescent ultrasmall MXene sheets, *ACS Nano*, 2017, **11**(11), 11559–11565.

222 P. Eklund, J. Rosen and P. O. Å. Persson, Layered ternary $M_{n+1}AX_n$ phases and their 2D derivative MXene: an overview from a thin-film perspective, *J. Phys. D: Appl. Phys.*, 2017, **50**(11), 113001.

223 M. Ashton, K. Mathew, R. G. Hennig and S. B. Sinnott, Predicted surface composition and thermodynamic stability of MXenes in solution. *The*, *J. Phys. Chem. C*, 2016, **120**(6), 3550–3556.

224 C. J. Zhang and V. Nicolosi, Graphene and MXene-based transparent conductive electrodes and supercapacitors, *Energy Storage Mater.*, 2019, **16**, 102–125.